# COMPARING THE MECHANISM OF THE *E. COLI* AND *S. CEREVISIAE* CLAMP LOADERS

By

JACLYN HAYNER

A DISSERTATION PRESENTED TO THE GRADUATE SCHOOL
OF THE UNIVERSITY OF FLORIDA IN PARTIAL FULFILLMENT
OF THE REQUIREMENTS FOR THE DEGREE OF
DOCTOR OF PHILOSOPHY

UNIVERSITY OF FLORIDA

2013

To my family and friends for being so supportive

ACKNOWLEDGMENTS

I thank my family and friends for their unwavering support and encouragement. I would like to especially thank Ben Looney for help and understanding throughout the years. I thank my fellow lab members, past and present, for their friendship and training. I thank my committee members for their advice and guidance. I would also like to thank Dr. Linda Bloom for her patience and mentoring.

TABLE OF CONTENTS

page

LIST OF TABLES

LIST OF FIGURES

## LIST OF ABBREVIATIONS

| | |
|---|---|
| 3’DNA | p/t DNA with a recessed 3’ end |
| 5’DNA | p/t DNA with a recessed 5’ end |
| Amp | Ampicillin |
| AF488 | Alexa Fluor 488 maleimide |
| ATP | Adenosine 5’-triphosphate |
| ATPγS | Adenosine 5′-[γ-thio]triphosphate tetralithium |
| Cm | Chloromphenicol |
| DEPC | Diethylpyrocarbonate |
| DMF | Dimethylformamide |
| DMSO | Dimethyl sulfoxide |
| dsDNA | Double-stranded DNA, blunt DNA |
| DTT | Dithiothreitol |
| EDTA | Ethylenediaminetetraacetic acid |
| EM | Electron microscopy |
| flRFC | RFC containing a full length Rfc1 subunit |
| FRET | Fluorescence Resonance Energy Transfer |
| HEPES | 4-(2-hydroxyethyl)-1-piperazineethanesulfonic acid |
| IPTG | Isopropyl β-D-1-thiogalactopyranoside |
| $K_d$ | Dissociation constant |
| $k_{obs}$ | Observed rate |
| LB | Luria broth |
| MDCC` | 7-diethylamino-3-((((2-maleimidyl)ethyl)amino)carbonyl)coumarin |

| | |
|---|---|
| MeG | 7-Methylguanosine 5′-triphosphate |
| MWCO | Molecular weight cut off |
| nt | Nucleotide |
| PAGE | Polyacrylamide Gel Electrophoresis |
| PBP | Phosphate binding protein |
| PCNA | Proliferating Cell Nuclear Antigen |
| $P_i$ | Inorganic phosphate |
| PNPase | Polynucleotide phosphorylase |
| p/t DNA | primer/template DNA |
| PY | N - (1 - Pyrene) maleimide |
| RFC | Replication Factor C |
| RhX | Rhodamine X isothiocyanate |
| RPA | Replication Protein A |
| SDS-PAGE | Sodium dodecyl sulfate polyacrylamide gel electrophoresis |
| SSB | Single-stranded binding protein |
| ssDNA | Single-stranded DNA |
| SSO | Single stranded overhang |
| TCEP | Tris (2-carboxyethyl) phosphine |
| trRFC | RFC containing a Rfc1 subunit lacking the first 282 amino acids |

Abstract of Dissertation Presented to the Graduate School
of the University of Florida in Partial Fulfillment of the
Requirements for the Degree of Doctor of Philosophy

# COMPARING THE MECHANISM OF THE *E. COLI* AND *S. CEREVISIAE* CLAMP LOADERS

By

Jaclyn Hayner

August 2013

Chair: Linda Bloom
Major: Medical Sciences—Biochemistry and Molecular Biology

Clamp loaders and sliding clamps are present in all kingdoms of life, playing a vital role in the DNA replication and repair pathways to ensure accurate transmission of genetic material. The ring-shaped sliding clamps are assembled onto DNA by clamp loaders, which function as molecular machines using ATP to load these clamps around DNA. Specifically, clamp loaders bind and open clamps, then bind DNA, and finally close and release clamps around DNA. In *E. coli*, one clamp and clamp loader pair are known, $\beta$ and $\gamma$ complex, which play roles in both DNA replication and repair. In *S. cerevisiae*, multiple clamp and clamp loader pairs have been identified. One pair, PCNA and RFC, is involved primarily in DNA replication, but also has roles in repair processes as well. Another pair, 9-1-1 and Rad24-RFC, is involved in signaling DNA damage. Any aberration in activity of these clamps and clamp loaders can lead to incomplete or inaccurate duplication of the genome.

For DNA replication, a new clamp is needed every 2 – 3 seconds, so clamp loaders must be fine-tuned and efficient machines to complete this reaction in the appropriate timeframe. The first general question asked is: how are various steps in the

clamp loading reactions coordinated to allow for efficient clamp loading? In addition, clamp loaders need to load clamps in a specific orientation at specific DNA sites, which consist of double-stranded DNA or an RNA:DNA hybrid with a single-stranded DNA overhang. The second general question addressed is: how do clamp loaders recognize the correct DNA structures for loading clamps?

Fluorescence-based assays were used to measure different steps of the clamp loading reaction for the *E. coli* and *S. cerevisiae* clamp loaders. Results from these assays give a better understanding of the organization and timing of events that promote efficient clamp loading. In addition, these assays were used in conjunction with multiple DNA substrates to understand what aspects of the DNA architecture are important to promote clamp loading. These studies help to determine common mechanisms between the conserved clamp loaders as well as identify key differences that have evolved to suit the niche of each clamp loader.

# CHAPTER 1
# INTRODUCTION

## Sliding Clamps and Clamp Loaders in DNA Replication and Repair

Sliding clamps and clamp loaders are found in all kingdoms of life. Sliding clamps are ring shaped proteins that encircle DNA and serve as a mobile platform to coordinate DNA metabolic enzymes. Clamp loaders are required to load sliding clamps onto DNA and they perform this function through the use of ATP binding and hydrolysis. In *E. coli,* the sliding clamp β is loaded onto DNA by the clamp loader γ complex. The analogous sliding clamp and clamp loader in *S. cerevisiae*, is Replication Factor C (RFC), which loads the proliferating cell nuclear antigen (PCNA) clamp.

The *E. coli* β and *S. cerevisiae* PCNA clamps were first discovered in the DNA replication pathway as processivity factors for DNA polymerases. The ring shaped nature of sliding clamps allows the clamp to encircle the template DNA and serve as a traveling platform that anchors the DNA polymerase to the DNA template, preventing frequent dissociation (1-4). DNA polymerases are not highly processive on their own, and frequently dissociate from the DNA template being copied, therefore, sliding clamps are needed to increase the processivity of DNA polymerases from tens of nucleotides per binding event to thousands of nucleotides per binding event (5, 6).

At the *E. coli* replication fork, the clamp loader helps to coordinate leading and lagging strand synthesis. The clamp loaders make direct contacts with the DNA polymerases on both the leading and lagging strand as well as the helicase (7-9). These contacts prevent the helicase from unwinding DNA too fast and coordinate the DNA polymerases on both strands to prevent replication fork collapse. Human RFC on the other hand has been shown to disengage from PCNA after loading and does not

associate with the PCNA•polymerase complex (10). It is still unclear if the eukaryotic replication fork is held together in a similar fashion to the *E. coli* replication fork, and if so, the factor holding the replication fork together is currently unknown. In eukaryotes, DNA replication is complicated by higher order chromatin structure, coordination of sister chromatids, and cell cycle control. PCNA plays a role in these processes by interacting with and coordinating chromatin remodeling proteins, cell cycle signaling molecules, cohesin assembly factors, DNA methylation factors, and histone chaperones and remodeling complexes (reviewed (11)).

The β and PCNA clamps also have a role in coordinating the enzymes responsible for processing the lagging strand Okazaki fragments. Lagging strand synthesis is performed discontinuously using RNA primed regions, which must be removed after DNA replication. This process is performed by DNA polymerase I and DNA ligase in *E. coli*, which both interact with the β clamp (12). In eukaryotes, Okazaki fragment maturation is performed by multiple enzymes that interact with the PCNA clamp: Rad27 (hFen1) and/or Dna2, DNA ligase I, and DNA polymerase δ (reviewed (13)). It is not clear if all of the enzymes acting at the Okazaki fragment bind the sliding clamps at the same time, or if they trade on and off the clamp to remove the Okazaki fragment. Work with archaeal *S. solfataricus* suggests that a single PCNA clamp coordinates Fen1, DNA ligase, and DNA polymerase simultaneously for each Okazaki fragment (14). This has not been clearly observed for the *E. coli* or *S. cerevisiae* sliding clamps, however.

These sliding clamps also play a role in coordinating enzymes involved in DNA repair processes. Both β and PCNA interact with enzymes involved in mismatch repair

(15-21). This process prevents single-base mismatches as well as small insertions or deletions from being propagated. Both sliding clamps also interact with translesion synthesis (TLS) polymerases, which are low-fidelity polymerases recruited to replicate past lesions that the replicative polymerases cannot bypass. β interacts with the TLS polymerases II, IV, and V (12, 22-25). Post-translational modification of PCNA with ubiquitin stimulates interaction with the TLS polymerases η, ι, ζ, κ, and Rev1 (26-29).

Alternative sliding clamps and clamp loaders exist that play roles in other aspects of DNA metabolism. One such clamp loader is Rad24-RFC, which has only a single subunit difference from the RFC clamp loader. This alternative clamp loader loads a clamp composed of Ddc1-Rad17-Mec3 (Rad9, Rad1, Hus1 in humans, or 9-1-1). The 9-1-1 clamp is loaded in response to DNA damage and serves to coordinate and propagate the DNA damage signal. The C-terminal region of Ddc1 (hRad9) is hyperphosphorylated in response to DNA damage, and recruits Dpb11 (hTOPBP1) (reviewed (30)). hRad9 contains approximately 10 residues that are phosphorylated in response to DNA damage (31-34). This subunit also contains conserved tryptophan residues that are important for Mec1 (hATR) activation (35).

## Sliding Clamp Structure

The sliding clamps form highly conserved ring shaped structures despite little sequence similarity. β is a homodimer (Figure 1-1 A), PCNA is a homotrimer (Figure 1-1 B), and 9-1-1 is a heterotrimer (Figure 1-1 C). The subunits are composed of globular domains connected by loops referred to as inter-domain connecting loops (IDCL). The subunits are arranged in a head to tail fashion creating an asymmetry of the two faces. The center hole is approximately 35 Å to fit around either DNA:DNA or RNA:DNA

duplexes (1-3, 36-39). The interior hole is also lined with positively charged residues that interact with the negatively charged phosphate backbone of DNA. Residues of the interior hole of β and PCNA have been shown to be important for clamp loading and were suggested to help position the DNA within the clamp-clamp loader complex (3, 40, 41). The clamps are highly stable in the closed ring shape: the half-life of β on DNA was measured to be about 72 minutes (42) whereas the half-life of PCNA on DNA is 24 minutes (43, 44)

The 9-1-1 clamp forms a core conserved ring shape like the other sliding clamps, but it also has extensions on the Ddc1 (hRad9) subunit not shown in the crystal structure. The C-terminal extension of Ddc1 has approximately 230 residues that are unstructured and are involved in signaling DNA damage (45, 46).

**Clamp Loader Structure**

The clamp loaders are members of the AAA+ ATPase family, characterized by the use of ATP binding and hydrolysis to promote conformational changes that rearrange and remodel macromolecular substrates. AAA+ proteins contain multiple subunits that interact with one another to propagate conformational changes across the oligomeric protein. Each subunit of this ATPase family contains highly conserved residues that sense and respond to ATP binding and promote ATP hydrolysis (reviewed (47)). Clamp loaders contain three domains, two of which contain the conserved AAA+ residues. The third domain, in the C-terminal region of the subunit, is less conserved with other AAA+ ATPases but is common to clamp loaders. This C-terminal domain is responsible for oligomerization of the clamp loader subunits to form a conserved cap-like structure.

The core of the *E. coli* clamp loader, γ complex (Figure 1-2 A), is composed of five subunits, three γ subunits, a δ and δ' subunit. The γ subunits each bind and hydrolyze one molecule of ATP (48-50). These five subunits oligomerize to form the conserved cap-like clamp loader structure (51). γ complex also has two accessory subunits, ψ and χ, not shown in the crystal structure, that help stabilize the clamp loader structure and mediate clamp loader•SSB interactions (52-54).

The *S. cerevisiae* clamp loader, RFC (Figure 1-2 B), is composed of five subunits, Rfc1 – Rfc5, which also oligomerize to form a cap-like structure (55). All RFC subunits contain the conserved AAA+ ATPase domains as well as the C-terminal oligomerization domain, but the Rfc1 subunit contains additional domains at the N and C terminal region. The extra C-terminal region is partially visible in the crystal structure, whereas the extra N-terminal domain (NTD) was truncated and omitted the crystal structure. The NTD of Rfc1 contains homology to ligase, and contains BRCT and PARP domains, but it is unclear what role this region plays in clamp loading (56, 57).

Rad24-RFC contains Rfc2 – 5 subunits, but replaces Rfc1 with Rad24 (58, 59). There is currently no high-resolution structure of Rad24-RFC; however, electron microscopy (EM) studies with the human homologue indicate that this alternative clamp loader makes a similar globular shape as RFC, and thus has a similar overall structure (60, 61). Figure 1-2 C shows a structural model of the Rad24-RFC clamp loader, where the Rad24 subunit structure was modeled based on homology with the Rfc1 subunit.

## Clamp Loading Reaction

The clamp loading reaction for both γ complex and RFC have the same basic characteristics. Both enzymes are members of the $AAA^+$ ATPase family, characterized

by the use of ATP binding and hydrolysis to drive conformational changes that modulate the affinity of the clamp loader for the sliding clamp and DNA (reviewed (62)). ATP binding is required for the clamp loaders to have high affinity for DNA and sliding clamps (63-68). Both γ complex and RFC bind β and PCNA, respectively, before opening them, indicating the clamp loaders do not simply trap open clamps in solution (46, 69). DNA binding triggers a burst of ATP hydrolysis and results in release of the clamp around DNA (66, 70-72). Release of the clamp is hypothesized to be the rate-limiting step in both clamp loading reactions (73, 74). This is illustrated in Figure 1-3.

There are subtle differences in the mechanisms of each clamp loader, however. The γ complex binds three ATP molecules before binding β, one for each γ subunit (48-50, 73). RFC can bind five molecules of ATP, but only hydrolyzes four, one each in Rfc1 – 4 (63, 72). ATP binding by RFC is correlated with specific steps in the clamp loading reaction, where 2 ATP molecules bind, activating RFC for either PCNA or DNA binding. This reveals a third ATP binding site, which allows RFC•PCNA•DNA complex formation. This complex allows for binding of the last ATP molecule resulting in a complex competent for clamp loading (63). It is less clear if the ATP binding site in Rfc1 is important for clamp loading activity because mutations in conserved ATPase residues in this subunit have a minimal effect on clamp loading ((75), Marzahn, in preparation).

Less rigorous analysis has been performed with Rad24-RFC, but the general clamp loading mechanism is similar to that of γ complex and RFC. ATP binding is required for Rad24-RFC to bind the 9-1-1 clamp and DNA (76, 77). ATP hydrolysis is then required for Rad24-RFC to release 9-1-1 around DNA (77). This process was suggested to be dependent on the presence of the single-stranded DNA binding protein,

RPA (78). It is currently unclear how many ATP molecules are bound and hydrolyzed by Rad24-RFC. Since Rad24-RFC shares Rfc2 – 5 subunits with RFC, it can be assumed that these subunits also bind ATP molecules but only Rfc2 – 4 hydrolyze ATP. Based on sequence alignment, the *S. pombe* homologue of the Rad24 subunit, Rad17, contains a putative nucleotide binding site, but cells were still viable when this site was mutated (79). However, other work with the *S. cerevisiae* Rad24 subunit indicated that loss of a highly conserved ATP binding residue led to defects in Rad24-RFC activity (77, 80). Therefore, it is not clear if binding of an ATP molecule to the Rad24 subunit is required for Rad24-RFC activity.

**Clamp Loader•Clamp Interactions**

Most proteins that interact with the β and PCNA sliding clamps contain conserved motifs, referred to as PIP motifs (named for PCNA-interacting motifs), which bind to the sliding clamps in hydrophobic regions in the inter-domain connecting loops (IDCL) (12, 81, 82). Each clamp contains multiple IDCL regions with a hydrophobic pocket, so in theory several proteins could interact with the clamp at once assuming they only make a single interaction. This is referred to as the “toolbelt” model, which hypothesizes that multiple proteins can bind a sliding clamp at once. The proteins would then take turns performing the function they were recruited for. Clamp loaders interact with multiple hydrophobic pockets at once, so a clamp loader must release the sliding clamp before subsequent proteins can bind to the clamp.

The 9-1-1 clamp is a heterotrimer, and therefore has asymmetry, so there would be defined interactions between individual clamp and clamp loader subunits. The Rad24 subunit likely interacts with the Rad17 (hRad9) subunit of the clamp (83-85). Based on

this result, it was predicted that the Rfc3 subunit would interact with Mec3 (hHus1) and the Rfc5 subunit would interact with Ddc1 (hRad9), implying that the clamp loader opens the Rad17 – Ddc1 interface (86). Two structural studies with h9-1-1 suggested that this interface was opened by the clamp loader because it had the weakest interface interactions (36, 38). Another h9-1-1 structural study however suggested that the Ddc1-Mec3 interface is opened as it most closely resembles the PCNA interface (37). Rad24-RFC can also interact with PCNA, albeit weakly, and can unload PCNA from DNA *in vitro* (46, 76, 87). It is not clear if this is a physiologically relevant function of Rad24-RFC, however.

**Clamp Loader•DNA Interaction**

Recently, crystal structures of the *E. coli* and the T4 bacteriophage clamp loaders were solved in complex with primer/template (p/t) DNA (51, 88). The crystal structure of $\gamma$ complex with DNA is shown in Figure 1-4. Both structures show similar DNA binding by the clamp loaders, where the duplex portion of the DNA sits inside the cap of the clamp loader while the single-stranded overhang exits via a gap between the first and fifth clamp loader subunit. Both crystal structures show that the clamp loader interacts with the template strand of the p/t DNA, presumably to allow for interaction with both RNA:DNA and DND:DNA p/t structures. This interaction is mediated via positively charged residues on the inside of the clamp loader cap and the negatively charged phosphate backbone of the DNA. This supported previous mutational studies in $\gamma$ complex, which showed that positively charged residues on the interior of the clamp loader are required for efficient DNA binding (89).

Because clamp loader•DNA interactions are mediated through the template strand only, it is not clear how the clamp loader differentiates between the two polarities of p/t DNA. Both polarities of p/t DNA form right-handed helixes with the same spiral and pitch, and therefore would be expected to make similar contacts with the clamp loader. Previous work suggested that γ complex received polarity information from the duplex region of the p/t junction, but it was unclear what aspect of this region was important for DNA specificity (90). Because the duplex region is important for DNA specificity, then this would indicate that there could be more contacts between the clamp loader and duplex region of the p/t DNA that are present to sense the orientation within the cap. This is certainly possible, as the γ complex and T4 crystal structures have 3 – 4 Å resolution, which is not high enough to rule out any other clamp loader•DNA interactions.

In both the *E. coli* and T4 crystal structures, the single-stranded overhang (SSO) is shown exiting the clamp loader through the gap between the first and fifth subunit. Each clamp loader was incubated with DNA containing a 10nt SSO, but only 4nt are present in the structure. This indicates that these 4nt are held in a rigid position while the last 6nt are not. It is not clear if the 4nt are held in the same position because clamp loader contacts with the SSO are important for clamp loader activity or if the SSO position is simply stabilized by interactions with these residues. The W279 residue of the δ subunit of γ complex crosslinks to the first nucleotide of the SSO, and mutational studies on this residue indicated that interactions with the SSO are important for γ complex activity (91, 92). The importance of other residues that interact with the SSO have not been determined, therefore it is not clear how long of an SSO is necessary for

efficient clamp loading.

RFC is also required to load clamps at a p/t junction with a 3' recessed end, similar to γ complex. There is no structure of RFC bound to DNA; however, it is presumed to bind DNA in a similar fashion, with the duplex region inserted inside the cap structure and the SSO exiting through the gap between Rfc1 and Rfc5. The SSO was shown to crosslink to the Rfc1 subunit, indicating a similar general DNA binding mechanism exists for RFC as for γ complex (91). RFC has been shown to be more promiscuous in its DNA specificity (43, 56, 93-99), so it is not clear what interactions with DNA are important for DNA recognition. RPA plays a role in promoting RFC activity on DNA with a recessed 3'end (100). Rad24-RFC differs by only one subunit from RFC, therefore it is also presumed to have similar general interactions with DNA, even though less is known about this clamp loader. Rad24-RFC loads clamps onto p/t DNA with recessed 5' ends (78), and RPA also plays a role in targeting Rad24-RFC to this site (100). It is possible that for DNA recognition, the two eukaryotic clamp loaders rely less on specific DNA contacts than on interactions with RPA.

**Clamp•DNA Interactions**

The sliding clamps also make contacts with DNA that play an important role in clamp loader activity. Both free β and PCNA sit on DNA at an angle making contacts with the DNA (3, 40). Mutation of positively charged residues on the interior of both clamps alters clamp loading activity, indicating DNA contacts by the sliding clamps are required for maximum clamp loader efficiency (3, 40, 41). A combination of molecular dynamics simulations and EM studies on the PCNA and 9-1-1 clamps bound to DNA and Fen1 showed that both sliding clamps make contacts with DNA via positive

residues on the interior of the clamp. Because PCNA is positioned on DNA at an angle, it makes asymmetrical contacts with the DNA, where one subunit would make a majority of the DNA contacts. This was thought to facilitate PCNA sliding along DNA. Interestingly, the 9-1-1 clamp appears to make more symmetrical contacts with DNA, where each subunit appears to contact DNA equally. It is not clear if these symmetrical contacts are important for clamp loading activity by Rad24-RFC, but the authors suggested this may play a role reducing the mobility of 9-1-1 on DNA (101).

## Statement of Problem and Research Design

Clamp loaders are fine-tuned molecular machines that must quickly and efficiently assemble sliding clamps on DNA. The clamp loader must bind the clamp, bind the correct DNA structure, load the clamp around DNA, and finally release the clamp•DNA complex all in a matter of a few seconds. For DNA replication, a new clamp is needed every 2 – 3 seconds, one for each Okazaki fragment, so clamp loaders must be able to quickly and efficiently load clamps at the appropriate sites on DNA. To perform this reaction efficiently, the clamp loaders must have a defined mechanism to ensure that clamps are loaded without wasting ATP or slowing the replication fork. Specifically, in Chapter 3, the temporal order of events in the clamp loading cycle following DNA binding was investigated for both the *E. coli* and *S. cerevisiae* replicative clamp loaders. These steps were measured using pre-steady state fluorescence-based assays that report on ATP hydrolysis, clamp closing, and clamp release. Results from this section help to understand the distinct timing of clamp loading events as well as compare the mechanism between the two clamp loaders. In Chapter 6, a comparison was made between two RFC clamp loaders, wild type (flRFC), and RFC containing an

Rfc1 subunit lacking the first 282 amino acids (trRFC). Using fluorescence-based assays, different steps of the clamp loading cycle were measured and compared between clamp loaders. This serves not only to understand the mechanism of RFC, but also to compare the clamp loaders and determine the function of the first 282 amino acids of the Rfc1 subunit.

Clamp loaders also play a role in targeting the sliding clamp to a specific location on DNA. For γ complex and RFC, this location is a p/t junction with a 3' recessed end, as this is where a new clamp would be loaded for DNA replication. For Rad24-RFC, a p/t junction with a 5' recessed end is recognized because this site is where 9-1-1 is loaded to signal DNA damage. To understand how these clamp loaders target specific structures of DNA, fluorescence-based assays reporting on various aspects of the clamp loading cycle were used to measure activity on different DNA structures. In Chapter 4, the DNA specificity of γ complex was investigated using pre-steady state β closing and release assays. Closing and release was measured on DNA with different lengths of single-stranded overhangs, and DNA with different polarities to determine what aspect of the DNA is recognized by γ complex. In addition, the presence of SSB was investigated to determine if it plays a role in clamp loader specificity. In Chapter 5 steady-state DNA binding assays were used to compare DNA binding by RFC and Rad24-RFC to different DNA structures. RFC specificity for DNA was further investigated using pre-steady state PCNA closing and release assays to monitor PCNA loading on different structures of DNA. RPA was also included in these studies to determine the effect of protein•protein interactions on DNA specificity. These studies help to understand what DNA structures are ideal for clamp loading and therefore give

insight into the mechanism of DNA recognition by clamp loaders. This work also serves as a comparison of the clamp loaders to identify conserved mechanisms as well as areas where the clamp loaders differ in their DNA recognition mechanism.

## Medical Relevance

The sliding clamps and clamp loaders play integral roles in the processes of DNA replication and repair. Aberration in function or activity of these proteins could lead to DNA replication defects and propagation of DNA damage. Haploinsufficiency of clamp loader subunit Rfc2, among other proteins, was discovered in patients with the neuro-developmental disorder Williams-Beuren Syndrome. This syndrome is characterized by growth and developmental defects, which could in part be caused by DNA replication defects associated with the haploinsufficiency of Rfc2 (102). In addition it has been reported that cells afflicted with Hutchinson-Guilford Progeria Syndrome (HGPS) contain RFC clamp loaders with deletions of the N-terminal region of the Rfc1 subunit. HGPS is caused by mutations in lamin proteins that weaken the structure of the nucleus. In HGPS cells, the authors observed RFC clamp loaders that had approximately 75 kD truncations of the Rfc1 subunit, which could be reversed if serine protease inhibitors were present. The authors hypothesized that the weak nuclear structure caused by HGPS allows cytoplasmic serine proteases access to nuclear proteins, resulting in aberrant proteolysis of the Rfc1 subunit. Truncation of Rfc1 could result in clamp loaders that are not proficient in clamp loading, and thus may explain replication defects characteristic of HGPS (103).

Mutations in clamp loader or clamp subunits have been identified in a variety of cancer cells. A haploinsufficiency of the hAtad5 subunit of the alternative clamp loader

Atad5-RFC (Elg1-RFC in *S. cerevisiae*) results in a predisposition to cancer, and is present in 5% of endometrial cancers screened (104). Deletions and truncations of RFC3 were present in approximately 10% of the gastric and colorectal cancers tested (105). The mutation, H239R in hRad9 (ScDdc1), was shown to be present in 16% of non-small cell lung carcinomas tested (106).

Because of their vital role in cell function, the sliding clamps and clamp loaders are excellent targets for anti-bacterial and chemotherapeutic agents. Small molecules have already been designed that target these clamps (107-114). Interestingly, no small molecules have been designed targeting the clamp loaders, so this remains an unexplored option for therapeutic agents. Understanding the nuances of the clamp loading mechanism and how they compare between species can help uncover new targets for small molecule inhibitors.

A.

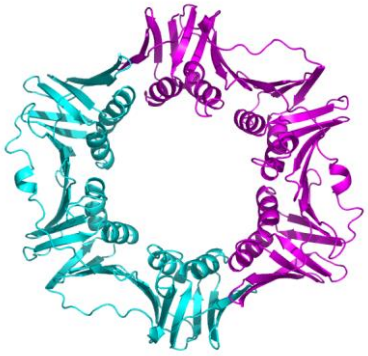

B.

C.

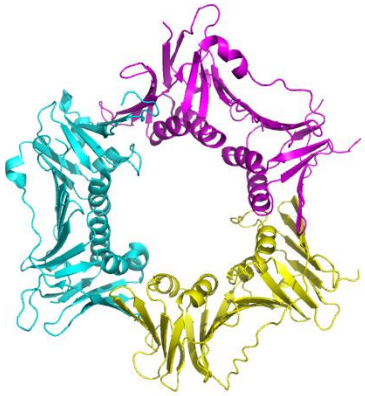

Figure 1-1. Crystal structures of the sliding clamps. A shows the structure of *E. coli* β (1). B shows the structure of human PCNA (2). A crystal structure of human 9-1-1 is shown in C (66). In blue is hRad9 (Ddc1), in yellow is hRad1 (Rad17) and in pink is hHus1 (Mec3).

A.

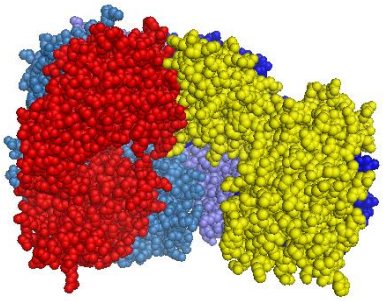

B.

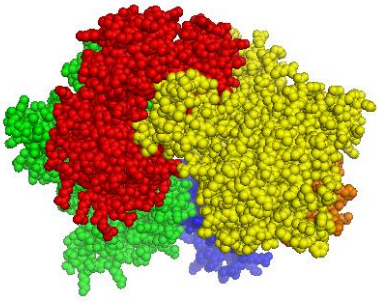

C.

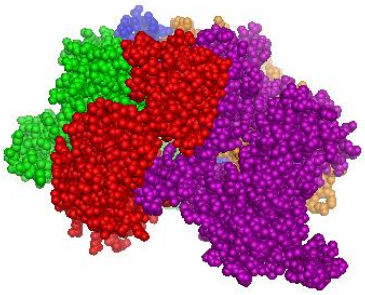

Figure 1-2. Clamp loader structures. Panel A shows the structure of *E. coli* γ complex, with δ in blue, the three γ subunits in blue and δ' in red (70). Shown in B is the structure of *S. cerevisiae* RFC, with Rfc1 in yellow, Rfc2 in green, Rfc3 in blue, Rfc 4 in orange, and Rfc5 in red (37). Panel C shows a model of the Rad24 subunit aligned with Rfc1 to give a predicted Rad24-RFC structure. The RFC structure is the same as in B, with Rad24 represented in purple.

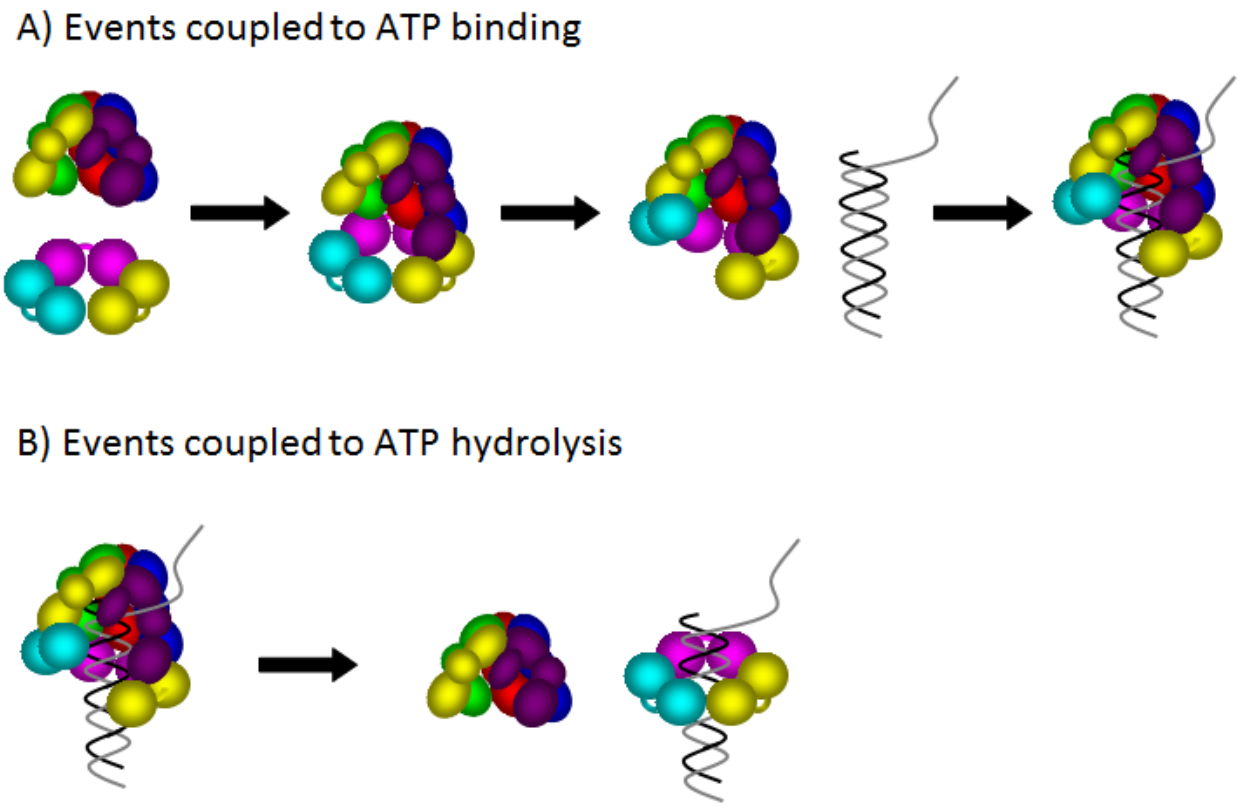


Figure 1-3. Events in the clamp loading cycle. Events are shown above and are grouped by their association with ATP binding or ATP hydrolysis. The timing of events coupled to ATP binding has been studied in more detail than events coupled to ATP hydrolysis. ATP binding is required for the clamp loader to bind the clamp efficiently, open the clamp, and bind DNA. ATP hydrolysis results in a loaded clamp around DNA.

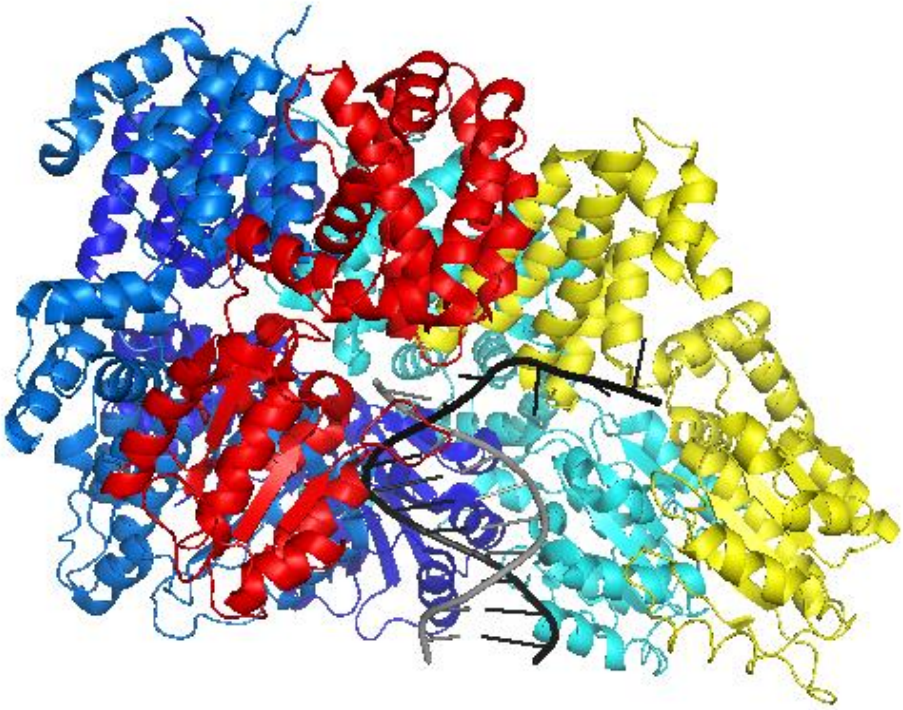

Figure 1-4. Crystal structure of γ complex bound to p/t DNA. The γ subunits are shown in shades of blue, δ is in yellow, and δ' is in red. The primer strand of the p/t DNA is shown in gray and the template strand is shown in black. This structure shows that the DNA sits inside the cap of γ complex, while the template strand exits near the δ subunit (70).

# CHAPTER 2
# MATERIALS AND METHODS

## Reagents

### Buffers

Unlabeled β was stored in a buffer containing 20 mM Tris pH 7.5, 10% glycerol, 0.5 mM EDTA and 2 mM DTT, whereas fluorescently labeled β clamps were stored in the same buffer without DTT. Storage buffer for γ complex was the same as β storage buffer with the addition of 50 mM NaCl. Pre-steady state assays with γ complex and β had final buffer concentrations of 20 mM Tris pH 7.5, 50 mM NaCl, 4% glycerol, 0.5 mM EDTA, 2 mM DTT, 8 mM $MgCl_2$, and 0.5 mM ATP.

Unlabeled PCNA was stored in 30 mM HEPES pH 7.5, 150 mM NaCl, 10% glycerol, 0.5 mM EDTA, and 2 mM DTT, while fluorescently labeled PCNA clamps were stored in the same buffer, but lacking DTT. Rad24-RFC was stored in the same buffer as unlabeled PCNA, while RFC was stored in the same buffer with 300 mM NaCl. Equilibrium assays with RFC, Rad24-RFC, and PCNA had final buffer concentrations of 30 mM HEPES pH 7.5, 150 mM NaCl, 10% glycerol, 10 mM $MgCl_2$, and 0.5 mM ATP. Pre-steady state reactions had the same final concentrations with the addition of 0.5 mM EDTA and 2 mM DTT. During the course of these studies, the composition of RFC storage buffer was changed to include 750 mM maltose to aid in stability, and 100 mM maltose was included in the assay buffers to keep the maltose concentration constant.

### ATP and ATPγS

ATP (Amersham Biosciences) was dissolved in 20 mM Tris pH 7.5 for reactions with γ complex and β, while ATP was dissolved in 30 mM HEPES pH 7.5 for reactions with RFC, Rad24-RFC and PCNA. The concentration of ATP was determined by

measuring the absorbance at 259 nm using the extinction coefficient of 15,400 $M^{-1}$ $cm^{-1}$. A 100 mM ATPγS solution was purchased from Roche, and used as is.

**Oligonucleotides**

Oligonucleotides used in these studies are listed in Tables 2-1 and 2-2 below. Oligonucleotides (Integrated DNA Technology) were purified using 10 – 12% denaturing polyacrylamide gels to ensure any shorter DNA byproducts were removed. Oligonucleotides 40 base pairs or longer were purified using a 10% gel, while shorter oligomers were purified using 12% gels. Gels were run 16 – 18 hours overnight at 8 – 9 watts. DNA bands were visualized using a handheld UV lamp and were excised. The DNA was eluted from the excised gel by soaking in 50 mM Tris pH 7.5, 50 mM NaCl and 0.5 mM EDTA for approximately 24 hours. Buffer solution containing the oligonucleotide was dialyzed against 2 L of 20 mM Tris pH 7.5 and 50 mM NaCl, followed by 2 dialyses against 2 L of water. The oligonucleotide solution was concentrated using a speed-vac to a volume of approximately 200 – 500 μL. The concentration of oligonucleotides was determined by measuring the absorbance at 260 nm using the sequence-based extinction coefficients provided by IDT.

An RNA oligonucleotide was purified using a modified version of the protocol above. All buffer solutions containing Tris were instead made with HEPES pH 7.5 (except for the running buffer) to allow for treatment with 0.1% diethyl pyrocarbonate (DEPC, Sigma). DEPC treatment of the buffer solutions and water was performed by adding DEPC to a final concentration of 0.1%, shaking the solutions vigorously, allowing the solution to sit overnight to inactivate RNases, and finally autoclaving the solution for 20 min to break down the DEPC. All glass plates, combs, spacers, plasticware and glassware were treated with RNase ZAP (Invitrogen) to remove RNase contamination. Unfortunately, after purification,

the yield of RNA oligomer was very low. Additionally, the RNA solution appeared opaque, which could indicate RNA precipitation. In future preparations of RNA, a higher amount of RNA should be ordered from IDT to compensate for the loss of RNA throughout the purification process. Also, the potential precipitation of RNA would need to be addressed.

Some oligonucleotides shown in Table 2-1 above contained thymine bases modified with an amino linker (indicated by **t**), which allowed covalent labeling by the succinimidyl ester derivatives of the RhX fluorophore. A 20-fold molar excess of RhX in DMF was mixed with purified oligonucleotides, and this was incubated overnight at 37°C with agitation. The labeled oligonucleotide was purified from excess fluorophore using a desalting column. The desalting column was composed of BioRad P6 desalting resin with a 6,000 MWCO, hand packed into a 50-cm, Flex-column (Fisher) with an 88-mL volume. DNA eluted in the void volume, while the excess fluorophore was retained on the column. Labeled oligonucleotide was purified from unlabeled oligonucleotide using the denaturing polyacrylamide gel protocol above. Modification of the oligomer with RhX caused it to run on a gel as if it was 1 – 2 nt longer than unmodified oligomer.

Some oligonucleotides in Table 2-2 were phosphorylated on the 5' end after purification using T4 polynucleotide kinase. The final 30-μL reaction contained 10 nmoles of oligomers, 3 mM ATP, 1X T4 forward buffer (New England Biolabs) and 0.17 U/mL T4 kinase (New England Biolabs). This reaction was incubated at 37°C for 1 hr. Kinase reactions were inactivated by heating to 65°C for 20 min. The reaction was mixed with 30 μL glycerol and loaded onto a 10 – 12% denaturing polyacrylamide gel. The oligomers were purified as described above. The phosphorylation state of the oligomers was tested by running 10 μL of the kinase treated oligomers alongside 10μL

of untreated oligomers. Phosphorylated oligomers ran faster on the gel than untreated oligomers.

For assays, oligonucleotides were annealed to produce the double stranded DNA substrates. Annealing DNA entailed heating the solution of oligonucleotides and buffer to 85 °C for 5 min and then cooling to room temperature overnight. For reactions with γ complex and β, the final buffer contained 20 mM Tris pH 7.5 and 50 mM NaCl. For RFC, Rad24-RFC or PCNA reactions, final buffer concentration is 30 mM HEPES pH 7.5, 150 mM NaCl.

## Proteins

### Purification of RFC with full length Rfc1 subunit

Previous preparations of RFC contained an Rfc1 subunit with a deletion of the first 282 amino acids. The plasmid for the full length RFC (flRFC) was a gift from the M. Hingorani laboratory. The pET-11a based plasmid contained all five subunits of the RFC complex. BL21 (DE3) Rosetta *E. coli* cells (Novagen) were used, which contain a plasmid that codes for rare tRNAs to prevent limitations in RFC expression because of *E. coli* codon bias. The rare tRNAs included code for AGG, AGA, AUA, CUA, CCC, and GGA.

The RFC plasmid was transformed into the BL21 (DE3) Rosetta cells and colonies were selected for based on growth on both ampicillin (Amp) for the pET-11a flRFC plasmid and chloramphenicol (Cm) for the Rosetta plasmid for rare tRNAs. A single colony was picked and grown in overnight in 2 mL of LB media with Amp and Cm at 37°C. The 2-mL culture was used to inoculate four 600-mL LB media cultures. The cells in the 2-mL culture were isolated by centrifugation at 6,810 x g for 5 minutes. The

cells were resuspended in 2 mL of fresh LB media, and isolated a second time by centrifugation. This cell pellet was resuspended in 2 mL fresh LB media, and this was used to inoculate four 600-mL LB Amp and Cm cultures. The 600-mL cultures were grown at 37°C to an OD of 0.6 – 0.7 as measured by the absorbance at 600 nm. Cultures were cooled to 25°C on ice and protein expression was induced by adding IPTG to a final concentration of 1 mM. After incubation for 8 hours at 25°C, cells were pelleted by centrifugation at 4,650 x g for 30 min at 4°C. Cell pellets were stored at -80°C.

The cells were lysed using a French Press in 60 mL of 30 mM HEPES pH 7.5, 300 mM NaCl, 10% glycerol, 0.5 mM EDTA, 2 mM DTT, and protease inhibitors (SigmaFast Protease inhibitor cocktail tablets, Sigma). Lysate was run through the French Press four times to ensure complete lysis. Cell lysate was centrifuged at 17,400 x g for 30 min at 4°C. Three chromatographic steps described below, were used to purify flRFC.

First, the soluble lysate was loaded at a rate of 3 mL/min onto two 5-mL HiTrap SP columns (GE Healthcare) attached back-to-back. Once the lysate was loaded, the column was washed with 50 mL of buffer containing 300 mM NaCl. A 150-mL linear gradient from 300 mM to 600 mM NaCl was used to elute flRFC. The protein eluted in approximately 450 – 500 mM NaCl. These fractions were pooled and dialyzed against 30 mM HEPES pH 7.5, 300 mM NaCl, and 10% glycerol, 0.5 mM EDTA, and 2 mM DTT.

The dialyzed flRFC was loaded onto the second column, a 5-mL HiTrap heparin (GE Healthcare), at a rate of 1.5 mL/min. The heparin column was first washed with 25

mL of buffer containing 300 mM NaCl. A 150-mL linear gradient from 300 mM NaCl to 1 M NaCl was used to elute flRFC. The protein eluted in approximately 700 mM NaCl. The fractions were pooled and dialyzed against 30 mM HEPES pH 7.5, 0.5 mM EDTA, 10% glycerol, 300 mM NaCl, and 2 mM DTT.

Prior to loading flRFC on the 8-mL MonoQ column (Pharmacia Biotech), it was diluted to 110 mM NaCl by adding buffer containing no NaCl, 10 mL at a time. The diluted protein was loaded at a rate of 1 mL/min. The column was washed with 40 mL of buffer containing 110 mM NaCl. The protein was eluted from the MonoQ with an 80-mL linear NaCl gradient from 110 – 500 mM. The flRFC peak eluted at approximately 250 mM NaCl. The final protein was dialyzed against in 30 mM HEPES pH 7.5, 300 mM NaCl, 10% glycerol, 0.5 mM EDTA, 2 mM DTT, and 750 mM maltose. Protein concentration was determined by denatured absorbance at 280 nm using the calculated extinction coefficient of 163,520 $M^{-1}$ $cm^{-1}$. An SDS-PAGE gel of the purification steps is shown in Figure 2-1.

**Size exclusion of flRFC**

To ensure that flRFC was a single complex, the purified protein was analyzed by size exclusion column. Specifically, a 120-mL Superdex (GE Healthcare) was used to measure the size of the flRFC complex. First, protein standards ranging from 1.35 – 670 kD (BioRad) were run to calibrate the column and correlate molecular weight to elution volume. Both protein standards and flRFC were run on the column in the RFC storage buffer. Standards were plotted as a function of the log of the elution volume to obtain a standard curve shown below in Figure 2-2 A. flRFC elution profile is shown below in Figure 2-2 B; flRFC eluted at 52 mL. Using the standard curve, the size of flRFC was

calculated to be 290 kD, which is consistent with 250 kD calculated for a flRFC complex containing all subunits.

### Other proteins

Other proteins used in these studies were purified by members of the Bloom laboratory. These proteins include γ complex (115-118), unlabeled β (119), β and γ complex mutants for fluorescent labeling (69, 73, 120), SSB (121), RFC (truncated) (122, 123), unlabeled PCNA (124, 125), PCNA mutants (46) (Marzahn, in preparation). RPA, Rad24-RFC, and γ complex lacking the χ subunit were gifts from the O'Donnell laboratory.

## Protein Labelings

### Fluorescent β and PCNA opening/closing clamps

To measure clamp opening and closing by γ complex and RFC, clamps were selectively labeled at both ends of the interface with AF488 (46, 69). To label these sites specifically, the native cysteine residues at position 260 and 333 in β and 22, 62, and 81 in PCNA were mutated to serine. The I305 and R103 sites in β and the I111 and I181 sites in PCNA were mutated to cysteine residues, which were covalently labeled using maleimide derivatives AF488.

To label these clamps, 2 mg of protein was first treated with 50 mM TCEP at 37°C for 1 hour to reduce any disulfide bonds that may have formed at the clamp interfaces. The clamps were then incubated with a 10 – 20 fold excess of AF488 fluorophore relative to the cysteine concentration. The labeling reaction was incubated at room temperature for 2 hours and then incubated at 4°C overnight. The excess fluorophore was removed by using the hand-packed desalting column described above

for DNA labelings. The clamps eluted in the void volume, while the fluorophore was retained on the column. The resulting protein was loaded onto a 1-mL HiTrap Q (GE Healthcare) at a rate of 0.5 mL/min. The column was washed with 5 mL of buffer containing no NaCl. A 10-mL linear gradient of NaCl from 0 mM to 1 M was used for elution; the clamps eluted at approximately 500 mM NaCl. Final clamp concentration was determined using a Bradford assay using β or PCNA standards where appropriate. AF488 concentration was determined by measuring the absorbance at 519 nm using the extinction coefficient of 73,000 $M^{-1}$ $cm^{-1}$, provided by Invitrogen.

**Fluorescent β and PCNA binding/release mutants**

To measure clamp binding and release by γ complex and RFC, sliding clamps were selectively labeled on the surface that interacts with the clamp loader (120) (Marzahn, in preparation). The native cysteine residues listed above were mutated to serine while Q299 in β and S43 in PCNA were mutated to cysteine. These cysteine residues were covalently labeled with maleimide derivatives of pyrene (PY) for β and MDCC for PCNA. A similar protocol was used to label these clamps as described above, except incubation with 50 mM TCEP was omitted. Final clamp concentrations were determined using a Bradford assay using β or PCNA standards as required. PY concentration was determined by measuring the absorbance at 338 nm using the extinction coefficient of 40,000 $M^{-1}$ $cm^{-1}$, as provided by Invitrogen. MDCC concentration was determined by measuring the absorbance at 419 nm using the extinction coefficient of 50,000 $M^{-1}$ $cm^{-1}$ provided by Invitrogen.

**Labeling phosphate binding protein with MDCC**

Phosphate binding protein (PBP) labeled with MDCC was used to report on inorganic phosphate ($P_i$) release from ATP hydrolysis reactions, thus serving as a read-out for ATP hydrolysis by the clamp loaders (49, 126). PBP-MDCC used in these assays was initially purchased from Invitrogen, but a second PBP-MDCC preparation was purified and labeled in our laboratory. The plasmid containing PBP with an A197C mutation was a gift from the Webb laboratory, which was used to purify PBP by a previous laboratory member. To label PBP, 28 mg of PBP was incubated with a 5-fold molar excess of MDCC in buffer containing 20 mM Tris pH 8.1, 200 μM 7-methyl guanosine (MeG, Santa Cruz), 0.2 U/mL purine nucleoside phosphorylase (PNPase, Sigma), and 5 μM $MnCl_2$ in a final volume of 2.7 mL. The labeling reaction was incubated at room temperature for 2.5 hours and then incubated at 4°C overnight. To purify away the excess MDCC, the desalting column described above for DNA labelings was used. Before the labeling reaction could be loaded onto the desalting column, it was concentrated to a final volume of 1 mL using 3 kD MWCO 0.5-mL centrifugal filters (Amicon). PBP eluted from the desalting column in the void volume and free MDCC was retained on the column.

To separate labeled PBP from unlabeled PBP, a 5-mL HiTrap Q column (GE Healthcare) was used. PBP-MDCC was loaded at a rate of 1 mL/min. The column was washed with 25 mL of buffer with no NaCl, and PBP-MDCC was eluted with a linear 400 mL gradient from 0 – 50 mM NaCl. Two peaks eluted, the first peak at approximately 15 mM NaCl, represented labeled PBP and was yellow. The second peak, which eluted at approximately 40 mM NaCl, represented unlabeled PBP and was uncolored.

To separate responsive MDCC-PBP from unresponsive MDCC-PBP, 100 μM $KH_2PO_4$ was included in the buffer. The PBP-MDCC was loaded at a rate of 1 mL/min on an 8-mL MonoQ column (Pharmacia Biotech). Once the protein was loaded, the column was washed with 40 mL of buffer containing no NaCl. PBP-MDCC was eluted with an 80 mL linear gradient from 0 – 50 mM. Again, two peaks eluted, the first peak at approximately 20 mM NaCl represents responsive MDCC-PBP, while the second peak at approximately 40 mM NaCl represents the unresponsive peak. The responsive peak was pooled and stored in 10 mM Tris pH8. To determine concentration of PBP, the denatured absorbance at 280 nm was measured and the extinction coefficient of 60,880 was used. The concentration of MDCC was determined by measuring the absorbance at 430 nm and using the extinction coefficient of 46,800 $M^{-1}$ $cm^{-1}$.

To determine the active concentration of MDCC-PBP, titrations of known concentrations of $KH_2PO_4$ were performed to determine the concentration at which MDCC-PBP is saturated. Briefly, 5 μM MDCC-PBP was titrated with concentrations of $KH_2PO_4$ ranging from 0 – 50 μM. As the concentration of $KH_2PO_4$ increased, the fluorescence of MDCC-PBP increased, but only to the point where all PBP-MDCC was saturated with $P_i$. This saturation point could be calculated to determine the active concentration of PBP-MDCC; this is shown in Figure 2-3.

**Fluorescence-Based Equilibrium Assays**

All equilibrium measurements were made using a QuantaMaster Spectrofluorometer (Photon Technology International). All reagents were mixed in a 3x3 mm quartz cuvette (Hellma) with a final volume of 80 μL for approximately 30 s before readings were taken. All equilibrium reactions were performed at room

temperature. Data was analyzed using KaleidaGraph, and the averages reported for each experiment are from three independent experiments.

**DNA binding**

To measure DNA binding, a fluorescence-based anisotropy assay was used. The DNA structures in Table 2-1 were used to make four DNA structures labeled with RhX: single-stranded (ssDNA), double-stranded (dsDNA), and two primed-template (p/t) structures, one with a 3' recessed junction (3'DNA), and one with a 5' recessed junction (5'DNA). Samples were excited at 590 nm and emission was measured at 610 nm with 8 nm bandpass. Polarizers were used to vertically and horizontally polarize the excitation and emission light.

To measure DNA binding at 25 nM DNA-RhX, anisotropy values were measured for multiple concentrations of clamp loader. To obtain anisotropy values, four polarized emission readings were taken ($I_{VV}$, $I_{VH}$, $I_{HV}$, and $I_{HH}$). First, a background signal was measured for assay buffer and 0.5 mM ATP$\gamma$S in the cuvette. Second, DNA-RhX was added to the cuvette and polarized intensities for free DNA were measured. Third, clamp loader was added to the cuvette to measure clamp loader binding to DNA. Finally, PCNA was added to the cuvette and polarized emission readings were taken.

To obtain an anisotropy value from these raw data, the g factor was first calculated using Equation 2-1. The g factor corrects for the bias in the emission detectors.

$$g = \frac{I_{HV(DNA)} - I_{HV(buff)}}{I_{HH(DNA)} - I_{HH(buff)}} \quad (2\text{-}1)$$

The g factor was used to calculate the anisotropy (r) for each clamp loader concentration using Equation 2-2.

$$r = \frac{(\mathrm{I}_{VV} - I_{vv(buff)}) - g(I_{VH} - I_{VH(buff)})}{(I_{VV} - I_{VV(buff)}) + 2g(I_{VH} - I_{VH(buff)})} \quad (2\text{-}2)$$

Anisotropy was plotted as a function of clamp loader concentration. The $K_d$ value was calculated using Equation 2-3, where $I_{max}$ is the maximum anisotropy, $I_{min}$ is the minimum anisotropy, RFC is the total clamp loader concentration, and DNA is the total DNA concentration.

$$I_{obs} = \frac{(K_d + RFC + DNA) - \sqrt{(K_d + RFC + DNA)^2 - 4(RFC)(DNA)}}{2(DNA)} \times (I_{max} - I_{min}) + I_{min} \quad (2\text{-}3)$$

**PCNA binding assay**

To measure PCNA binding by RFC, the PCNA-MDCC mutant was used. MDCC was excited at 425 nm and emission was measured from 450 nm to 500 nm with a 4 nm band-pass. To measure PCNA binding, three measurements were taken: the first is a buffer background with 0.5 mM ATP, the second is free PCNA-MDCC, and the third is with RFC. To generate the data points, the intensities at 468 nm were used. The intensities were corrected for dilution factor, and then the buffer intensity was subtracted from the free PCNA and the RFC intensities. The RFC intensity was then divided by the free PCNA intensity giving the relative change in intensity due to RFC binding. The $K_d$ was calculated using Equation 2-3, with PCNA-MDCC concentration in place of DNA concentration.

### PCNA opening assay

To measure PCNA opening by RFC, the PCNA-AF488 mutant was used. AF488 was excited at 490 nm and emission was measured from 500 nm to 550 nm with a 2.4 nm band-pass. As with the PCNA binding assay, three measurements were taken: buffer, free PCNA, and RFC. To generate the data points, the intensities at 517 nm were used. The intensities were corrected for dilution factor and the buffer background intensity was subtracted from the free PCNA and RFC intensities. The RFC intensity was divided by the free PCNA intensity to give relative opening intensity. The $K_d$ was calculated using Equation 2-3, with PCNA-AF488 concentration in place of DNA concentration.

## Fluorescence-Based Pre-Steady State Kinetic Assays

Pre-steady state reactions were measured using an Applied Photophysics SX20 MV stopped-flow spectrophotometer. All reactions were performed at 20°C. This device rapidly mixes solutions together to begin measuring fluorescence intensity on a millisecond timescale. All reactions were performed in sequential mixing mode, where clamp, clamp loader, and ATP were mixed together for 1 – 4 seconds to allow for ATP•clamp loader•clamp complex formation. This solution was mixed with syringe 3 containing DNA and ATP (Figure 2-4). For clamp closing and release assays, unlabeled clamp was included in syringe 3 to limit the fluorescent reaction to one turnover. Representative traces presented were normalized so that the fluorescence intensity changes from 1 to 0. For ATP hydrolysis assays, PBP-MDCC and ATPγS were included in syringe 3 and unlabeled β was used in place of the labeled β clamps (Figure 2-5).

KaleidaGraph was used to analyze data and calculate observed rates from the raw data.

**β closing reactions**

To measure β closing, β-AF488 was used. β closing reactions were excited at 490 nm and emission was measured with a 515 nm cut-on filter. Observed closing rates were calculated from raw data using an exponential decay equation shown in Equation 2-4, where a is the amplitude, $k_{obs}$ is the observed rate constant, t is time, and c is a constant.

$$y = a(e^{-k_{obs}t}) + c \tag{2-4}$$

**β release reactions**

Two assays were used to measure β release. The first assay uses the β-PY mutant described above. PY was excited at 345 nm and emission was measured using a 365 nm cut-on filter. Observed β-PY release rates were calculated from raw data using a double exponential decay equation shown in Equation 2-5.

$$y = a_{fast}\left(e^{-k_{fast}t}\right) + a_{slow}(e^{-k_{slow}t}) + c \tag{2-5}$$

The second assay used to measure β release was a FRET-based assay, where the δ' subunit of γ complex is labeled with AF488, and β is labeled with the non-fluorescent quencher QSY9 (73). AF488 was excited at 490 nm and emission was measured with a 515 nm cut-on filter. Observed rates were calculated from raw data using a double exponential increase equation shown in Equation 2-6.

$$y = a_{fast}\left(1 - e^{-k_{fast}t}\right) + a_{slow}(1 - e^{-k_{slow}t}) + c \tag{2-6}$$

**ATP hydrolysis assay**

ATP hydrolysis was measured using phosphate-binding protein (PBP) labeled with MDCC. All solutions contained 168 μM 7-methyl guanosine (MeG-Santa Cruz) and 0.2 U/mL polynucleotide phosphorylase (PNPase-Sigma). PNPase catalyzes the addition of $P_i$ to the MeG, thus removing free $P_i$ from the buffers and reagents before the ATP hydrolysis reaction is initiated. Solutions with MeG and PNPase were incubated at room temperature for 45 min to allow for complete removal of free $P_i$. The stopped-flow was also incubated with buffer containing MeG and PNPase for 45 min to remove $P_i$ present in the instrument. MDCC was excited at 425 nm and emission was measured with a 455 nm cut-on filter.

**PCNA closing assay**

PCNA closing was measured using the PCNA-AF488 mutant described above. AF488 was excited at 490 nm and emission was measured using a 515 nm cut-on filter. Observed rates for the closing time courses were calculated using a double exponential decrease equation shown in Equation 2-5.

**PCNA release**

PCNA release was measured using the PCNA-MDCC mutant described above. MDCC was excited at 425 nm and emission was measured with a 455nm cut-on filter. Observed rates for the release time courses were calculated using a double exponential decrease equation shown in Equation 2-5.

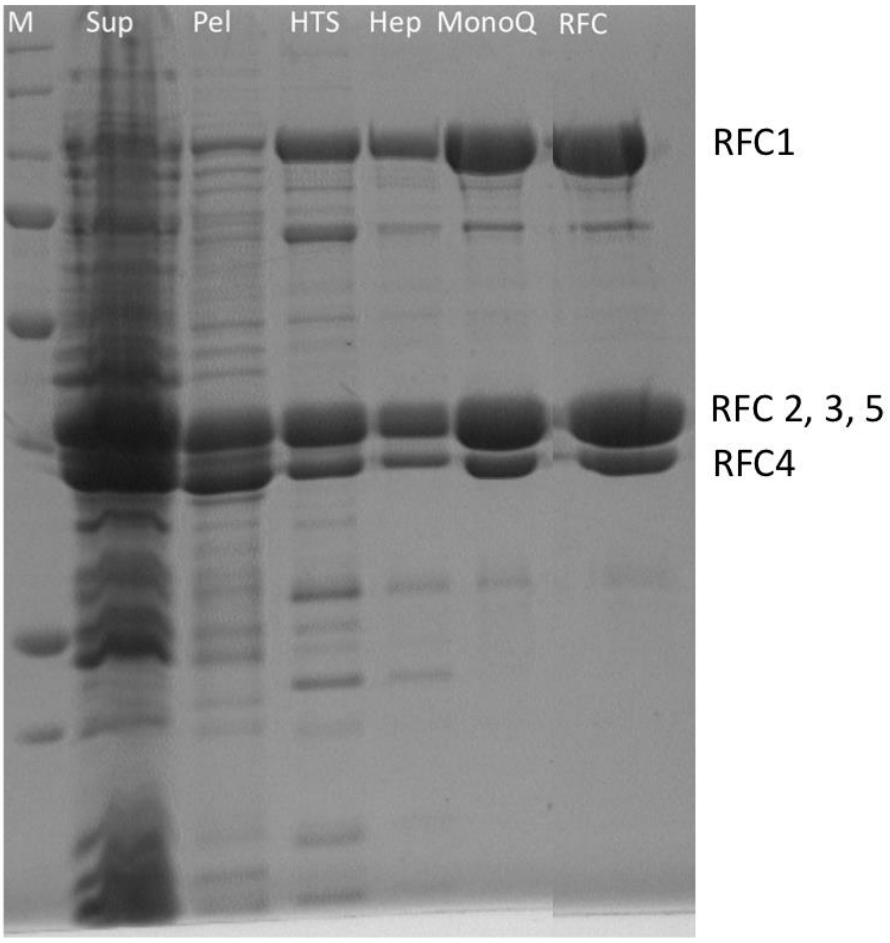


Figure 2-1. SDS PAGE gel showing flRFC after each purification step. The first lane on the left (M) is unstained protein molecular weight marker (BioRad). The second column (Sup) is the soluble protein supernatant after the lysate was spun, while the next column (Pel) shows the insoluble pellet. The next three lanes represent flRFC after purification on the HiTrap SP (HTS), the HiTrap heparin (Hep) and the MonoQ. The last lane shows final dialyzed flRFC product (RFC).

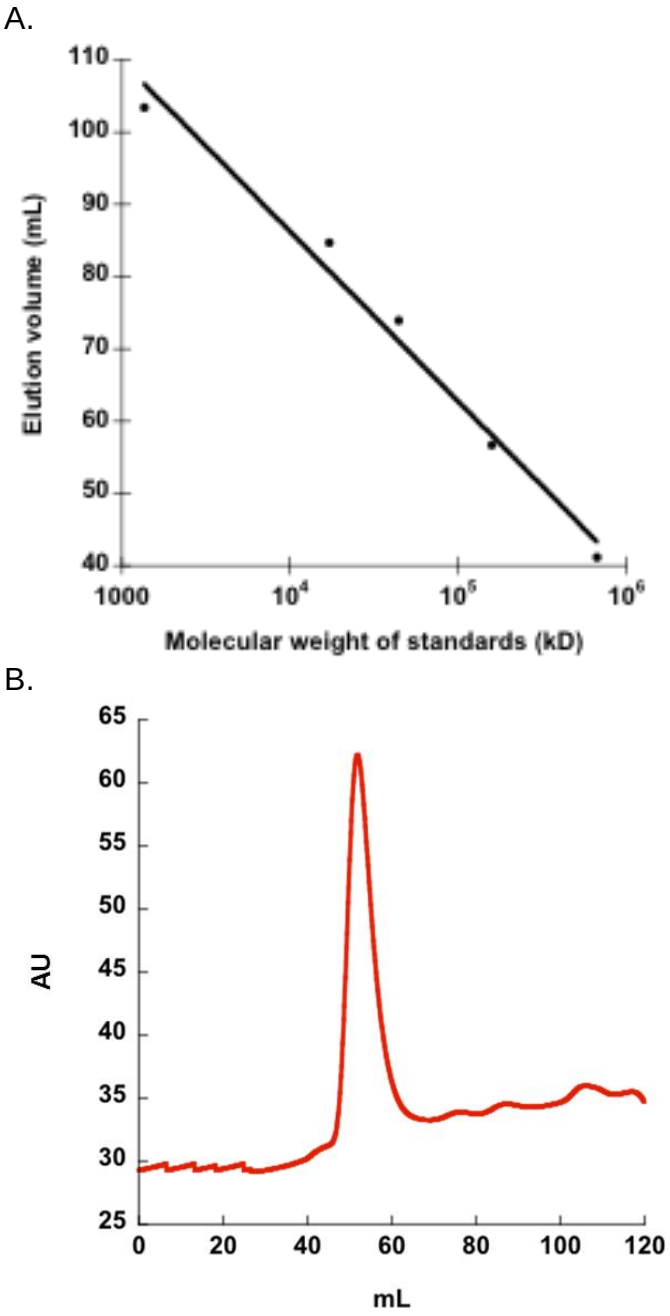


Figure 2-2. Size exclusion of flRFC. Panel A shows molecular weight standards run on the Superdex size exclusion column. The elution volume of each standard is plotted as a function of the log of protein standard mass. The points were fit resulting in the following equation: $y = 190.29 - 23.511\log(x)$. Panel B shows the size exclusion elution profile of flRFC. The major peak eluted at 52 mL, which based on the equation from A corresponds to 290 kD.

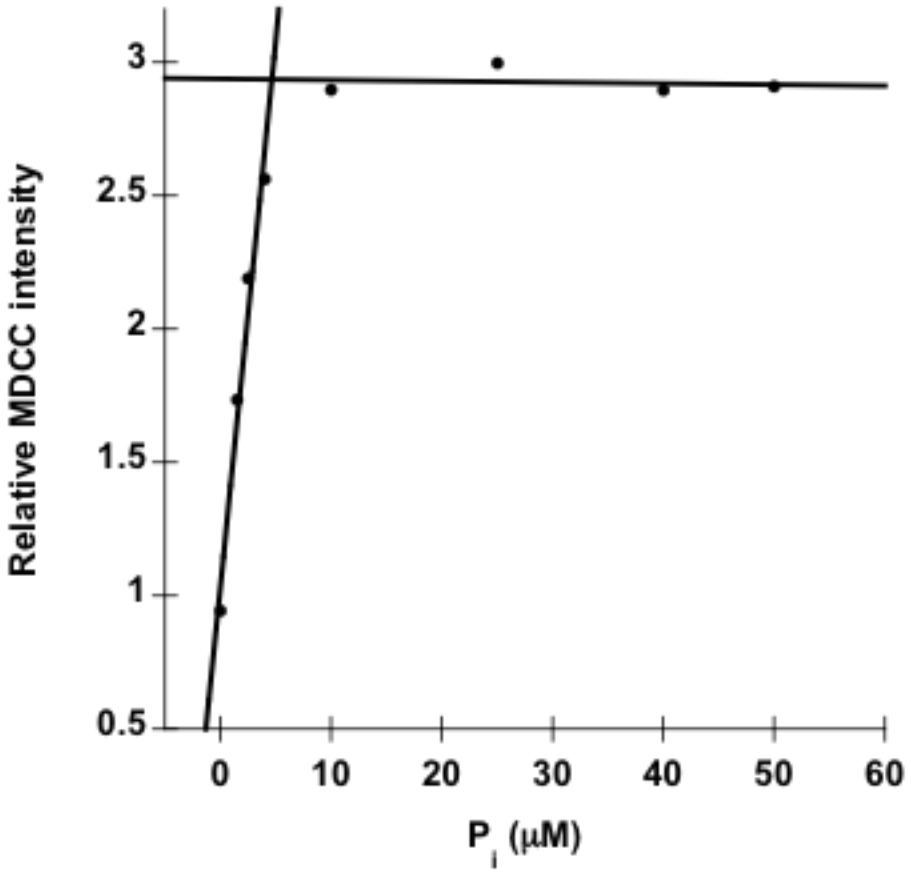


Figure 2-3. Titration of $P_i$ to determine the active concentration of PBP-MDCC: The relative intensity of PBP-MDCC is plotted as a function of $P_i$ concentration. The first half of the data where the $P_i$ concentration is not saturating PBP-MDCC, and the second half of the data where the $P_i$ concentration is saturating were individually fit to lines via linear regression. Because $P_i$ binds PBP-MDCC in a 1:1 ratio, the intersection of these lines indicates the concentration at which $P_i$ is saturating, and therefore the concentration of active PBP-MDCC.

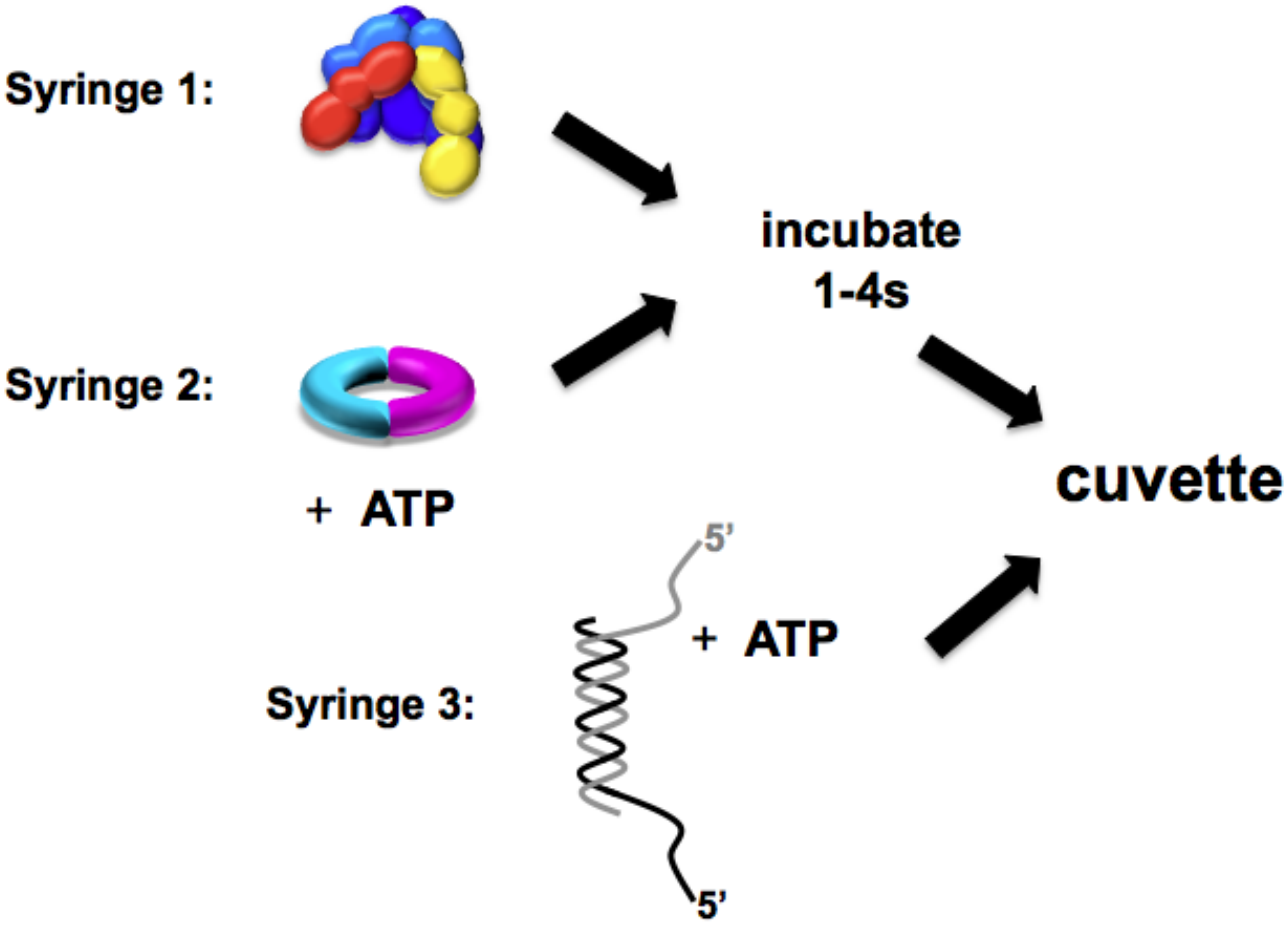


Figure 2-4. The mixing scheme for pre-steady state clamp loading assays. Syringe 1 and 2 mix and incubate for 4 s. This allows the clamp loader to form a complex with ATP and the clamp. This solution is mixed with the contents of syringe 3 as the solutions enter the cuvette.

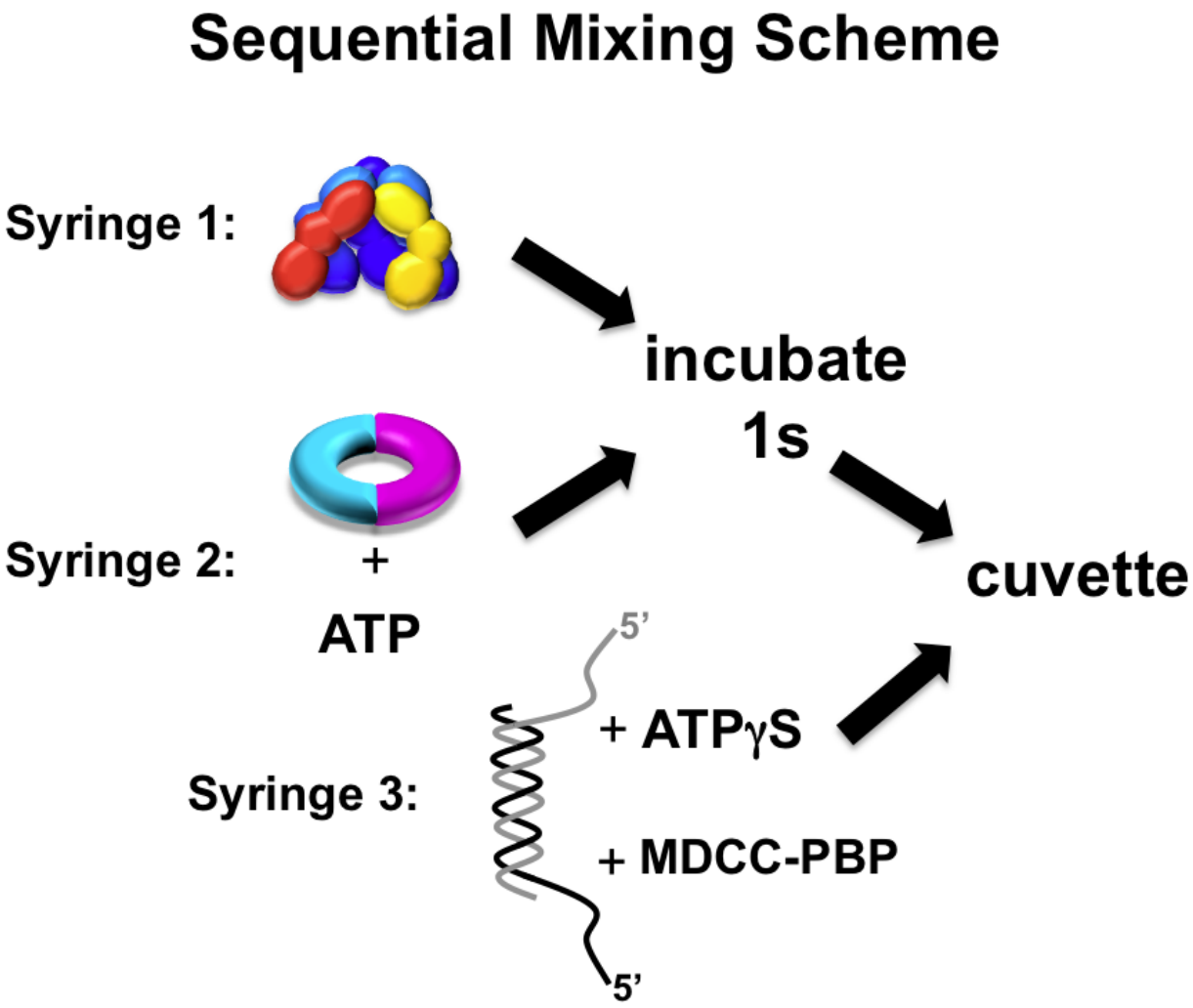


Figure 2-5. The mixing scheme for pre-steady state ATPase assays. Syringe 1 and 2 mix and incubate for 1 s. This allows the clamp loader to form a complex with ATP and the clamp. This solution is mixed with the contents of syringe 3 as the solutions enter the cuvette.

Table 2-1. DNA sequences for DNA-RhX anisotropy assays

| Oligo | Sequence | Use |
|---|---|---|
| **pIIIp2** | ACACGACCAGTAATAAAAGGGACATTCTGG | Pairs with pIIItI-60-RhX to make 3'DNA-RhX structure |
| **pIIItI-60-RhX** | T***t***CAGGTCAGAAGGGTTCTATCTCTGTTGGC CAGAATGTCCCTTTTATTACTGGTCGTGT | Pairs with pIIIp2 to make 3'DNA-RhX structure |
| **JH1-RhX** | TTCAGGTCAGAAGGGTTCTATCTCTGTTGG CCAGAAGTCCCTTTTATTACTGGTCG***t***CT | Pairs with JH2 to make 5'DNA-RhX structure and JH3 to make blunt structure |
| **JH2** | CCAACAGAGATAGAACCCTTCTGACCTGAA | Pairs with JH1-RhX to make 5'DNA-RhX structure |
| **JH3** | ACACGACCAGTAATAAAAGGGACATTCTGG CCAACAGAGATAGAACCCTTCTGACCTGAA | Pairs with JH1-RhX to make blunt-RhX structure |

***t*** denotes a dT with a C6 amino modifier used to label DNA with RhX.

Table 2-2 DNA sequences for symmetrical overhang substrates.

| Oligo | Sequence | Use |
|---|---|---|
| pIIIpI | ACGACCAGTAATAAAAGGGACATTCTGGCC | pIIIpI and JH4 pair to make 0nt blunt structure |
| JH4 | GGCCAGAATGTCCCTTTTATTACTGGTCGT | |
| JH5 | GTCACACGACCAGTAATAAAAGGGACATTCTGGCC | JH5 and JH6 pair to make 5nt structure |
| JH6 | CTGTTGGCCAGAATGTCCCTTTTATTACTGGTCGT | |
| JH7 | CACCAGTCACACGACCAGTAATAAAAGGGACATTCTGGCC | JH7 and JH8 pair to make 10nt structure |
| JH8 | TATCTCTGTTGGCCAGAATGTCCCTTTTATTACTGGTCGT | |
| JH9 | ATTATTTACATTGGCAGATTCACCAGTCACACGACCAGTAATAAAAGGGACATTCTGGCC | JH9 and JH10 pair to make 30nt 3'DNA (JH10 also pairs with JH15 to make 5'DNA) |
| JH10 | CTTTCAGGTCAGAAGGGTTCTATCTCTGTTGGCCAGAATGTCCCTTTTATTACTGGTCGT | |
| JH11 | CACACGACCAGTAATAAAAGGGACATTCTGGCC | JH11 and JH12 pair to make 3nt structure |
| JH12 | GTTGGCCAGAATGTCCCTTTTATTACTGGTCGT | |
| JH13 | CACGACCAGT AATAAAAGGGACATTCTGGCC | JH13 and JH14 pair to make 1nt structure |
| JH14 | TGGCCAGAATGTCCCTTTTATTACTGGTCGT | |
| JH15 | AACAGAGATAGAACCCTTCTGACCTGAAAGCGTAAGAATACGTGGCACAGACAATAGTCA | Pair with JH10 to make 5'DNA structure |

# CHAPTER 3
# TEMPORAL CORRELATION OF ATP HYDROLYSIS, CLAMP CLOSING, AND CLAMP RELEASE BY *E. COLI* AND *S. CEREVISIAE* CLAMP LOADERS

## Background

Clamp loaders are fine-tuned machines that catalyze the loading of sliding clamps around DNA for various metabolic processes. The clamp loaders use ATP binding and hydrolysis to drive conformational changes that allow the clamp loader to have high affinity for the sliding clamp and DNA to bring the two macromolecules together, but then must decrease the affinity for these macromolecules to release the clamp•DNA (Reviewed in (127)). For DNA replication, a new sliding clamp is needed every 2 – 3 seconds, one for each Okazaki fragment, so clamp loaders must have an efficient method for completing these steps to keep pace with the replication fork. Any perturbation in clamp loading may result in replication fork collapse and could lead to DNA damage and inaccurate transmission of genetic information to the next generation.

The clamp loading reaction for both γ complex and RFC have the same basic characteristics. Both enzymes are members of the $AAA^+$ ATPase family, characterized by the use of ATP binding and hydrolysis to drive conformational changes that rearrange macromolecules (reviewed in (62, 127)). γ complex binds and hydrolyzes three ATP molecules, one for each γ subunit (48-50, 73). RFC can bind five molecules of ATP, but only hydrolyzes four, one in each of the Rfc1-4 subunits (63, 72). ATP binding is required for both clamp loaders to bind the clamps and DNA (63-68). DNA binding triggers ATP hydrolysis and results in release of the clamp around DNA (66, 70-72). This is summarized in Figure 1-3.

Although the general mechanism has been elucidated, there are intermediary steps in which the order of events are not yet clear. For example, it is not yet known if the clamp loaders close the sliding clamps around DNA before releasing the clamp•DNA complex, or if they simply release the sliding clamps to "snap shut" on their own. It also is not clear if hydrolysis of the individual ATP molecules results in conformational changes associated with individual steps, or if ATP hydrolysis occurs in an all-or-none fashion before the subsequent step can occur. To address the timing of these steps, pre-steady state fluorescence-based assays were used to report on ATP hydrolysis, clamp closing, and clamp release. The timing of these events was compared to determine the order of events.

## Temporal Correlation of *E. coli* Clamp Loading Events

### β closing and release

To determine the relative timing of β closing and release, fluorescence-based assays were used to report on these aspects of the clamp loading cycle. Clamp closing was measured using a β-clamp labeled on each monomer at the interface with Alexa Fluor 488 (AF488). When β-AF488 is open, the AF488 fluorophores are far enough apart that there is no interaction between them, and they fluoresce. When the clamp closes, the fluorophores return to a position in which they are close enough to self-quench, decreasing the signal (69). Clamp release was measured using a clamp labeled with pyrene (PY) on the surface to which the clamp loader binds. When β-PY is bound by γ complex, PY is about two times more fluorescent than when the clamp is released and unbound (120). Clamp loading reactions were initiated by adding a solution of γ complex, labeled β, and ATP to a solution of DNA, ATP, and 10-fold excess

unlabeled β (Figure 2-4). The unlabeled β limited the monitored reactions to a single-turnover. Experiments were performed three separate times, and a representative time course for β closing is shown in Figure 3-1 (green trace).

In the first approximately 40 ms of each β closing time course (green), there is a small increase in fluorescence (see Figure 3-7 for an expanded time scale). This small increase is caused by a dilution effect as the preformed γ complex•β is diluted 2-fold with the contents of syringe 3. Stopped-flow controls were performed in which a solution of γ complex•β was mixed with buffer (Figure 3-2 A) and where γ complex•β was mixed with another syringe containing an equal concentration of γ complex•β (Figure 3-2 B). In the first case, γ complex•β is diluted with buffer, and the small increase is visible. In the second case, γ complex•β is not diluted, it is simply mixed with itself, and no small increase is visible. Because a unique fit to the rate of the small rise was difficult to obtain, the β closing time course was fit to a single exponential decay (Equation 2-4) to calculate an observed rate of closing. The average rate calculated from three separate closing reactions was 6.2 ± 1.3 $s^{-1}$.

Time courses for β release were biphasic decreases in PY fluorescence (Figure 3-1, blue trace). This biphasic decrease is consistent with previous equilibrium binding studies that show the fluorescence of PY is sensitive to the γ complex• β conformation. In the absence of ATP, γ complex can bind but not open β (65, 66, 69). This bound but closed conformation of γ complex•β results in a lower level of PY fluorescence than a bound and open conformation (69). Therefore, the initial decrease in fluorescence represents the conformational change in the γ complex•β associated with β closing and the second rate represents β release. The biphasic decrease likely does not represent

two populations of γ complex•β releasing at different rates, as the rates and amplitudes of each phase are consistent from multiple preparations of β complex as well as multiple concentrations of DNA. Also, the β closing reactions show no indication of two populations of γ complex•β closing at different rates. Fits of the data to a double exponential decay (Equation 2-5) gave an initial rate of 6.3 ± 0.3 $s^{-1}$, and a second rate of 0.85 ± 0.04 $s^{-1}$. The rapid rate of 6.3 $s^{-1}$ is the same as the observed rate determined in β-AF488 closing assays, which supports the interpretation that this rapid decrease in fluorescence reflects β closing. The slower rate of 0.85 $s^{-1}$ then reflects the rate of β release by the clamp loader.

An alternative interpretation of the biphasic nature of the β-PY release traces is that the first rate reflects β-PY release, and the second rate reflects loss of the interaction between β-PY and DNA as the clamp slides off the short linear substrates. To test this possibility, two experiments were performed. In the first experiment, β closing and release were measured on p/t-DNA bound by SSB to block the ends and prevent β from sliding off the DNA. *In vitro* DNA replication assays demonstrated that a single-stranded DNA overhang of 25-nt is of sufficient length to bind SSB and stabilize β on DNA to form a pre-initiation complex to which the core polymerase can bind (128). In assays with SSB coated p/t-DNA, the decrease in PY fluorescence remained biphasic (Figure 3-3). Moreover, the calculated rates measured in the β-AF488 and β-PY assay were about the same as measured in the absence of SSB (Table 1), indicating protein•protein interactions with SSB via the χ subunit (52, 53) of the γ complex have little influence the rates of β closing and release. If the slower rate measured in the β-PY

assay had corresponded to β-PY sliding off DNA, this rate should have decreased in assays with SSB.

The second experiment used an alternative FRET-based assay to measure β release. In this assay, the δ' subunit of γ complex is labeled with a fluorescent AF488 donor, and the β clamp is labeled with the non-fluorescent QSY9 quencher (73). When β-QSY9 is bound to γ complex-AF488, the quencher is in proximity to the AF488 fluorophore, so the fluorescent signal is quenched. When the clamp is released, the QSY9 is no longer close enough to quench the AF488 signal. This assay was performed with a similar mixing scheme as above (Figure 2-4), with γ complex-AF488 incubated with β-QSY9 for 4 s before the addition of DNA and excess unlabeled β. Time courses for this reaction were also biphasic, with an initial calculated rate of 4.1 ± 0.2 $s^{-1}$ and a second calculated rate of 0.82 ± 0.06 $s^{-1}$ (Figure 3-4). The slow rate calculated from the FRET assay time courses matches the second rate calculated from the β-PY assay. Because β-QSY9 is not fluorescent, interactions with DNA cannot be responsible for the biphasic rates. Therefore, the rapid decrease in fluorescence in β-PY assays most likely reflects β closing and the slow decrease reflects β release.

**DNA-dependent ATP hydrolysis is required for β closing before release**

Clamps can dissociate from the γ complex by two mechanisms, a productive clamp loading reaction in which β is released on DNA, and a passive dissociation reaction reflecting the equilibrium interaction between β and the γ complex. In the absence of DNA, passive dissociation is the only mechanism by which β can dissociate from the γ complex. To determine if β closing is also faster than β release when the

clamp passively dissociates from the clamp loader, closing and release assays were performed in the absence of DNA (Figure 3-5 A). To determine if DNA binding alone is required to activate clamp closing prior to release or whether ATP hydrolysis is also required, closing and release were measured in assays in which the non-hydrolyzable analog, ATPγS, was substituted for ATP (Figure 3-5 B).

When DNA is omitted, both the closing and release rates are much slower than for a productive clamp loading reaction on DNA; the closing rate is about 200 times slower in assays without DNA (Table 3-1). Interestingly, the clamp release trace was no longer biphasic and could be fit by a single rate. In addition, rates calculated for β closing and release in the absence of DNA are within standard deviation of one another, indicating clamp closing is not faster than release in the passive dissociation reaction. Clamp closing and release may be simultaneous, or more likely the clamp may close rapidly on its own after dissociation from the γ complex.

Time courses for reactions with ATPγS were similar to time courses for reactions lacking DNA (Figure 3-5 B). Calculated rates for clamp closing and release were about the same in reactions with ATPγS as in reactions lacking DNA (Table 3-1). As with reactions lacking DNA, the calculated rate of clamp closing was the same as the rate of clamp release. Most likely, clamp closing and release occur via a passive dissociation mechanism rather than an active clamp loading mechanism in reactions with ATPγS (129).

These data show that DNA dependent ATP hydrolysis promotes β closing prior to β release. Given that DNA binding is a bimolecular reaction, the rates of clamp closing and release may increase with increasing DNA concentrations. To determine how

clamp closing and release rates are influenced by DNA concentration, both reactions were measured at DNA concentrations of 20, 40, and 100 nM (Figure 3-6). Increasing the DNA concentration had no effect on time courses for clamp closing (A) or release (B). This indicates that these steps must be limited by the rate of some intramolecular reaction such as a DNA-induced conformational change in the clamp loader•clamp complex or ATP hydrolysis.

Together, these data show that DNA-dependent ATP hydrolysis is required for the γ complex to close β before releasing it. It also shows that the rate of clamp closing and release is limited by an intramolecular reaction in the ternary clamp loader•clamp•DNA complex. When DNA is omitted from the reactions or ATPγS is present, the observed β closing and release rates are slower than when DNA is present and occur at the same rates.

**The relative timing of β closing and ATP hydrolysis**

A fluorescent ATPase assay was used to measure the timing of ATP hydrolysis relative to β closing. ATP hydrolysis is measured using phosphate-binding protein (PBP) labeled with MDCC, which increases in fluorescence when the inorganic phosphate ($P_i$) product of ATP hydrolysis binds to MDCC-PBP (126, 130). ATPase assays were performed using a sequential mixing scheme in which a solution of γ complex and a solution of β and ATP were incubated for 1 s before mixing with a syringe containing DNA, PBP-MDCC, and excess ATPγS (Figure 2-5). ATP hydrolysis reactions were limited to a single turnover by the addition of non-hydrolyzable ATPγS. Final concentrations were 200 nM γ complex, 200 nM β, 400 nM DNA, 200 μM ATP, 2 mM ATPγS, and 2 μM PBP. Clamp closing assays were done using identical concentrations

except that 200 nM β-AF488 and 2 μM unlabeled β were used instead of PBP-MDCC and ATPγS. Figure 3-7 shows the time course for ATP hydrolysis by γ complex (blue) overlaid on a time course for β closing (green). A burst of ATP hydrolysis is complete in just over 0.1 s whereas the decrease in β-AF488 fluorescence is only about 20% complete in the same time showing that ATP is hydrolyzed before the clamp closes.

The γ complex contains three active ATP sites, one in each γ subunit, and can hydrolyze up to three molecules of ATP. Based on the amplitude of the burst of ATP hydrolysis, 1.5 – 1.7 molecules of $P_i$ per γ complex were released in the rapid burst. Previous work has shown that the γ complex binds three molecules of ATP (50) and all ATP sites hydrolyze ATP within this burst phase (48, 49, 131). It is not clear why our burst amplitudes correspond to fewer than three molecules of ATP, but this was observed in multiple preparations of γ complex. Possibilities include that some of the sites exchange ATP for ATPγS faster than ATP is hydrolyzed, a fraction of our clamp loaders or ATP sites are not active for hydrolysis, or the last inorganic phosphate molecule is released too slowly to be seen in our assay. Any molecules of ATP hydrolyzed after clamp closing would have given rise to a phase of ATP hydrolysis limited by the slower 6 $s^{-1}$ closing rate. Regardless of the number of ATP molecules hydrolyzed, the important point here is that ATP is hydrolyzed prior to clamp closing by at least two of the ATP sites.

## Temporal Correlation of *S. cerevisiae* PCNA Closing and Release

### PCNA closing and release

To determine the relative timing of PCNA closing and release, the fluorescence-based assays described above for γ complex and β were adapted for *S. cerevisiae* RFC

and PCNA. PCNA closing was measured using a PCNA clamp labeled with AF488 on either end of the interfaces. When PCNA-AF488 is closed, the fluorophores self-quench, but when the clamp is open, the fluorophores move apart and relieve the self-quench (46). PCNA release was measured using a PCNA clamp labeled with MDCC on the surface to which RFC binds. When RFC binds PCNA-MDCC, the fluorescence is about 2-fold higher than when the clamp is free (Marzahn in preparation). As with the $\gamma$ complex and $\beta$ reactions above, reactions were performed in the stopped-flow to measure the first few seconds of the reaction using the mixing scheme outlined in Figure 2-4. RFC, fluorescent PCNA, and ATP were incubated for 4 s before mixing with a solution of DNA, ATP, and 10-fold excess unlabeled PCNA. Unlabeled PCNA was included as a trap, limiting the fluorescent reaction to one turnover. RFC used in these experiments contained a truncation of the first 282 amino acids in the Rfc1 subunit. Experiments were performed three independent times and representative time courses for PCNA closing (green) and PCNA release (blue) are shown in Figure 3-8.

Calculated observed rates for both time courses were obtained by fitting to a double exponential decay (Equation 2-4). The average calculated rate for PCNA closing was 3.5 ± 0.32 $s^{-1}$ and 0.09 ± 0.05 $s^{-1}$. The average calculated rate for PCNA release was 0.37 ± 0.06 $s^{-1}$ and 0.09 ± 0.03 $s^{-1}$. The biphasic nature of these time courses supports previous work suggesting that two populations of RFC•PCNA form and are loaded at different rates. The first set of calculated observed rates for closing and release represents a population of RFC•PCNA loaded in an active, ATP hydrolysis dependent manner. The second set of observed closing and release rates represents a population RFC•PCNA loaded in a passive, ATP hydrolysis independent manner (45).

The slow closing and release rates are within standard deviation of the rates calculated for closing and release in the absence of DNA dependent ATP hydrolysis (see below, Table 3-2), therefore, this second slower rate likely represents passive release of a subset of RFC•PCNA complexes. The first observed rate for PCNA closing, representing an active clamp closing reaction, is 10-fold higher than the first observed rate for PCNA release. Based on these data, PCNA closing occurs before release, as seen with the *E. coli* sliding clamp and clamp loader.

**DNA dependent ATP hydrolysis is required for PCNA closing before release**

As with β and γ complex, PCNA can dissociate passively from RFC in the absence of DNA. To determine if PCNA is closed before released during passive dissociation, PCNA closing and release reactions were measured in the absence of DNA. The observed rates for passive closing and release were calculated using a single exponential decay (Equation 2-3) and are listed in Table 3-2. As with β and γ complex, the observed rates of passive PCNA closing and release are slower without DNA and are now within standard deviation of one another. Therefore, DNA is required to promote PCNA closing before release. However, DNA binding alone is not sufficient to support PCNA closing before release. Reactions with the non-hydrolyzable ATP analog, ATPγS, in place of ATP yielded calculated observed rates similar to reactions without DNA (Table 3-2). This indicates DNA-dependent ATP hydrolysis is required to observe the mechanism of PCNA closing before release.

The DNA concentration dependence of PCNA closing and release were tested to determine if the bimolecular reaction of RFC•PCNA binding to DNA affects the rates of closing and release. DNA concentrations of 20 nM, 40 nM, and 100 nM were used in

closing and release reactions, but the changes in DNA concentration had no effect on the PCNA closing and release time courses (Figure 3-9). Thus, like γ complex and β, the rate of PCNA closing and release is restricted by an intramolecular reaction in the RFC•PCNA•DNA complex.

## Conclusions

These data show that clamp loaders from both *E. coli* and *S. cerevisiae* close sliding clamps around DNA before releasing them in a manner reliant on DNA dependent ATP hydrolysis. This is opposed to a mechanism in which the sliding clamps are released first and then allowed to snap shut on their own. This likely serves to prevent DNA from slipping out of an open clamp, resulting in an unsuccessful clamp loading event. In addition, a burst of ATP hydrolysis occurs before β clamp closing in the *E.* coli system. This would indicate that ATP hydrolysis mediated conformational changes are required for clamp closing.

There are several possible mechanisms that would facilitate clamp closing prior to release from the clamp loaders; two possibilities are described below for each clamp loader. The first possibility is that an ATP hydrolysis-induced conformational change in the clamp loader forces the clamp closed. This type of mechanism is supported by molecular dynamics simulations for γ complex and β (132). Simulations indicated that β is held closed under spring tension, which would facilitate clamp opening by the δ subunit of the clamp loader, but would require energy to close the clamp (132, 133). It is possible that there is more effort required for the γ complex to close the β clamp than to open it.

On the other hand, while the δ subunit can open clamps transiently to unload them from DNA (132), the δ subunit alone does not sufficiently stabilize the clamp in an open conformation in solution to produce a measurable population of open clamps; formation of open clamps requires intact clamp loaders (69). Therefore, a second possible mechanism for β closure is that ATP hydrolysis-induced conformational changes in the γ complex remove clamp loader•clamp interactions that stabilize an open conformation of the clamp, without destabilizing the complex enough to promote clamp dissociation. This type of mechanism is supported by the high stability of the closed β conformation and the requirement for binding to the clamp loader to maintain a relatively large fraction of clamps in an open conformation (69).

Molecular dynamics simulations with PCNA do not indicate the presence of spring tension as with β, in fact the authors report little to no energetic barrier required for PCNA to reclose (134). This would indicate a closing mechanism in which conformational changes in RFC destabilize the open PCNA conformation allowing PCNA to close on its own, followed by PCNA release. This is also supported by the high stability of PCNA in the closed conformation.

β release in the absence of DNA or in the presence of ATPγS is 10 – 20 times slower than in the presence of DNA-dependent ATP hydrolysis, while PCNA release is about 5 – 10 times slower. Structural studies with both RFC•PCNA as well as the bacteriophage T4 clamp loader•clamp yield an explanation for this result (55, 88). In these structures, there are fewer contacts with the closed clamp than an open one, decreasing the affinity of the clamp loader for the clamp. Passive dissociation of the

open clamp loader•clamp complex may be slower because it would have to break more contacts to dissociate.

The clamp loading reaction is complex and composed of multiple steps driven by ATP binding and hydrolysis at multiple sites and interactions with two other ligands, the sliding clamp and DNA. These interactions with the clamp, DNA, and ATP likely promote conformational changes in the clamp loader that facilitate the next step in the reaction cycle to generate an ordered clamp loading mechanism that ensures the clamp is loaded quickly, in the correct position, and with as little wasted effort as possible. This type of mechanism could give the clamp loading reaction the efficiency required to keep pace with the moving replication fork.

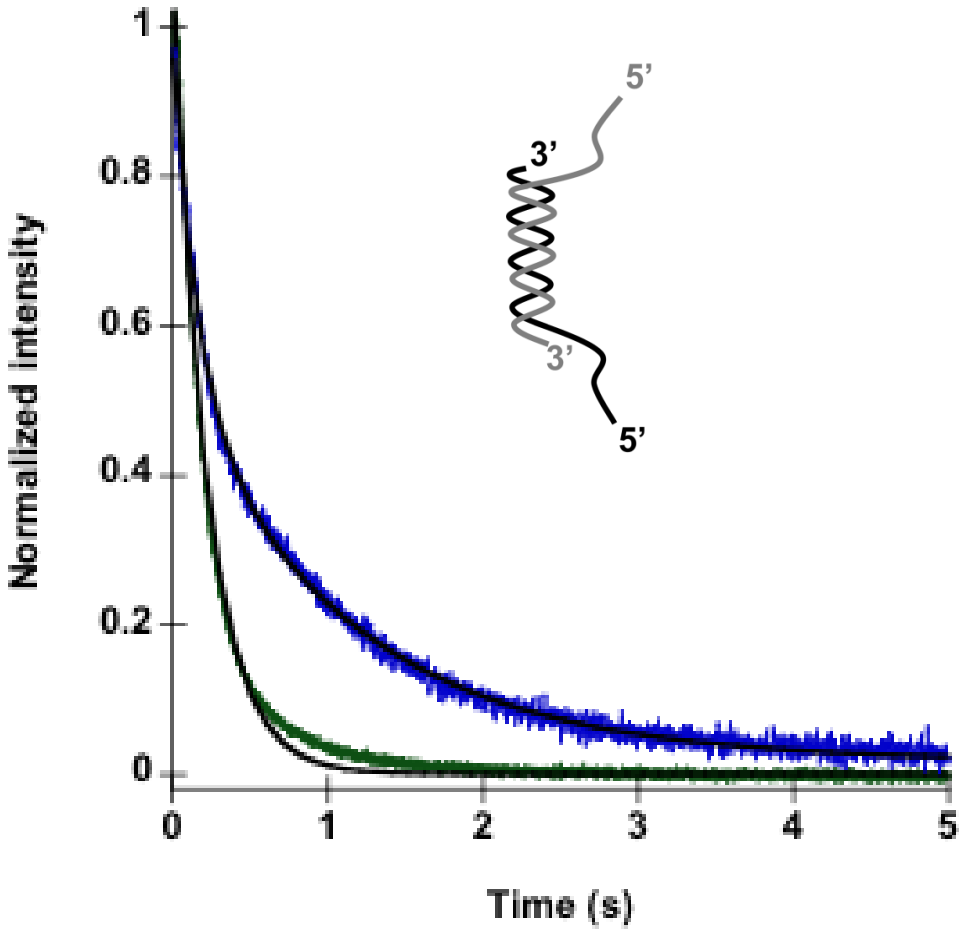


Figure 3-1. β clamps are closed before they are released. Representative time courses for β closing (green) and β release (blue) are shown. Reactions contained 20 nM γ complex, 20 nM fluorescent β, 0.5 mM ATP, 40 nM DNA, and 200 nM unlabeled β.

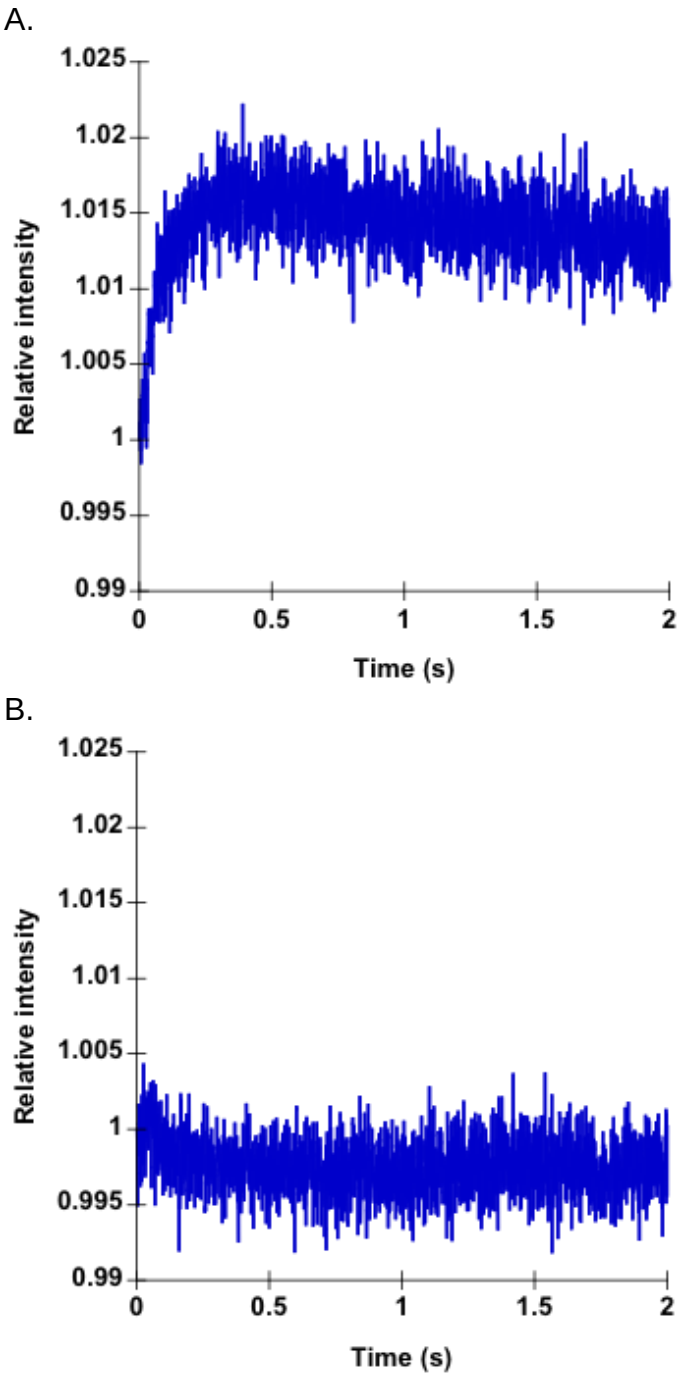


Figure 3-2. The small increase in the beginning of each β closing time course. Shown above in Panel A is a reaction in which a syringe containing 40nM γ complex, 40 nM β-AF488 and 0.5 mM ATP is mixed with a syringe containing buffer. This time course contains a small increase in signal in the first few ms. Shown in Panel B is a reaction in which a syringe containing 40nM γ complex, 40 nM β-AF488 and 0.5 mM ATP was mixed with another syringe containing the same components. In this case, after mixing, the concentration of γ complex, β-AF488 and ATP remained unchanged.

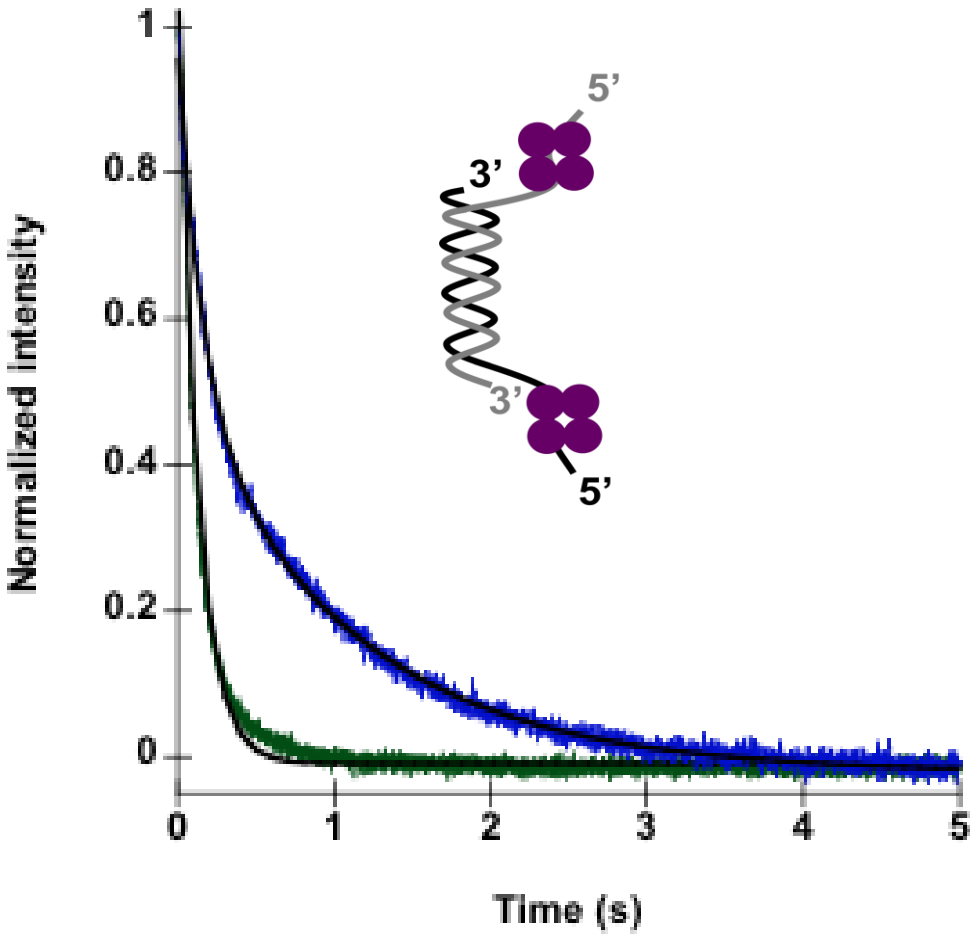


Figure 3-3. β closing and release reactions in the presence of SSB. Closing (green) and release (blue) are unchanged from reactions excluding SSB. Reactions contained 20 nM γ complex, 20 nM fluorescent β, 0.5 mM ATP, 40 nM DNA, 400 nM SSB, and 200 nM unlabeled β.

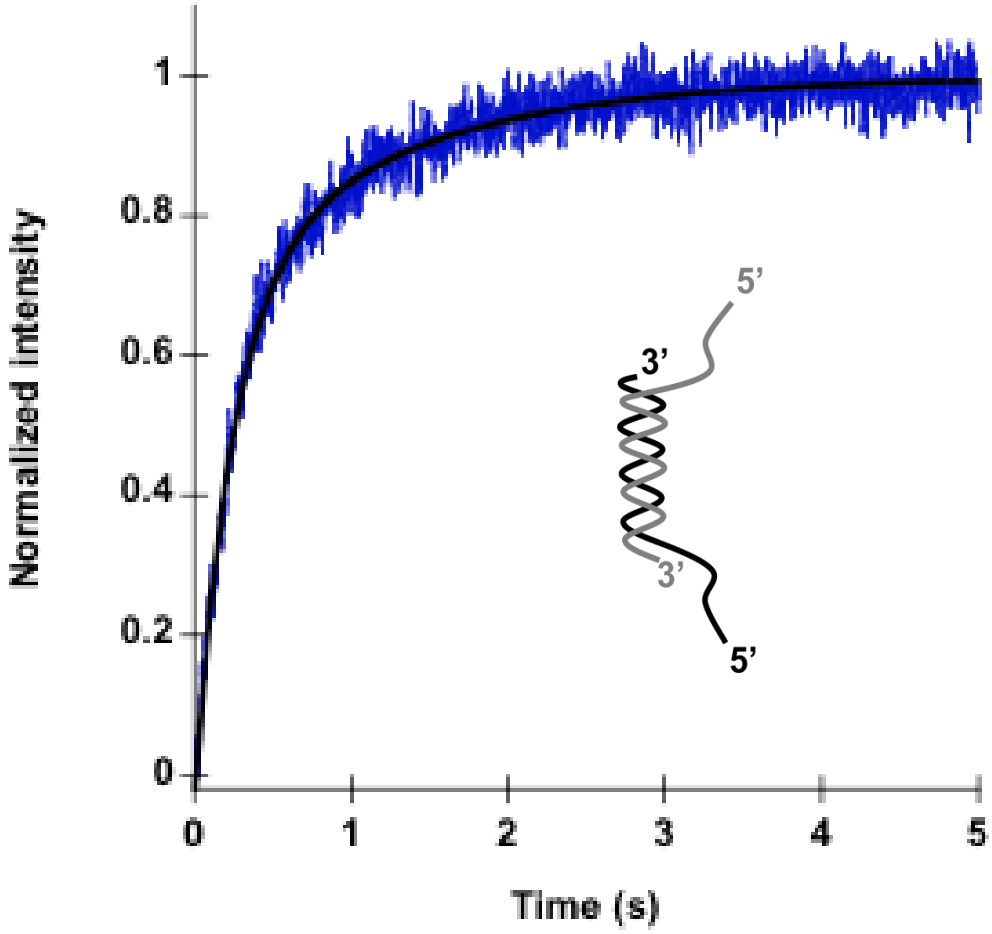


Figure 3-4. β release time course using the alternative FRET-based release assay. Reactions contained 20 nM γ complex-AF488, 20 nM β-QSY9, 40 nM DNA, 0.5 mM ATP and 200 nM unlabeled β. This time course was fit with a double exponential increase (Equation 2-6).

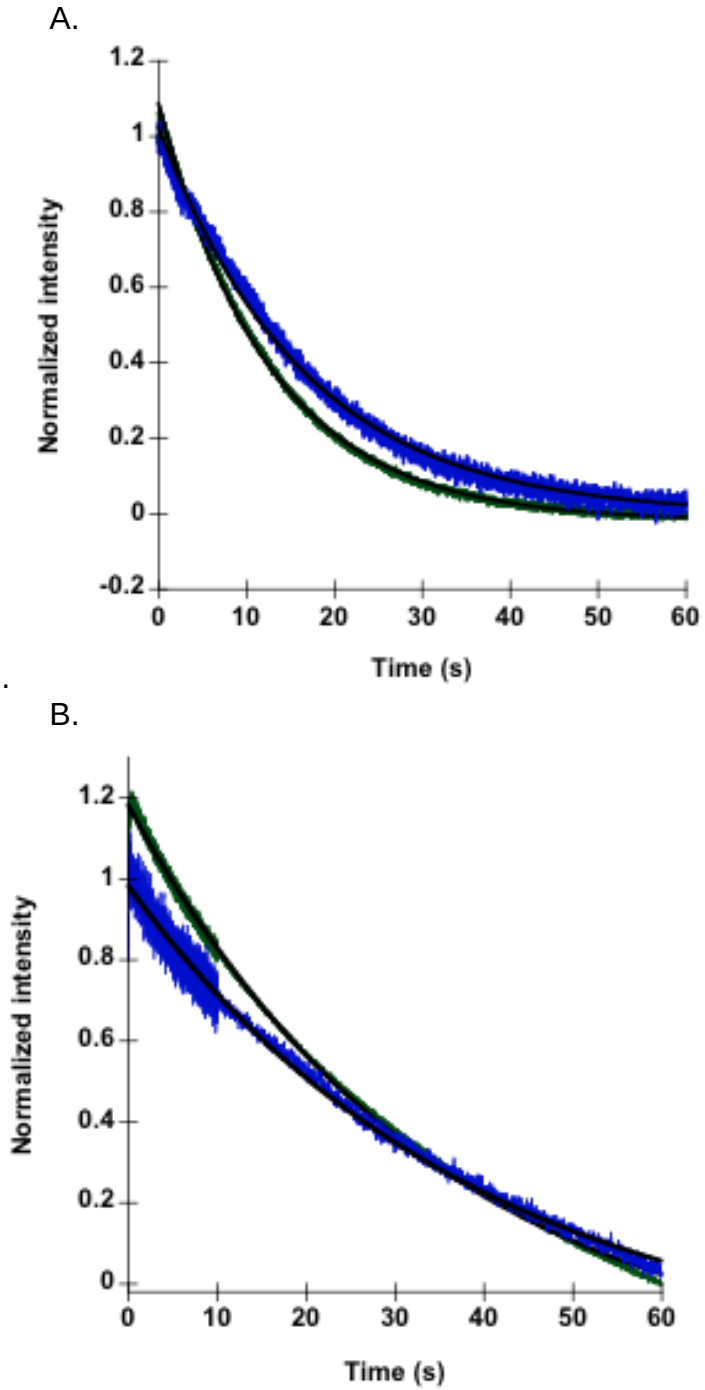


Figure 3-5. Passive β closing and release. Closing (green) and release (blue) time courses are shown for reactions omitting DNA (A) or in the presence of DNA and ATPγS (B). In both reactions, β closes at the same time as it is released, indicating DNA dependent ATP hydrolysis is required to promote β closing prior to β release. Reactions in A contained 20 nM γ complex, 20 nM fluorescent β, 500 μM ATPand 200 nM unlabeled β. Reactions in B contained the same components as A, with the addition of 40 nM DNA and the substitution of ATPγS for ATP.

A.

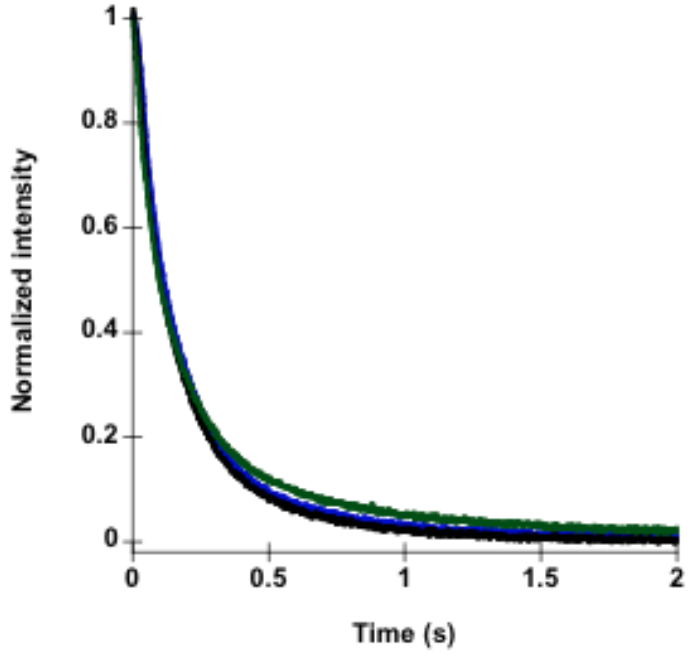


B.

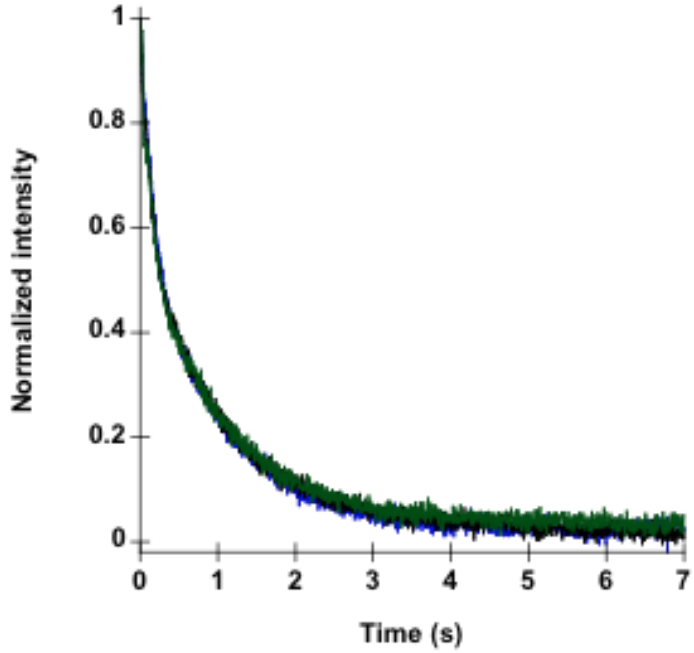


Figure 3-6. β closing and release as a function of DNA concentration. Closing (A) and release (B) was measured as a function of DNA concentration to determine if DNA binding is limiting the rate of these steps. Reactions contained 20 nM γ complex, 20 nM fluorescent β, 0.5 mM ATP and 200 nM unlabeled β with either 20 nM (black), 40 nM (blue) or 100 nM (green) DNA.

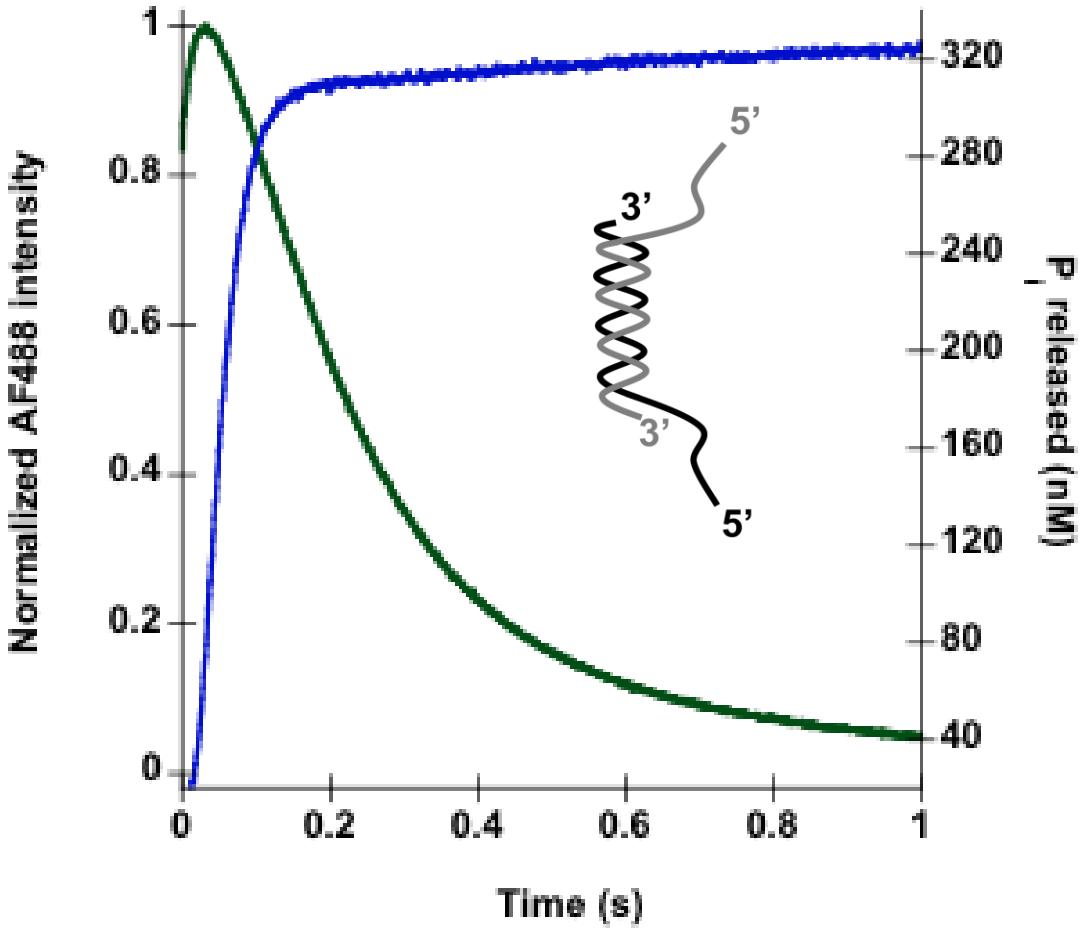


Figure 3-7. The temporal correlation of β closing and ATP hydrolysis. Time courses for β closing (green) and ATP hydrolysis (blue) are shown. The fluorescence of PBP-MDCC was converted to the concentration of $P_i$ released by γ complex during the ATP hydrolysis reaction. β closing reactions contained 200 nM γ complex, 200 nM β-AF488, 400 nM DNA, 0.5 mM ATP, and 200 nM unlabeled β. ATP hydrolysis reactions contained 200 nM γ complex, 200 nM β, 400 nM DNA, 0.2 μM ATP and 2 μM ATPγS and 2 μM PBP-MDCC.

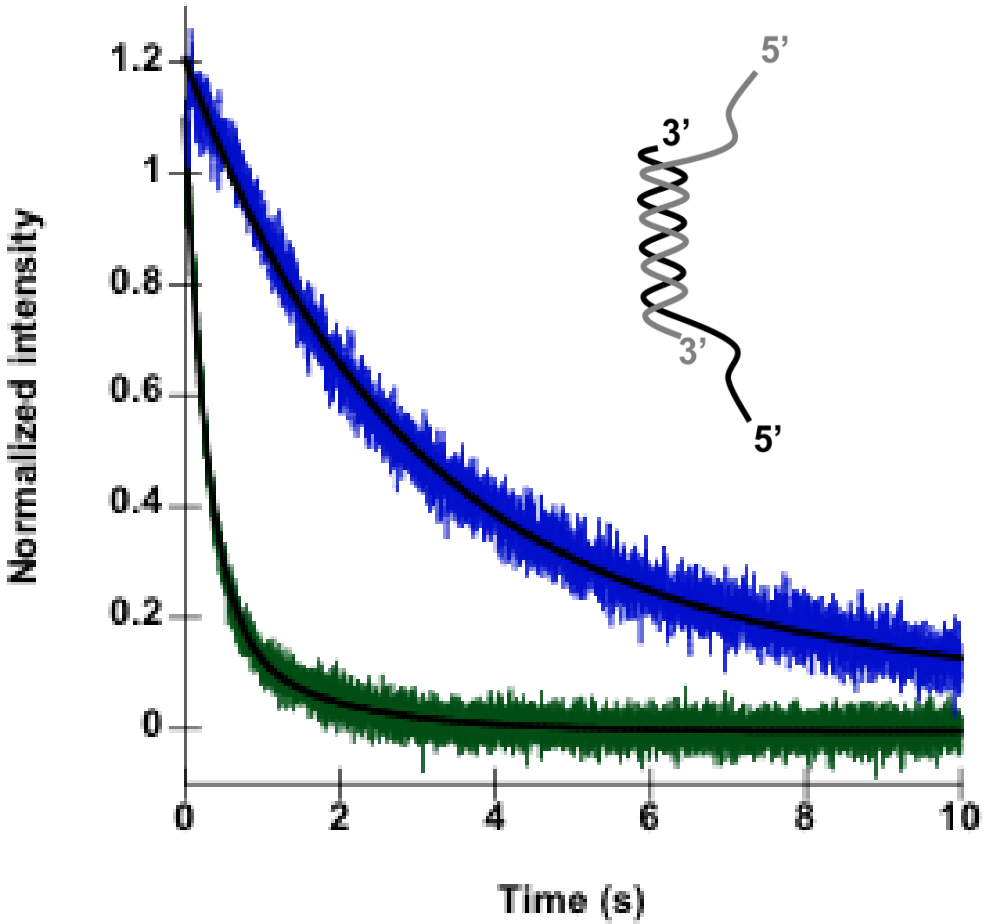


Figure 3-8. PCNA closing is faster than PCNA release. Time courses for PCNA closing (green) and PCNA release (blue) are shown. Reactions contained 20 nM RFC, 20 nM PCNA-AF488, 40 nM DNA, 0.5 mM ATP, and 200 nM unlabeled PCNA as chase.

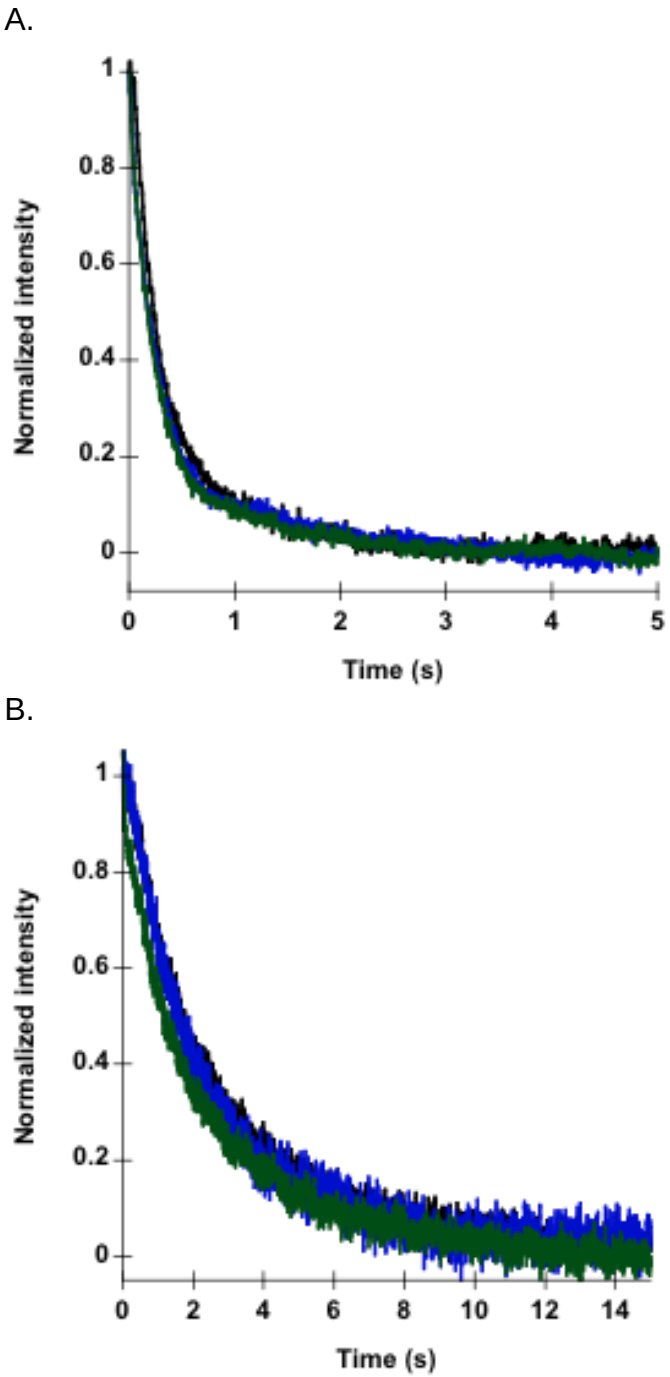


Figure 3-9. PCNA closing as a function of DNA concentration. Representative time courses for PCNA closing (A) and release (B) as a function of DNA concentration are shown. The reaction included 20 nM RFC, 20 nM fluorescent PCNA, 0.5 mM ATP, 200 nM unlabeled PCNA chase, and either 20 nM (black), 40 nM (blue), or 100 nM (green) DNA.

Table 3-1. Calculated observed rates for β closing and release

| **Substrates** | **Closing** | **Release** | |
|---|---|---|---|
| | $k_{obs}$ ($s^{-1}$) | $k_{obs1}$ ($s^{-1}$) | $k_{obs2}$ ($s^{-1}$) |
| p/t DNA | 6.2 ± 1.3 | 6.3 ± 0.3 | 0.85 ± 0.04 |
| p/t DNA + SSB | 8.7 ± 0.6 | 6.2 ± 0.6 | 0.73 ± 0.2 |
| No DNA | 0.03 ± 0.01 | 0.04 ± 0.02 | N/A |
| p/t DNA + ATPγS | 0.08 ± 0.002 | 0.06 ± 0.007 | N/A |

N/A indicates that no $k_{obs2}$ was present for these reactions.

Table 3-2. Calculated observed rates for PCNA closing and release

| **DNA substrate** | **PCNA closing** | | **PCNA release** | |
|---|---|---|---|---|
| | $k_{obs1}$ ($s^{-1}$) | $k_{obs2}$ ($s^{-1}$) | $k_{obs1}$ ($s^{-1}$) | $k_{obs2}$ ($s^{-1}$) |
| **p/t DNA** | 3.5 ± 0.32 | 0.09 ± 0.05 | 0.37 ± 0.06 | 0.09 ± 0.03 |
| **No DNA** | 0.03 ± 0.01 | N/A | 0.07 ± 0.02 | N/A |
| **ATPγS** | 0.05 ± 0.01 | N/A | 0.09 ± 0.03 | N/A |

N/A indicates that no $k_{obs2}$ was present for these reactions.

# CHAPTER 4
# THE CONTRIBUTION OF DNA STRUCTURE TO THE CLAMP LOADING REACTION BY THE *E. COLI* CLAMP LOADER γ COMPLEX

## Background

Clamp loaders use the power of ATP binding and hydrolysis to assemble sliding clamps around DNA for use in a variety of functions involving DNA metabolism. Clamp loaders must not only load clamps on DNA, but they must also target clamps to the correct location on DNA and must load the clamps in the correct orientation to be useful for binding by the subsequent protein. One such downstream protein, DNA polymerase, binds the sliding clamp at the replication fork, and this interaction prevents frequent dissociation of the polymerase from the template DNA. A new sliding clamp is needed every 2 – 3 seconds on the lagging strand for each Okazaki fragment, so the clamp loader must be able to target the p/t junction quickly and load a clamp in the proper position and orientation to support processive replication (reviewed in (135)). Disruption of this process could result in uncoupling of the replication fork, potentially leading to DNA strand breaks.

For DNA replication, the γ complex clamp loader must load the β sliding clamp at primer/template (p/t) junctions with a recessed 3' end. It is still not clear which aspects of this p/t DNA architecture are targeted by the γ complex to either promote clamp loading at the correct DNA site, or inhibit clamp loading at the incorrect site. A recent crystal structure of γ complex with p/t DNA gives insight into DNA binding by the clamp loaders (Figure 1-4) (51).

In this structure, the subunits of the clamp loader spiral in a pitch similar to DNA. Positively charged residues on the inside of the clamp loader cap make contacts with

the phosphate backbone of the template strand in the duplex region of the DNA (51). If this is the only contact made by the clamp loader to the duplex of DNA, it does not explain how the clamp loader can discern the correct from incorrect polarity of DNA. In fact, the opposite polarity of DNA was modeled into the structure of γ complex, and the same contacts between the duplex DNA and the inside of the clamp were observed (90). If clamp loading occurs on the incorrect polarity, ATP will have been wasted as the sliding clamp will not be available for the polymerase and therefore will slow down the replication fork progression as another clamp is loaded.

Another interesting aspect of the crystal structure is the single-stranded overhang (SSO), which exits the cap through the gap between δ and δ'. The γ complex was incubated with p/t DNA containing a 10nt SSO, but the solved structure shows only 4nt visible, indicating that these 4nt are held in a rigid position in each molecule, while the last 6nt of the SSO are not. This signifies that the first 4nt must be important to be held in such a rigid position in each molecule in the structure.

Pre-steady state fluorescence-based assays were used to examine the effect of different DNA structures on clamp loading by γ complex. Two basic questions were asked. First, how does the length of the p/t SSO affect clamp loading? This question was addressed by measuring pre-steady state clamp loading triggered by DNA structures of varying SSO length. The second question is: how does the γ complex discriminate between different polarities of DNA found at the p/t junction? This question was addressed by measuring pre-steady state clamp loading on DNA of different polarities with and without single-stranded binding protein (SSB).

## The Role of the DNA Single-Stranded Overhang in γ complex Clamp Loading

### β closing and release on DNA with different lengths of single-stranded overhangs

To measure the role that the SSO plays in triggering clamp loading by the γ complex, DNA oligomers were designed such that multiple structures could be made with different lengths of SSO (Table 2-2). To measure γ complex clamp loading, the same fluorescent closing and release assays described in Chapter 3 were used. Briefly, β closing was monitored using a β clamp labeled at the interface with AF488; when the clamp is in the closed conformation the fluorophores are close enough to self-quench, but when β opens, the fluorophores move apart to relieve the self-quench (69). Clamp release was measured using β labeled with pyrene on the surface so that when γ complex binds, the fluorescence increases approximately 2-fold over free β-PY (120). Clamp closing and release reactions were performed in a stopped-flow apparatus to allow rapid mixing and detection of the first few seconds of the reaction. A sequential mixing scheme (Figure 2-4) was used to mix γ complex, labeled β, and ATP for 4 s, before mixing with a syringe containing DNA, ATP, and excess unlabeled β. Excess unlabeled β was added to limit the reaction to a single turnover. Final concentrations of the proteins and DNA in these reactions are 20 nM γ complex, 20 nM labeled β, 0.5 mM ATP, 40 nM DNA, and 200 nM unlabeled β.

Figure 4-1 shows representative time courses for β closing reactions comparing γ complex activity on DNA with 30nt (black), 3nt (blue), and 0nt (green) SSO. Observed β closing rates were calculated using a single exponential decay equation (Equation 2-4) and the average rates of three independent experiments for these structures as well as

DNA structures with other lengths of SSO are shown in Table 4-1. DNA with 30nt, 10nt, and 5nt SSO have similar observed closing rates of 6 – 7 $s^{-1}$ while DNA with 3nt and 1nt have observed rates of approximately 2 – 3 $s^{-1}$. DNA with no overhang (0nt SSO) triggered the slowest clamp closing, with an observed rate of 0.35 $s^{-1}$.

Figure 4-2 shows representative time courses for β release reactions for 30nt (black), 3nt (blue), and 0nt (green) SSO. Corresponding calculated average observed rates of three independent experiments for β release reactions are shown in Table 4-1. β release time courses are biphasic for all DNA structures except 0nt, ssDNA, and no DNA. The first phase in the β-PY release time courses represent a conformational change as γ complex closes the clamp, and the second phase represents the change in fluorescence as β-PY is released (see Chapter 3). For each DNA structure giving a biphasic β-PY time course, the calculated observed rate for the first phase of the β-PY release scaled with the calculated rate for β closing measured with the β-AF488 assay. The corresponding second β-PY observed rates were all 0.8 – 0.9 $s^{-1}$. From this point forward, when referring to the observed β release rate, the second phase of the biphasic reactions will be referenced, as this rate corresponds to β release. For the ssDNA, 0nt DNA, and no DNA, the observed release rates are no longer biphasic and match the observed β closing rate for those structures. In this situation, it appears that β closing is so slow that it limits the rate β release.

Based on this data, it appears that γ complex requires only 1nt of SSO for efficient clamp loading, as DNA with a 1nt SSO triggered β closing with a 10-fold higher observed rate than DNA with 0nt SSO. Interestingly, the observed release rates did not

change for DNA structures with 1nt SSO or longer, even though observed closing rates changed 2-fold when increasing the SSO from 3nt to 5nt. Clamp closing rates appear to be more sensitive to DNA conformation than clamp release rates, indicating that even though β clamps are released onto DNA at the same rate, the mechanism by which they are loaded changes depending on the DNA structure.

**DNA concentration dependence of β closing and release reactions**

DNA binding by γ complex•β is required to trigger the rapid clamp closing and release rates reported in Table 4-1. This is a bimolecular reaction, so the concentration of DNA could influence the observed β closing and release rates. To address this, β closing reactions were performed at a variety of DNA concentrations for each DNA structure. For 10nt, 5nt, 3nt, and 1nt DNA structures, DNA concentrations of 20 nM, 60 nM, 150 nM, 200 nM, and 300 nM were used. For 0nt DNA, the previous concentrations were tested as well as 500 nM, 1000 nM, 1500 nM, 2000 nM, and 3000 nM DNA. Concentrations of the protein and ATP remained constant at 20 nM γ complex, 20 nM β-AF488, 0.5 mM ATP, and 200 nM unlabeled β.

Figure 4-3 A shows representative results of these titrations for 0nt DNA. The individual closing time courses were fit to an exponential decrease (Equation 2-4) to obtain the observed rate of closing. The observed rate was then plotted as a function of DNA concentration to obtain the graph in Figure 4-3 B. DNA concentration dependent titrations for each DNA structure were fit with the Michaelis-Menten equation (Equation 4-1) to yield two constants. First, the maximum closing rate, ($k_{max}$), which is a measure of the observed closing rate when DNA binding is no longer rate limiting, and therefore represents the highest observed rate that can be reached with these substrates. The

second constant is the DNA concentration at which half the $k_{max}$ is reached ($K_{0.5}$), which is a way to measure the concentration of DNA needed to reach half saturation. These values are reported in Table 4-2. The $K_{0.5}$ could not be calculated for 30nt DNA, because closing rates on this DNA structure do not change as a function of DNA concentration, even at the equimolar concentration of 20 nM DNA.

$$v = \frac{k_{max}[S]}{K_{0.5} + [S]} \quad (4\text{-}1)$$

Interestingly, for DNA structures with more than 5nt SSO, the $k_{max}$ decreases 2-fold, from 14 $s^{-1}$ for 5nt DNA to 6 $s^{-1}$ for 30nt DNA. The $K_{0.5}$ also decreases as a function of the SSO length, from 60 nM for 5nt DNA to presumably less than 20 nM for 30nt DNA. Although these changes are not dramatic, there is a trend of decreasing $k_{max}$ and $K_{0.5}$ as the SSO length increases above 5nt, which implies that the excess nucleotides on the SSO may be playing a slightly inhibitory role in clamp loading. $\gamma$ complex can bind ssDNA so it is possible that the excess SSO is trapping some of the $\gamma$ complex•$\beta$ molecules and slowing the ability of the complex to find the p/t junction.

Both 3nt and 1nt DNA reach a $k_{max}$ of approximately 6 – 9 $s^{-1}$. It is surprising that the $K_{0.5}$ value for 1nt DNA is lower than for 3nt DNA and is comparable to the $K_{0.5}$ value for 5nt and 10nt DNA. This could represent a different binding mode by the clamp loader on these this structures, and this possibility will be discussed below. DNA with a 1nt SSO has a higher $K_{0.5}$ values than DNA structures with longer SSO, indicating that a higher concentration of DNA with a 1nt SSO is needed for the clamp loading reaction to reach saturation.

The $K_{0.5}$ for 0nt DNA was the highest for all substrates tested. With 3 $\mu$M DNA, closing reactions were still not able to reach a maximum observed rate, but based on

fitting, a predicted $k_{max}$ of 8 $s^{-1}$ and a $K_{0.5}$ of 1600 nM were calculated. The γ complex can still load clamps on DNA with 0nt SSO; however it requires much higher concentrations of DNA to reach a saturating closing rate.

β release reactions were performed in the presence of 300 nM DNA, which is a saturating DNA concentration as measured by the β closing assays for all structures except 0nt DNA (Table 4-2). Again, all time courses show biphasic kinetics. The observed rates calculated from the first phase of the release time courses were higher than the rates calculated at 40 nM DNA (Table 4-1), with the exception of 30nt DNA. These rates instead scaled with the $k_{max}$ rates calculated from the β-AF488 closing reactions. This was expected, as the first phase represents a conformational change associated with clamp closing, which is DNA concentration dependent. The second phase of the release time courses, corresponding to release of β-PY from γ complex, are essentially unchanged from one another at about 1 – 1.2 $s^{-1}$. Based on this data, the rates of β closing are affected by DNA concentration, but the rates of β release are not.

**β closing on DNA with 5' phosphate**

The DNA structures above were chemically synthesized without 5'phosphates (5'P) that otherwise naturally occurs on DNA. This extra charge at the 5' end may change the way that γ complex interacts with the DNA, because interaction with the phosphate backbone is the only known mediator of γ complex•DNA interactions and this would give the clamp loader one more phosphate to interact with. The oligomers used above were treated with T4 kinase to add the 5'P. Clamp closing was measured on these structures to see how the 5'P affects the DNA substrate specificity of γ complex. Final concentrations of components are 20 nM γ complex, 20 nM β-AF488, 40 nM DNA,

500 μM ATP, and 200 nM β. Observed closing rates were calculated using an exponential decay (Equation 2-4) and are reported in Table 4-3.

The addition of 5'P to the DNA increased the observed rates of β closing for all DNA structures except 30nt and 1nt DNA-P. For 10nt and 5nt DNA-P, the calculated closing rates of 12 ± 1.1 $s^{-1}$ and 14 ± 0.8 $s^{-1}$ respectively, are within standard deviation of the $k_{max}$ rates calculated for 5nt and 10nt DNA lacking 5'P (Table 4-3). This would indicate that DNA concentration is not limiting the rate of β closing on these DNA structures. Closing reactions were repeated for 30nt, 10nt, and 5nt DNA-P at 20 nM and 80 nM DNA to determine if DNA binding is limiting the rate of β closing. Changing the concentration of DNA did not affect the observed β closing rates, therefore β closing on these structures is DNA concentration independent.

For 3nt, 1nt, and 0nt DNA-P, the concentration dependence of the closing rates was also investigated using 20 nM, 40 nM, 80 nM, and 200 nM DNA. The observed rates for these structures were dependent on DNA concentration and all reached a $k_{max}$ of 7 – 9 $s^{-1}$. For DNA with a 3nt SSO, the $K_{0.5}$ is about 20 nM, which is low compared to the $K_{0.5}$ of around 200 nM measured for 1nt and 0nt DNA-P. This $K_{0.5}$ is also much lower than the $K_{0.5}$ of about 200, calculated for 3nt DNA lacking the 5'P.

Comparing 0nt and 5nt DNA-P, there is now only about a 10-fold difference in observed closing rates, as compared to a 20-fold difference for 0nt and 5nt DNA lacking a 5'P. From this data, when a 5'P is present on the DNA, γ complex requires 3 – 5 nt of SSO for the most efficient clamp loading.

## The Role of Single Stranded Binding Protein and the 5'Phosphate in Promoting β Loading on the Correct Polarity of DNA

### β closing reactions on naked DNA

To be effective for DNA replication, β must be loaded onto the replication fork at the primer-template (p/t) junction with a recessed 3' end (3'DNA). Therefore, γ complex must be able to preferentially target this p/t junction instead of a p/t junction with a recessed 5' end (5'DNA). It was reported that γ complex receives polarity information from the duplex portion of the p/t junction, but it is not clear how (90). β closing was therefore measured using p/t structures with a 3' recessed end (3'DNA) and a 5' recessed end (5'DNA). The role of SSB and the 5'P in promoting clamp loading on the correct, 3'DNA polarity was also investigated.

Figure 4-4 A and B show representative β closing and release traces, respectively, with 3'DNA (green) and 5'DNA (blue). Reactions contained 20 nM γ complex, 20 nM fluorescent β, 40 nM DNA, 0.5 mM ATP, and 400 nM β. Average calculated observed rates for three independent experiments are reported in Table 4-4. β closing on the incorrect 5'DNA had only half the observed rate as the correct 3'DNA, and no change in the β release rate. One possible reason there is not a large difference observed between 3' and 5'DNA is that the synthetic oligonucleotides used do not have 5'P and therefore have a different charge at the 5' end of a p/t junction that could otherwise inhibit clamp loading on 5'DNA. To test this possibility, DNA oligomers chemically modified with 5'P were used to make the 3' and 5'DNA structures. These structures were used to measure β closing and β release in Figure 4-4 C and D. Average observed rates for three independent β closing and release experiments are

reported in Table 4-4. The addition of the 5'P to the DNA structures did not convey specificity for 3'DNA-P (green) over 5'DNA-P (blue) any further; there was still an approximately 2-fold difference in observed closing rates and no change in observed release rates.

**β closing and release in the presence of SSB**

Based on the data above, naked DNA is not enough to confer specificity to 3'DNA over 5'DNA; instead, other proteins at the replication fork, such as SSB, may confer specificity. To address this, the β closing and release reactions were performed on SSB coated 3'DNA and 5'DNA. Representative closing and release time courses for SSB coated 3'DNA (blue) and 5'DNA (green) are shown in Figure 4-5 A and B, respectively, with the average calculated observed rates of three independent experiments reported in Table 4-5. Interestingly, although the addition of SSB to 3'DNA did not significantly affect the observed rates of β closing or release, SSB significantly decreased these observed rates for 5'DNA. Addition of SSB to the 5'DNA decreased the observed closing rate about 10-fold compared to bare 5'DNA, and almost 50-fold compared to 3'DNA with SSB. β release time courses in the presence of SSB were slowed about 4-fold to a rate of about 0.2 $s^{-1}$ and were no longer biphasic, indicating β closing is now so slow that it is limiting the rate of clamp release.

Clamp closing and release were also measured with SSB coated DNA structures containing the 5'P modification (Figure 4-5 C and D and Table 4-5). In the presence of SSB, the observed rates of β closing and release on 3'DNA-P were unchanged compared to the absence of SSB. In the presence of SSB, closing on 5'DNA-P was approximately 100-fold slower than 3'DNA-P, while release was approximately 30-fold

slower. The observed rates calculated for both β closing and release on SSB coated 5'DNA-P are within standard deviation of rates calculated in the absence of DNA (Table 3-1). This would seem to indicate that γ complex•β is not able to bind these DNA structures and instead passively dissociates in the absence of DNA dependent ATP hydrolysis. From this data, SSB alone plays a role in preventing clamp loading on the incorrect 5' polarity of DNA, but this effect is amplified when a 5'P is present at the junction.

**β closing using a mutant γ complex lacking the χ subunit**

Based on the data above, SSB confers the specificity of γ complex for 3'DNA over 5'DNA. The χ subunit of γ complex is responsible for mediating the interaction with SSB (52, 53), therefore, if this subunit is lost, γ complex should no longer be able to interact with SSB. β closing reactions were performed with different polarities of DNA using γ complex lacking the χ subunit (γ complex-χ); average calculated observed rates for three independent experiments are shown in Table4-6.

Observed β closing rates for γ complex-χ in the absence of SSB remain unchanged from rates of closing by wild type γ complex. This indicates that the χ subunit does not affect the clamp loading reaction with naked DNA. In the presence of SSB, β closing on 3'DNA as well as 3'DNA-P slows about 2 – 3 fold with γ complex-χ compared to in the absence of SSB. This indicates the χ subunit is required for optimal clamp loading on SSB coated DNA.

Interestingly, on 5'DNA coated with SSB, two different results are observed, depending on if a 5'P is present or not. In the absence of a 5'P, closing on 5'DNA with SSB is about 10-fold faster when the χ subunit is missing than for wild type γ complex.

Therefore, the 50-fold difference in closing rates observed between SSB coated 3'DNA and 5'DNA with wild type γ complex is lost. Instead, in the absence of the χ subunit, the difference between SSB coated 3' and 5'DNA is now only about 2-fold, similar to wild type γ complex without any SSB present. This seems to indicate that interactions mediated by the χ subunit are required for the SSB to confer specificity to 3'DNA over 5'DNA.

In the presence of a 5'P however, closing on SSB coated 5'DNA-P is not affected by the absence of the χ subunit; β closing with both wild type and γ complex-χ yield observed rates of 0.06 $s^{-1}$. This indicates that interactions between SSB and the χ subunit are not required to prevent clamp closing on SSB coated 5'DNA-P, instead, interactions involving the 5'P are important to prevent clamp loading on SSB coated 5'DNA.

## Conclusions

The γ complex must load a new clamp every 2 – 3 seconds to keep pace with the replication fork, therefore, it must be able to quickly and accurately recognize the correct structure of DNA. To understand the mechanism by which γ complex recognizes the correct DNA structure, pre-steady state β closing and release assays were used to measure clamp loader activity triggered by different DNA structures. DNA structures tested contained varying lengths of single stranded overhangs (SSO) as well as different polarities of the p/t junction.

The γ complex appears to require only a single nucleotide of SSO for the most efficient clamp loading, because β closing is 10-fold faster and β release is 3-fold faster for this structure than for 0nt DNA. Increasing the length of SSO to 5nt had only a 2-fold

further effect on β closing and no further effect on β release. However, when a 5'P is present, γ complex loads clamps most efficiently on DNA structures with 3 – 5nt SSO.

There are a few possible reasons γ complex needs an SSO. It is possible that the SSO makes important and specific interactions in the δ subunit that would help to sense and lock the DNA into a position needed for optimal clamp loader activity. This would be supported by studies where mutational analysis was performed on the δ-W279 residue, which cross-links to the first nucleotide of the SSO (91). Losing the contact between the SSO and the δ–W279 via mutation weakened γ complex activity and thus would indicate that this specific interaction is important (92). It is also possible that γ complex needs a SSO not to make specific contacts, but to simply help orient the duplex DNA so that the DNA can make appropriate contacts within the clamp loader cap.

Interestingly, results from measuring the concentration dependence of β closing (Table 4-2) could suggest a role for the SSO in mediating binding to the p/t DNA, similar to a threading or sliding mechanism hypothesized for the T4 bacteriophage clamp loader (88). In this model, the clamp loader binds the SSO first, and then slides to the p/t junction to load the clamp (Figure 4-6 A). Evidence supports this mode of binding for DNA with 5nt SSO or longer, whereas a different DNA binding mechanism may exists for 1nt and 0nt DNA. For DNA structures with 5nt SSO and greater, both the $k_{max}$ and $K_{0.5}$ of β closing decrease as the SSO length increases. This could represent a situation in which γ complex binds the SSO and slides into the p/t junction. The longer the SSO, the longer it takes to slide to the p/t junction, therefore lowering the $k_{max}$. In other words, the maximum β closing rate for DNA structures with longer SSOs is limited by sliding of the clamp loader to the p/t junction.

For DNA with 1nt and 0nt SSO, the binding mechanism would change as the SSO is too short to mediate p/t DNA binding (Figure 4-6 B). This could explain the decrease in $K_{0.5}$ and the $k_{max}$ values compared to 3nt DNA. The 3nt DNA might be an intermediate structure, where $\gamma$ complex binds with either mechanism described above, and that could explain why the $K_{0.5}$ increases, but the $k_{max}$ decreases compared to 1nt DNA.

The sliding model is also supported by the data measuring clamp closing on DNA with a 5'P present (Table 4-3). For DNA structures with 5nt or 10nt SSO, the presence of the 5'P increases the observed $\beta$ closing rates compared to in the absence of the 5'P. In fact, these closing rates were no longer DNA concentration dependent, indicating these reactions had reached $k_{max}$. Based on the crystal structure (Figure 1-4), the additional 5'P for 10nt and 5nt DNA is far enough from the p/t junction that it should not influence $\gamma$ complex•$\beta$ binding directly to the p/t junction. Instead, in a model where $\gamma$ complex•$\beta$ binds the end of the SSO and slides to the p/t junction, the presence of the 5'P could stimulate binding to the end of the SSO, or facilitate sliding of the $\gamma$ complex•$\beta$ toward the p/t junction, thus resulting in the faster observed rates.

The presence of SSB on the SSO of p/t DNA, however, would question this sliding mechanism. In the presence of SSB, $\gamma$ complex is still able to load $\beta$ onto 3'DNA with a similar observed rate as in the absence of SSB (Table 4-4 and 5). This would indicate that this binding mechanism may only be valid for naked short linear DNA structures and not more complicated structures, such as those with SSB or DNA that is circular in nature.

To prevent β loading on the wrong polarity of DNA, γ complex relies on SSB. When SSB is present, β closing is slowed 50 – 100 fold on 5'DNA compared to 3'DNA (Table 4-5). In fact, closing on SSB coated 5'DNA-P is so slow, it is within a standard deviation of closing reactions in the absence of DNA (Table 4-1), indicating that the SSB could be preventing 5'DNA binding by γ complex•β. Interactions between SSB and γ complex are mediated by the χ subunit (52, 53). In the absence of the χ subunit, SSB can no longer prevent clamp loading on 5'DNA; closing on 3'DNA with SSB is only 2-fold faster than closing on 5'DNA with SSB (Table 4-6). Surprisingly, when a 5'P was present, the absence of the χ subunit appeared to have no effect on clamp closing on the 5'DNA. Clamp closing on 5'DNA-P was still 0.06 $s^{-1}$, the same as when the χ subunit is present. This would suggest that while χ•SSB interactions can play a role in preventing clamp loading on the wrong polarity of DNA, the 5'P also plays an important role.

These data presented here indicate that for efficient clamp loading, γ complex requires DNA with at least 1nt of SSO when a 5'P is absent from the DNA structure, but requires 3 – 5 nt of SSO when a 5'P is present. These data also show that γ complex relies on SSB to prevent clamp loading on the wrong polarity of p/t DNA. These studies help to define the aspects of the DNA structure required for γ complex to load clamps effectively as well as highlight protein•protein interactions that play a role in γ complex DNA specificity.

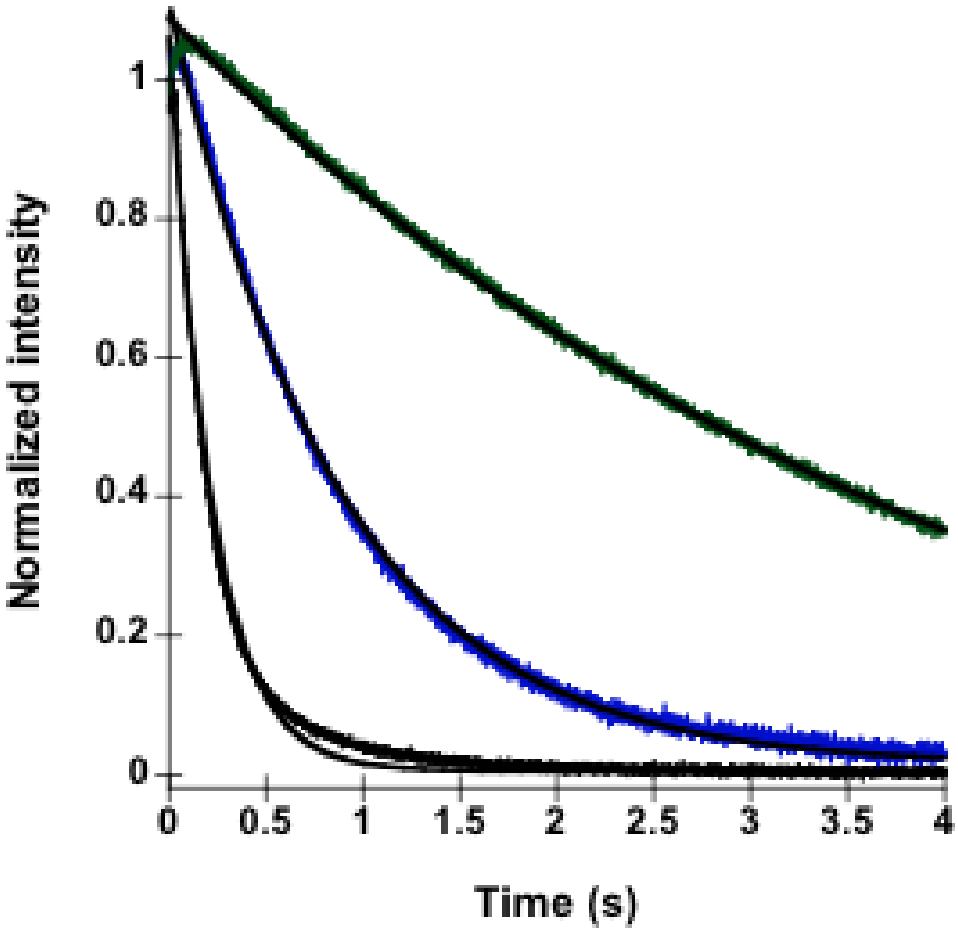


Figure 4-1. Representative traces for β closing using DNA with 30nt (black), 3nt (blue) and 1nt (green) SSO. Reactions included: 20 nM γ complex, 20 nM β-AF488, 40 nM DNA, 500 μM ATP and 200 nM unlabeled β.

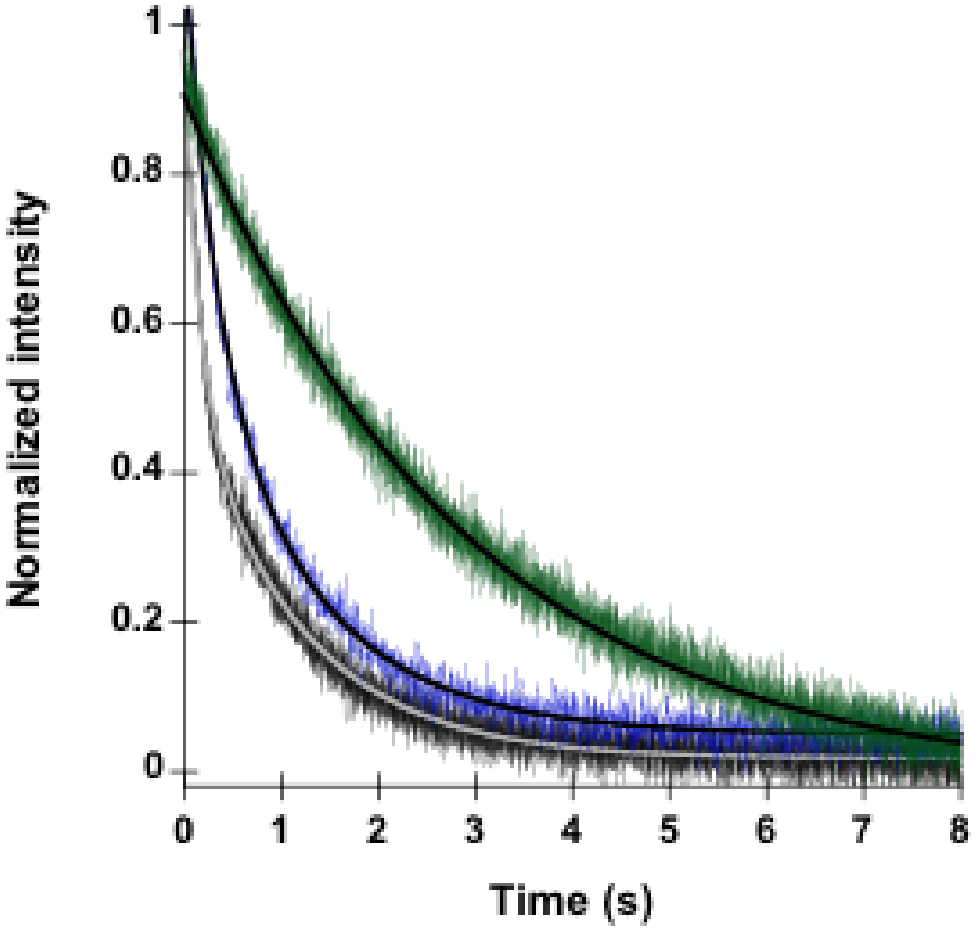


Figure 4-2. Representative β release time courses are shown for DNA with 30nt (black), 3nt (blue), and 0nt (green) SSO. Reactions included: 20 nM γ complex, 20 nM β-AF488, 40 nM DNA, 500 μM ATPand 200 nM unlabeled β.

A.

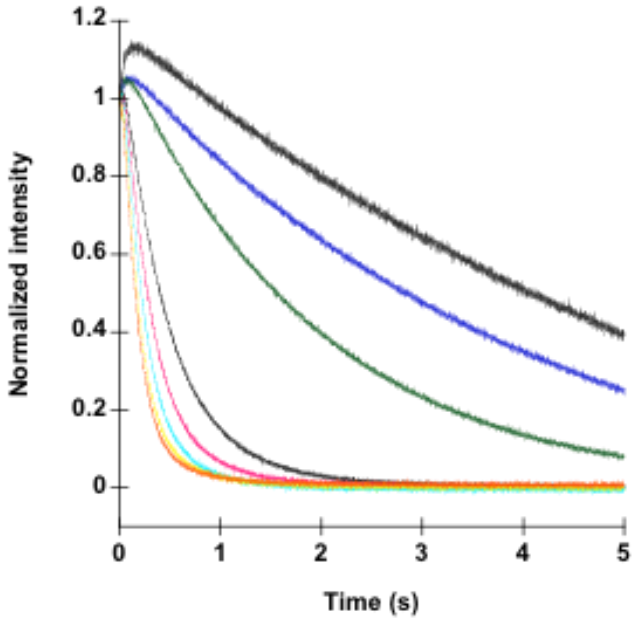


B.

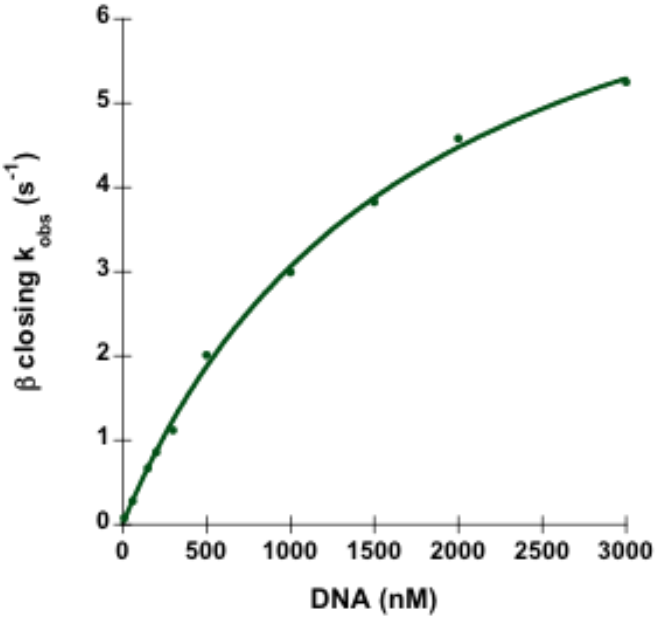


Figure 4-3. β closing as a function of DNA concentration. Reactions were performed with a variety of DNA concentrations ranging from 20 – 3000 nM; the time courses for each DNA concentration are shown in A. The observed rates were calculated from the time courses individually using Equation 2-4. The observed rates were then plotted as a function of DNA concentration to obtain the graph in B. This curve was fit using the Michaelis-Menten equation (Equation 4-1) to obtain DNA binding constants shown in Table 4-2.

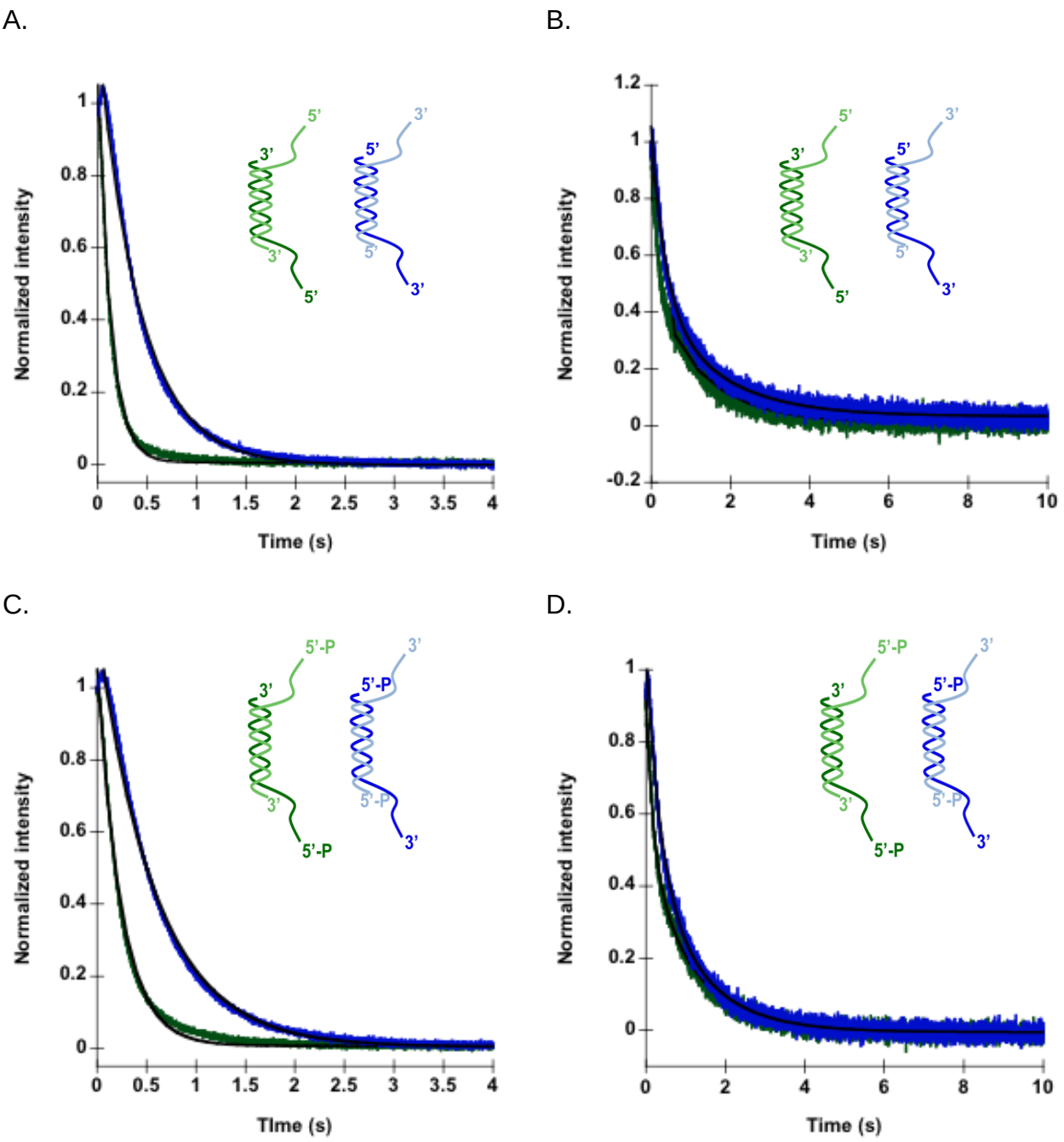


Figure 4-4. Representative β closing time courses for loading on different DNA polarities are shown, with calculated observed rates reported in Table 4-5. β closing was measured with 3'DNA (green) and 5'DNA (blue) for DNA without a 5'P in (A) and with a 5'P in (C). β release was measured with 3'DNA (green) and 5'DNA (blue) for DNA without a 5'P in (B) and with a 5'P in (D). Reactions contained 20 nM γ complex, 20 nM fluorescent β, 40 nM DNA, 500 μM ATP and 200 nM unlabeled β.

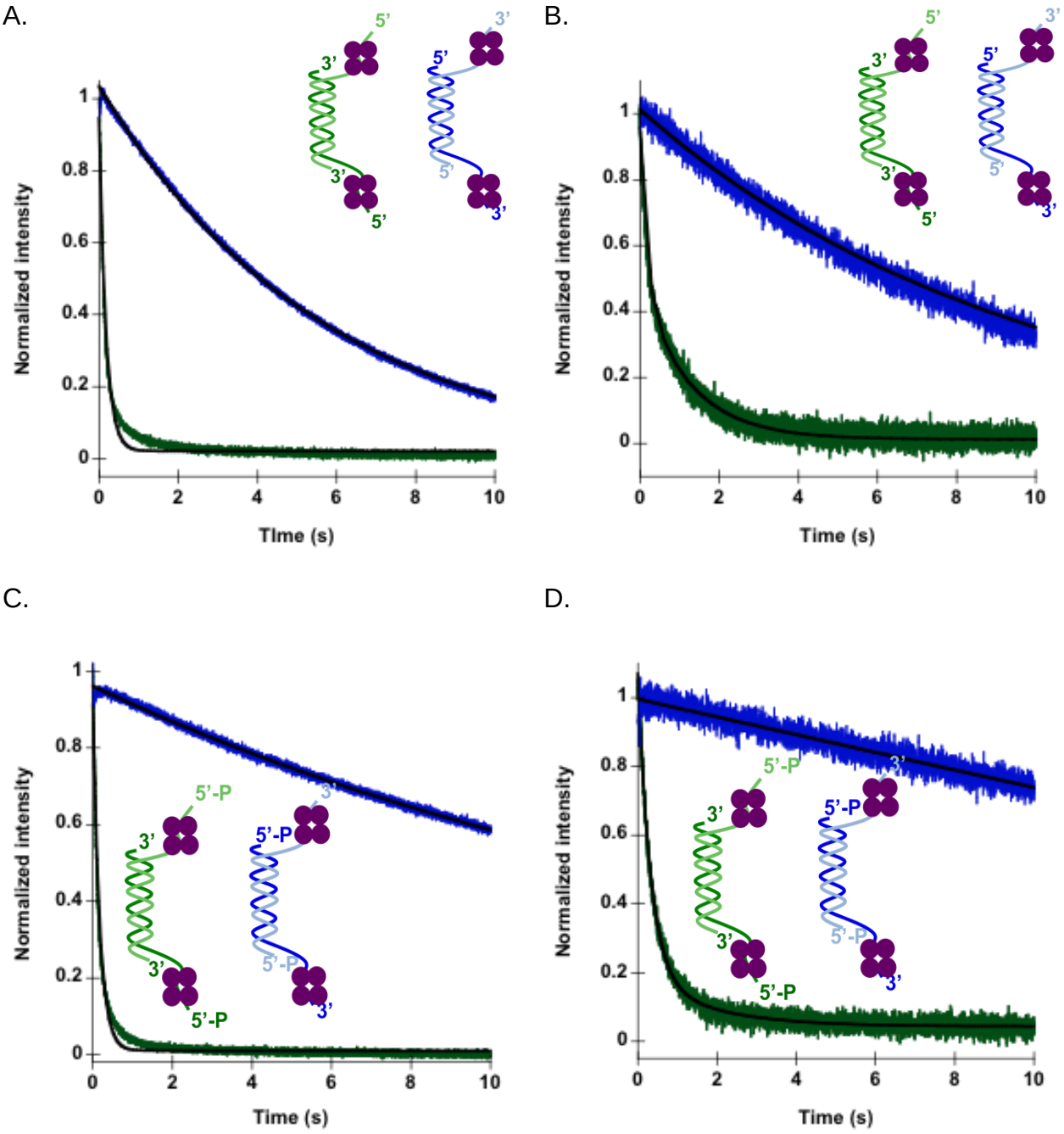


Figure 4-5. Representative closing time courses on different polarities of DNA in the presence of SSB. β closing traces are shown for 3'DNA+SSB (green) and 5'DNA+SSB (blue) without 5'P (A) and with 5'P (B). Observed rates were calculated and are reported in Table 4-6. Reactions contained 20 nM γ complex, 20 nM β-AF488, 40 nM DNA, 0.5 mM ATP, 200 nM unlabeled β and 800 nM SSB.

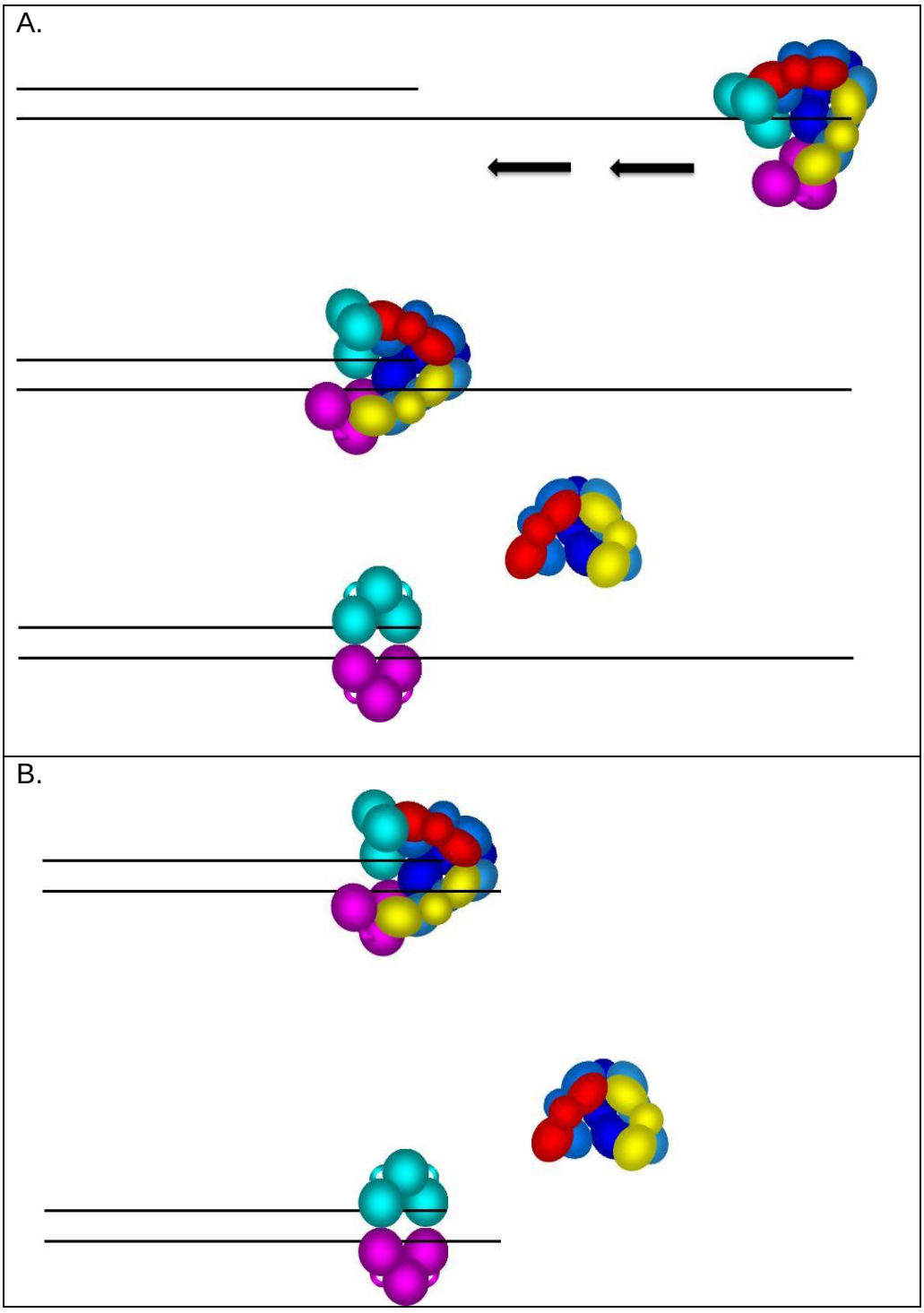


Figure 4-6. Two models for the mechanism of γ complex binding to p/t DNA. Panel A shows a model in which γ complex binding to the p/t DNA junction is mediated by interactions with the SSO. The γ complex•β is shown binding first to the SSO, and then sliding to the p/t junction where γ complex then loads a β clamp. Panel B shows a model in which the γ complex bi nds directly to the p/t junction to load clamps.

Table 4-1 β closing and release rate for DNA structures with different lengths of single-stranded overhangs.

| **DNA structure** | **Closing** | **Release** | |
|---|---|---|---|
| | $k_{obs}$ ($s^{-1}$) | $k_{obs1}$ ($s^{-1}$) | $k_{obs2}$ ($s^{-1}$) |
| **30nt** | 6.2 ± 1.3 | 6.3 ± 0.3 | 0.85 ± 0.04 |
| **10nt** | 6.9 ± 0.3 | 9.1 ± 0.13 | 1.0 ± 0.02 |
| **5nt** | 6.4 ± 0.9 | 9.2 ± 0.9 | 0.9 ± 0.03 |
| **3nt** | 1.2 ± 0.4 | 2.9 ± 0.04 | 0.84 ± 0.03 |
| **1nt** | 2.8 ± 0.3 | 5.1 ± 0.7 | 0.88 ± 0.03 |
| **0nt** | 0.35 ± 0.08 | 0.33 ± 0.03 | N/D |
| **ssDNA** | 0.3 ± 0.06 | 0.2 ± 0.08 | N/D |
| **No DNA** | 0.03 ± 0.01 | 0.04 ± 0.02 | N/A |

N/A indicates that no $k_{obs2}$ was present for these reactions.
N/D indicated not determined.

Table 4-2 DNA concentration dependence of clamp loading on DNA substrates with different lengths of single-stranded overhangs

| **DNA Structure** | **Closing at different DNA concentrations** | | **Release rates at saturating DNA concentrations ($s^{-1}$)** | |
|---|---|---|---|---|
| | $k_{max}$ ($s^{-1}$) | $K_{0.5}$ (nM) | $k_{obs1}$ ($s^{-1}$) | $k_{obs2}$ ($s^{-1}$) |
| 30nt | 6.2 | N/A | 7.4 | 1.1 |
| 10nt | 11 | 20 | 10 | 1.1 |
| 5nt | 14 | 60 | 11 | 1.0 |
| 3nt | 8.9 | 190 | 8.9 | 1.1 |
| 1nt | 5.5 | 45 | 6.9 | 1.2 |
| 0nt | 7.9 | 1600 | N/D | N/D |

N/D indicated not determined.

Table 4-3. Observed β closing rates on DNA with different lengths of SSO with 5'P added.

| **DNA structure** | **β closing ($s^{-1}$)** | **$k_{max}$ ($s^{-1}$)** | **$K_{0.5}$ (nM)** |
|---|---|---|---|
| **30nt-P** | 4.6 ± 0.4 | 5 | N/A |
| **10nt-P** | 12 ± 1.1 | 12 | N/A |
| **5nt-P** | 14 ± 0.8 | 14 | N/A |
| **3nt-P** | 6.4 ± 0.7 | 9 | 23 |
| **1nt-P** | 1.2 ± 0.2 | 7 | 220 |
| **0nt-P** | 1.5 ± 0.1 | 9 | 180 |

Table 4-4. β closing and release calculated observed rates are reported for 3'DNA and 5'DNA structures.

| DNA structure | β closing | β release | |
|---|---|---|---|
| | $k_{obs}$ ($s^{-1}$) | $k_{obs1}$ ($s^{-1}$) | $k_{obs2}$ ($s^{-1}$) |
| **3'DNA** | 6.2 ± 1.3 | 6.3 ± 0.3 | 0.85 ± 0.04 |
| **3'DNA-P** | 4.6 ± 0.4 | 7.0 ± 1.1 | 0.82 ± 0.07 |
| **5'DNA** | 2.5 ± 0.3 | 3.1 ± 0.6 | 0.68 ± 0.09 |
| **5'DNA-P** | 1.9 ± 0.3 | 2.4 ± 1.0 | 0.76 ± 0.04 |

Table 4-5. Calculated observed rates are reported for β closing and release on 3'DNA and 5'DNA in the presence of SSB

| DNA structure | β closing | β release | |
|---|---|---|---|
| | $k_{obs}$ ($s^{-1}$) | $k_{obs1}$ ($s^{-1}$) | $k_{obs2}$ ($s^{-1}$) |
| **3'DNA** | 8.7 ± 0.6 | 6.2 ± 0.6 | 0.73 ± 0.2 |
| **3'DNA-P** | 5.7 ± 0.3 | 4.1 ± 1.2 | 0.54 ± 0.05 |
| **5'DNA** | 0.18 ± 0.04 | 0.23 ± 0.11 | N/A |
| **5'DNA-P** | 0.06 ± 0.001 | 0.06 ± 0.03 | N/A |

N/A indicates that no $k_{obs2}$ was present for these reactions.

Table 4-6. Calculated observed β closing rates by γ complex-χ on 3'DNA and 5'DNA in the presence and absence of SSB

| DNA structure | β closing – SSB ($s^{-1}$) | β closing + SSB ($s^{-1}$) |
|---|---|---|
| **3'DNA** | 6.1 ± 0.4 | 2.7 ± 0.1 |
| **3'DNA-P** | 5.2 ± 0.2 | 1.8 ± 0.3 |
| **5'DNA** | 1.8 ± 0.2 | 1.0 ± 0.2 |
| **5'DNA-P** | 1.7 ± 0.1 | 0.06 ± 0.02 |

# CHAPTER 5
# DNA SUBSTRATE SPECIFICITY OF THE *S. CEREVISIAE* CLAMP LOADERS RFC AND RAD24-RFC

## Background

In *S. cerevisiae* there are multiple clamp and clamp loader systems, each playing different roles in the organism. For DNA replication, the RFC clamp loader loads the PCNA sliding clamp onto DNA for use as a processivity factor by DNA polymerases. For DNA damage response, the clamp loader Rad24-RFC loads the alternative sliding clamp Ddc1-Rad17-Mec3 (homologue of human Rad9-Rad1-Hus1 or 9-1-1). The 9-1-1 clamp is loaded at sites of DNA damage to initiate and propagate the damage checkpoint signal (reviewed in (127, 136)).

RFC and Rad24-RFC load clamps at primer/template (p/t) DNA structures, but RFC recognizes a recessed 3' end (3'DNA), whereas Rad24-RFC recognizes a recessed 5' end (5'DNA) (78, 100). The difference in DNA polarity recognized by the clamp loaders is dictated by the different roles required of the sliding clamps. PCNA is primarily used as a processivity factor for DNA polymerases, so RFC loads it on 3'DNA structures. During DNA replication, a new PCNA clamp is needed for each Okazaki fragment. Therefore, RFC must target this 3'DNA site with high accuracy and efficiency to prevent loading PCNA clamps in the wrong location, thus slowing the replication fork. The 9-1-1 clamp is loaded to signal DNA damage arising from many sources (reviewed in (137)). The damaged DNA is processed in a manner that results in a p/t junction with a recessed 5' end. Accuracy of Rad24-RFC clamp loading for these sites is essential; if 9-1-1 is loaded at another site, it may signal DNA damage when there is none, thus giving the cell a "false alarm."

RFC and Rad24-RFC differ structurally by only one subunit, and yet they recognize different clamps and different DNA substrates (58, 59, 78). Even though the DNA structure preference is known, the mechanism by which the clamp loaders recognize specific DNA structures is not known. To understand how DNA structure affects clamp loading, fluorescence-based assays were used to measure various aspects of the clamp loading reaction. DNA binding was measured using a fluorescent anisotropy-based DNA binding assay. Clamp loader binding to 3'DNA, 5'DNA, single-stranded DNA (ssDNA) and double stranded DNA (dsDNA) with and without PCNA was assayed. This would help to determine if the clamp loaders can discriminate between different DNA structures and how PCNA affects DNA specificity. The specificity of RFC for DNA was investigated further using pre-steady state PCNA closing and release assays to measure PCNA loading on these DNA structures.

**Equilibrium DNA Binding by RFC and Rad24-RFC**

DNA binding by the clamp loaders was measured using DNA structures labeled with X-Rhodamine (RhX). When the DNA-RhX is free in solution, it rotates rapidly leading to a depolarization of light and a low anisotropy value. When the clamp loaders bind DNA-RhX, the rotation of DNA-RhX slows, thus leading to a higher amount of polarized light and a higher anisotropy value. Four DNA structures were used: two primer/template (p/t) structures, single-stranded DNA (ssDNA) and duplex blunt DNA (dsDNA); the DNA sequences are shown in Table 2-2. One p/t DNA structure, 3'DNA, has a free 3'OH at the p/t junction, while the other p/t structure, 5'DNA, has a free 5'P at the p/t junction.

In these assays, a buffer background was obtained, followed by the anisotropy of free DNA-RhX signal to measure unbound DNA. Then clamp loader was added and anisotropy was measured to determine how well the clamp loader binds the DNA substrate alone. The last step is the addition of PCNA to determine if PCNA stimulates clamp loader binding to the different DNA substrates. Final concentrations are 25 nM RhX, 0.5 mM ATPγS, 500 nM PCNA, and 0 – 1500 nM clamp loader. $K_d$ values were calculated using Equation 2-3 and an average of three independent experiments are reported in the graphs.

**RFC binding to different DNA substrates in the presence and absence of PCNA**

RFC binding to 3'DNA (A), 5'DNA (B), ssDNA (C), and dsDNA (D) are shown in Figure 5-1. The RFC complex used in these equilibrium DNA binding assays contains an Rfc1 subunit lacking the N-terminal ligase homology domain, which has been shown to be dispensable for clamp loading (95, 138). The anisotropy of free DNA (red) for each substrate remained constant around 0.22 – 0.24 as expected. Each DNA substrate was titrated with RFC (blue) to measure clamp loader binding to the different DNA substrates alone. PCNA was added (green) to measure stimulation of DNA binding by RFC. Two pieces of information can be obtained from each graph: first, the $K_d$, which measures the affinity of RFC for the DNA structure, and second, the total anisotropy change, which indicates the extent of slowing of the DNA rotation as the clamp loader binds.

Figure 5-1 A shows RFC binding to 3'DNA, and the calculated $K_d$ values are reported. Addition of RFC to 3'DNA-RhX increased the anisotropy in an RFC concentration dependent manner until it saturated around 0.31. Comparison of the

calculated $K_d$ values for RFC with and without PCNA show that the addition of PCNA stimulates RFC binding to 3'DNA approximately 5-fold.

Figure 5-1 B shows the anisotropy values as a function of RFC concentration for 5'DNA. RFC appears to bind 5'DNA with higher affinity than 3'DNA both alone, and in complex with PCNA, as illustrated by lower $K_d$ values. This was surprising, as RFC is not supposed to load clamps on this structure. RFC also bound this DNA in such a way that the anisotropy saturated at a higher value than with 3'DNA. Anisotropy measures rotation of the DNA, and with this structure, RFC binds in a manner that slows the rotation more dramatically than for 3'DNA. This might indicate that RFC binds this structure tightly but not necessarily the physiologically relevant p/t region of the structure. Instead, RFC may bind the end of the single-stranded overhang, where the fluorophore is located, thus decreasing rotation of the fluorophore in this fashion.

RFC binding to ssDNA (Figure 5-1 C) has slight differences from the p/t structures above. Like the p/t DNA structures, ssDNA binding is RFC concentration dependent; however, RFC binding alone reaches a saturating anisotropy value that is about half of the total change in anisotropy in the presence of PCNA. This may represent a different binding mode of RFC on ssDNA or a different conformation of the DNA in the absence of PCNA. The addition of PCNA to these reactions strongly stimulates binding to ssDNA with a $K_d$ value that is about 20-fold lower in the presence of PCNA. Interestingly, in the presence of PCNA, RFC binding to ssDNA has about a 5-fold lower $K_d$ value than binding to 3'DNA, indicating RFC•PCNA binds ssDNA with higher affinity than 3'DNA.

RFC binding to dsDNA (Figure 5-1 D) has similarities to RFC binding to ssDNA. Alone, RFC binding to dsDNA is weak, represented by a large $K_d$ value and the low saturating anisotropy value. Addition of PCNA stimulates dsDNA by lowering the $K_d$ value approximately 2-fold and increasing the saturating anisotropy value. This stimulation by PCNA is not as dramatic as seen for ssDNA, but the trend of PCNA stimulation is still present.

Based on the calculated $K_d$ values, in the absence of PCNA, RFC binds 5'DNA with the highest affinity. This is surprising as this structure is not one that should be recognized physiologically. Addition of PCNA stimulates RFC binding to all DNA structures, with ssDNA having the largest fold stimulation. Based on $K_d$ values, RFC•PCNA binds ssDNA with slightly higher affinity than 5'DNA, and 5'DNA with higher affinity than 3'DNA. RFC•PCNA binding to dsDNA was the weakest.

**Rad24-RFC binding to different DNA substrates in the presence and absence of PCNA**

Similar experiments were performed with Rad24-RFC in the presence and absence of PCNA to measure DNA binding affinity to these DNA structures. As above, the anisotropy of free DNA was measured, followed by the anisotropy of Rad24-RFC bound to DNA, and finally the anisotropy of Rad24-RFC•PCNA bound to DNA. PCNA is not the sliding clamp normally recognized by Rad24-RFC, however, *in vitro*, Rad24-RFC unloads PCNA after it is bound to DNA (87). Therefore, Rad24-RFC has the capacity to interact with PCNA in some manner and so PCNA was included in these reactions. Figure 5-2 shows the DNA binding results from three independent experiments for Rad24-RFC in the presence and absence of PCNA.

The red points represent the free DNA-RhX anisotropy values, which remained constant at 0.22 – 0.24 as expected. The anisotropy of Rad24-RFC bound to DNA is shown in blue. For each DNA structure tested, the anisotropy value increases as a function of Rad24-RFC concentration, but DNA binding is weak. For 3'DNA and dsDNA, the total anisotropy change of approximately 0.01 – 0.02 is low compared to the total anisotropy change of about 0.05 for 5'DNA and ssDNA. The $K_d$ values calculated for Rad24-RFC binding to the various DNA structures is shown in each graph. Calculating the $K_d$ for these binding curves yielded values with high variability because the anisotropy values are not reaching saturation, and thus are not fit as accurately. The large standard deviation in $K_d$ values makes it hard to compare Rad24-RFC binding to one structure versus another because it is not clear if differences in $K_d$ values are significant. However, Rad24-RFC alone generally binds all structures weakly, with high $K_d$ values.

The green points represent Rad24-RFC binding to the DNA structures in the presence of PCNA. Addition of PCNA shows no stimulation for 3'DNA, ssDNA or dsDNA as evidenced by no additional increase in anisotropy value and either no change or an increase in $K_d$ values. Rad24-RFC binding to 5'DNA did appear to be stimulated by PCNA, however. Again, the large standard deviation in the $K_d$ values makes it hard to compare the differences between some structures, but for 5'DNA, addition of PCNA results in a lower $K_d$ value. Addition of PCNA also increases the total anisotropy value of 5'DNA to around 0.32, which is comparable to anisotropy values reached by RFC binding to the DNA structures (Figure 5-1).

## Conclusions

In the presence of PCNA, RFC does not show a strong specificity for 3'DNA. In fact, based on calculated $K_d$ values, RFC•PCNA binds to ssDNA and 5'DNA with higher affinity than 3'DNA. It is possible that the high affinity observed for 5'DNA may not be specific for the p/t junction, but instead may reflect RFC binding to the single-stranded overhang of the structure. *In vivo* bare ssDNA is not likely to be present; instead it would be coated with RPA, likely preventing clamp loading. Rad24-RFC did not appear to have a preference for any DNA structure tested; it bound all structures poorly. Addition of PCNA slightly stimulated Rad24-RFC binding to the 5'DNA structure, but in general, DNA binding was weak compared to DNA binding by RFC as measured by $K_d$ values. RPA could not be used in these anisotropy-based DNA binding studies because binding of RPA to DNA-RhX would yield a large increase in anisotropy. It is unlikely that the RPA coated DNA-RhX would be further sensitive to report on clamp loader binding.

## RFC Clamp Loading on Different DNA Substrates

Based on the equilibrium DNA binding data from Figure 5-1, RFC binds all DNA substrates tested in the presence of PCNA. Based on the calculated $K_d$ values, RFC•PCNA even has higher affinity for ssDNA and 5'DNA over the physiologically relevant 3'DNA structure. This raises the question of how RFC correctly targets a 3'DNA site *in vivo*. It is possible that even though RFC can bind other DNA structures, these alternative structures do not promote a productive PCNA loading event. It was suggested that the single-stranded DNA binding protein, RPA, plays a role in preventing clamp loading on the other DNA structures (78, 100). Pre-steady state PCNA closing and release assays were used to measure PCNA loading on unlabeled versions of the

DNA structures described above. RPA was also included to compare clamp loading on 3'DNA and 5'DNA. The RFC complex used in these pre-steady state assays contained a full-length Rfc1 subunit.

**PCNA closing and release on 3'DNA, dsDNA, and ssDNA.**

Pre-steady state PCNA closing and release assays were used to measure clamp loading on 3'DNA, ssDNA, and dsDNA. PCNA closing was measured using PCNA doubly labeled at the interface with AF488 (PCNA-AF488). When PCNA-AF488 is closed, the fluorophores are close enough to self-quench, but when PCNA-AF488 opens, the fluorophores move apart to relieve the self-quench, thus leading to an increase in signal (46). PCNA release was measured using a PCNA clamp selectively labeled with MDCC on the surface that interacts with RFC. When RFC binds PCNA-MDCC, the fluorescence of MDCC increases 2-fold over free PCNA-MDCC (Marzahn, in preparation). PCNA closing and release were measured using the stopped-flow, as with $\gamma$ complex in Figure 2-4, to permit rapid mixing and detection of PCNA closing and release in real time. Excess unlabeled PCNA was added to limit the fluorescent reactions to one turnover. Final concentrations of the proteins and DNA in these reactions are 20 nM RFC complex, 20 nM labeled PCNA, 0.5 mM ATP, 40 nM DNA, and 200 nM unlabeled PCNA. Representative time courses for PCNA closing (A) and release (B) are shown in Figure 5-3 for 3'DNA (green), ssDNA (blue), and dsDNA (black). Observed PCNA closing and release rates were calculated using a double exponential decrease equation (Equation 2-5) and the average rates of three independent experiments are reported in Table 5-1.

Again, both PCNA closing and release show biphasic kinetics, with a fast phase and a slow phase. The fast phase of each time course represents the population of RFC•PCNA that closes or releases in an active, ATP dependent manner. The slow phase of the closing time courses represents the clamp loader losing interaction with one of the fluorophores as PCNA is released. The slower phase of the release time courses represents a second population of RFC•PCNA released in a passive manner (see Chapter 6). The biphasic observed rates for PCNA closing and release are reported, however for simplicity, comparisons will only be made with the first rate of each biphasic fit from this point forward because the fast phases measure the active, DNA dependent clamp closing and release.

The calculated observed rate for PCNA closing on 3'DNA is only 1.5-fold faster than dsDNA, and only 3-fold faster than ssDNA. The PCNA release rates remain unchanged. Comparing these data to results from the *E. coli* $\gamma$ complex, RFC has less DNA specificity. Clamp closing by $\gamma$ complex on dsDNA structures (0nt) or ssDNA structures was 20-fold slower, and release was 3-fold slower (Table 4-1). RFC does not appear to share this specificity. It is interesting to note that PCNA closing appears to be more sensitive to the DNA substrate than clamp release. This observation is consistent with results from the *E. coli* $\gamma$ complex (Chapter 4).

RFC may not have specificity against ssDNA or dsDNA like $\gamma$ complex, but PCNA loading on these sites *in vivo* is still unlikely. ssDNA is not likely to exist in the cell without RPA present, so RPA may play a role in preventing RFC from loading on ssDNA. It is surprising that RFC can load clamps on dsDNA with observed rates comparable to those of clamp loading on 3'DNA; however, *in vivo*, these types of

structures are not likely to exist either. A structure resembling dsDNA would be recognized by the cell as DNA damage and would be bound by a host of other proteins that could prevent clamp loading as well as process the DNA, producing another DNA structure altogether. Therefore, RFC may rely on other factors to direct PCNA loading away from ssDNA and dsDNA structures. It is still interesting to note the differences between RFC and γ complex DNA specificity. The γ complex appears to rely more on DNA structural cues than RFC.

**PCNA closing and release comparing 3'DNA and 5'DNA**

DNA binding studies with RFC indicate that RFC•PCNA binds to 5'DNA with higher affinity than 3'DNA (Figure 5-1). To be effective for DNA replication, PCNA must be loaded at the replication fork at a 3'DNA site. Loading at a 5'DNA site would result in a clamp that could not be used by the downstream polymerase representing a wasted clamp loading event. To determine how RFC discriminates between the two p/t structures in the cell, pre-steady state PCNA closing and release assays were performed using 3'DNA and 5'DNA. Closing and release assays were performed as described in the previous section. First, PCNA closing and release were measured with bare p/t DNA structures.

Representative PCNA closing time courses comparing 3'DNA (green) and 5'DNA (blue) are shown in Figure 5-4 A while representative time courses for PCNA release are shown in Figure 5-4 B. PCNA closing with 5'DNA had only half the calculated observed closing rate as the correct 3'DNA. Observed release rates for 3'DNA and 5'DNA are within standard deviation and are essentially the same (Table 5-2). This negligible difference in observed rates supports the results from Figure 5-1; RFC does

not appear to differentiate between 3' and 5'DNA. One possible reason a larger difference is not observed between 3' and 5' DNA is that the synthetic oligonucleotides used do not have 5'P and therefore have a different charge at the 5' end of a p/t junction that could otherwise inhibit clamp loading on 5'DNA. To test this possibility, DNA oligomers chemically modified with 5'P were used to make the 3' and 5'DNA structures to measure PCNA closing and PCNA release. Representative PCNA closing time courses are shown in Figure 5-4 C, while PCNA release time courses are shown in Figure 5-D. Calculated observed rates for PCNA closing and release are reported in Table 5-2. The addition of the 5'P to the DNA structures did not convey specificity for 3'DNA-P (green) over 5'DNA-P (blue) any further. There was still an approximately 2-fold difference in observed closing rates and no change in observed release rates (Table 5-2).

Another possible reason there is not a larger difference between 3' and 5'DNA is that bare DNA is not enough to confer specificity to 3'DNA. Specificity may instead be conferred by other proteins at the replication fork, such as RPA (78, 100). To address this, PCNA closing and release reactions were performed on 3'DNA and 5'DNA with RPA bound. Representative closing and release time courses for RPA coated 3'DNA (green) and 5'DNA (blue) are shown in Figure 5-5 A and B respectively, with the calculated observed rates for reported in Table 5-3. Addition of RPA stimulated PCNA closing on 3'DNA, and slowed closing on 5'DNA giving a 5-fold difference in observed closing rates, but there was no change in release rates (Figure 5-5, Table 5-3). This small difference in closing rates was surprising as similar experiments with $\gamma$ complex

showed that SSB yielded an approximate 50-fold difference in β closing between 3'DNA and 5'DNA (Figure 4-6).

Again, the DNA substrates with a 5'P added were also tested in the presence of RPA to determine if this extra negative charge prevents clamp loading on the incorrect polarity. Representative PCNA closing and release time courses with RPA coated 3'DNA-P (green) and 5'DNA-P (blue) are shown in Figure 5-5 C and D. When bound to DNA containing a 5'P, RPA now shows a strong inhibitory affect toward clamp loading on 5'DNA, but no effect on 3'DNA. PCNA closing on RPA coated 5'DNA-P was reduced 50-fold compared to RPA coated 3'DNA-P (Table 5-3). PCNA release also gave similar results: release rates were not affected by the presence of RPA on the correct polarity, but the combination of the 5'P and RPA slowed release about 3-fold.

Interestingly, the decrease in signal for the PCNA closing and release time courses with RPA coated 5'DNA-P are no longer biphasic and are no longer different. The calculated observed rates from these time courses are similar to those calculated in the absence of DNA or with ATPγS present (Table 3-2). Figure 5-6 shows comparisons of the PCNA closing (A) and release (B) time courses in the absence of DNA (blue) or in the presence of RPA coated 5'DNA-P (green). In the absence of DNA, the RFC•PCNA complex dissociates in a passive manner, independent of ATP hydrolysis. Based on this comparison, RPA in conjunction with the 5'P is promoting passive dissociation of the RFC•PCNA complex, similar to when no DNA is present. This would suggest that the RPA and 5'P are preventing the RFC•PCNA complex from binding the wrong polarity of DNA.

The time course for PCNA closing without DNA and with 5'DNA-P and RPA (Figure 5-6 A) both contain a fast increase in signal in the first few seconds of the reaction. It is unclear what this increase in signal represents because it is not seen in other PCNA closing time courses. It is possible that RFC makes different contacts with PCNA-AF488 when it is passively released versus when it is actively released in an ATP hydrolysis dependent manner. These different contacts may result in secondary changes in fluorescence not due to the interface closing, but instead are because of conformational changes in RFC sensed by interactions with an AF488 fluorophore.

## Conclusions

Multiple clamp loaders exist in eukaryotic cells to perform numerous functions in the DNA replication and repair pathways. Each clamp loader is composed of five subunits, with four subunits in common, and one subunit switched out for each clamp loader. The RFC clamp loader, which is involved in loading the PCNA sliding clamp onto DNA during DNA replication, is composed of subunits Rfc1-5. Rad24-RFC, which loads the 9-1-1 clamp onto DNA during the early steps of DNA repair, replaces the Rfc1 subunit with Rad24. This single subunit difference between the clamp loaders changes the sliding clamp and DNA structure recognized. RFC has been shown to target p/t DNA with a 3' recessed end (3'DNA), while Rad24-RFC targets p/t DNA with a 5' recessed end (5'DNA) (78, 100). To address how these clamp loaders recognize these DNA sites, DNA binding was measured for the two clamp loaders to assay specificity for different DNA structures in the presence and absence of PCNA. RFC DNA specificity was explored further using fluorescent PCNA closing and release assays to report on clamp loading on various DNA structures.

Equilibrium DNA binding assays indicated that RFC alone has the highest affinity for 5'DNA, based on the low value of the calculated $K_d$. In the presence of PCNA, RFC binding is stimulated to all DNA structures tested, but has the highest affinity for ssDNA and 5'DNA (Figure 5-1). This is surprising as RFC should target 3'DNA junctions. Measuring PCNA closing and release on different DNA structures, RFC loads clamps onto 3'DNA, ssDNA, dsDNA, and 5'DNA with similar observed rates (Figure 5-3 and Table 5-1). RFC alone does not appear to differentiate between DNA substrates.

It is interesting to compare clamp closing and release on the 3'DNA, dsDNA, and ssDNA by *E. coli* γ complex and the *S. cerevisiae* RFC. The γ complex showed a 20-fold difference in closing rates and a 3-fold difference in release rates comparing 3'DNA (30nt) to ssDNA and dsDNA (0nt, Table 4-1).The γ complex can differentiate between the DNA structures, whereas RFC cannot. This suggests that RFC does not require similar DNA contacts to load clamps, thus allowing RFC to be less specific.

Addition of 5'phosphates to the DNA structures in combination with RPA slows the PCNA closing reaction on 5'DNA approximately 50-fold. As with γ complex, the single-stranded binding protein prevents clamp loading on the wrong polarity of DNA (Table 4-6 and Table 5-3). This represents a conserved mechanism between the two clamp loaders. It is interesting to note that the 5'P is required for RPA to prevent clamp loading on 5'DNA, as RPA bound to DNA without a 5'P had no effect on clamp loading. This is different from the *E. coli* system, where addition of SSB alone slowed closing 50-fold, while addition of the 5'P and SSB slowed closing an additional 2-fold. It is not clear why the 5'P is required to see this affect in RFC but not γ complex. RPA is thought to bind ssDNA with a defined polarity, with the Rpa1 subunit oriented toward the 5' end of

the ssDNA and the Rpa3 subunit oriented toward the 3' end (139, 140). It is possible that when RPA binds the ssDNA at the p/t junction, RFC binding is either stimulated or repelled by an interaction with as specific orientation of RPA.

However, the defined orientation of RPA is presumably unaffected by the presence of a 5'P at the p/t junction, so the presence of a 5'P is key to preventing clamp loading on 5'DNA. No structure of RPA bound to a p/t junction is known, and there is little to no information about how SSBs in general interact at a p/t junction. It is possible that RPA interacts with the p/t junction, and the presence of a 5'P could change the interaction preventing RFC from binding. For example, the 5'P could provide an additional interaction with RPA making the RPA more stable on the p/t junction. When RFC tries to load PCNA on these sites, the RPA may block the RFC•PCNA complex (Figure 5-7).

Another possibility is that the presence of RPA forces RFC to interact with the p/t DNA in such a way that the 5'P inhibits clamp loading. In these assays, RFC may bind DNA in multiple modes to load clamps on the p/t DNA structure in the absence of RPA, such as binding via the single-stranded DNA overhang. The presence of RPA could promote a specific RFC binding mode that forces interactions with the p/t junction and therefore the 5'P, which may be an unfavorable interaction. The 5'P at the junction could inhibit DNA binding on its own, but in the absence of RPA, RFC can bind DNA in alternate manners that allow it to evade inhibition by the 5'P (Figure 5-8).

The Rad24-RFC clamp loader does not show strong specificity toward 5'DNA alone or in the presence of PCNA. In fact, DNA binding by Rad24-RFC alone was weak compared to RFC, as evidenced by the high $K_d$ values. PCNA stimulated binding to

5’DNA about 2-fold, but this was still weak compared to PCNA stimulation of RFC DNA binding. It is interesting that PCNA stimulated Rad24-RFC binding to 5’DNA only.

Rad24-RFC is known to bind PCNA but not produce a stable open population of PCNA clamps (46). It would be interesting to determine how the 9-1-1 clamp affects DNA binding by Rad24-RFC; it would be expected to stimulate binding to 5’DNA, as this is the structure where 9-1-1 is loaded. There are currently no assays in place to measure 9-1-1 clamp closing and release to compare clamp loading triggered by different DNA structures. However, the fluorescent ATP hydrolysis assay described in Chapter 3 could be used to measure activity of Rad24-RFC on different DNA substrates. This would give a more dynamic perspective of DNA specificity for Rad24-RFC and help to determine how Rad24-RFC recognizes 5’DNA junctions.

Multiple clamp and clamp loader systems exist in *S. cerevisiae* to perform a variety of functions in the DNA replication and repair pathways. The clamp loaders must be able to target the correct DNA site and load clamps efficiently to prevent DNA replication stalls, DNA damage, and propagation of unrepaired DNA. Determining how these clamp loaders recognize the correct structure of DNA is important for understanding not only the mechanism of these clamp loaders, but also understanding how they compare to clamp loaders from other species.

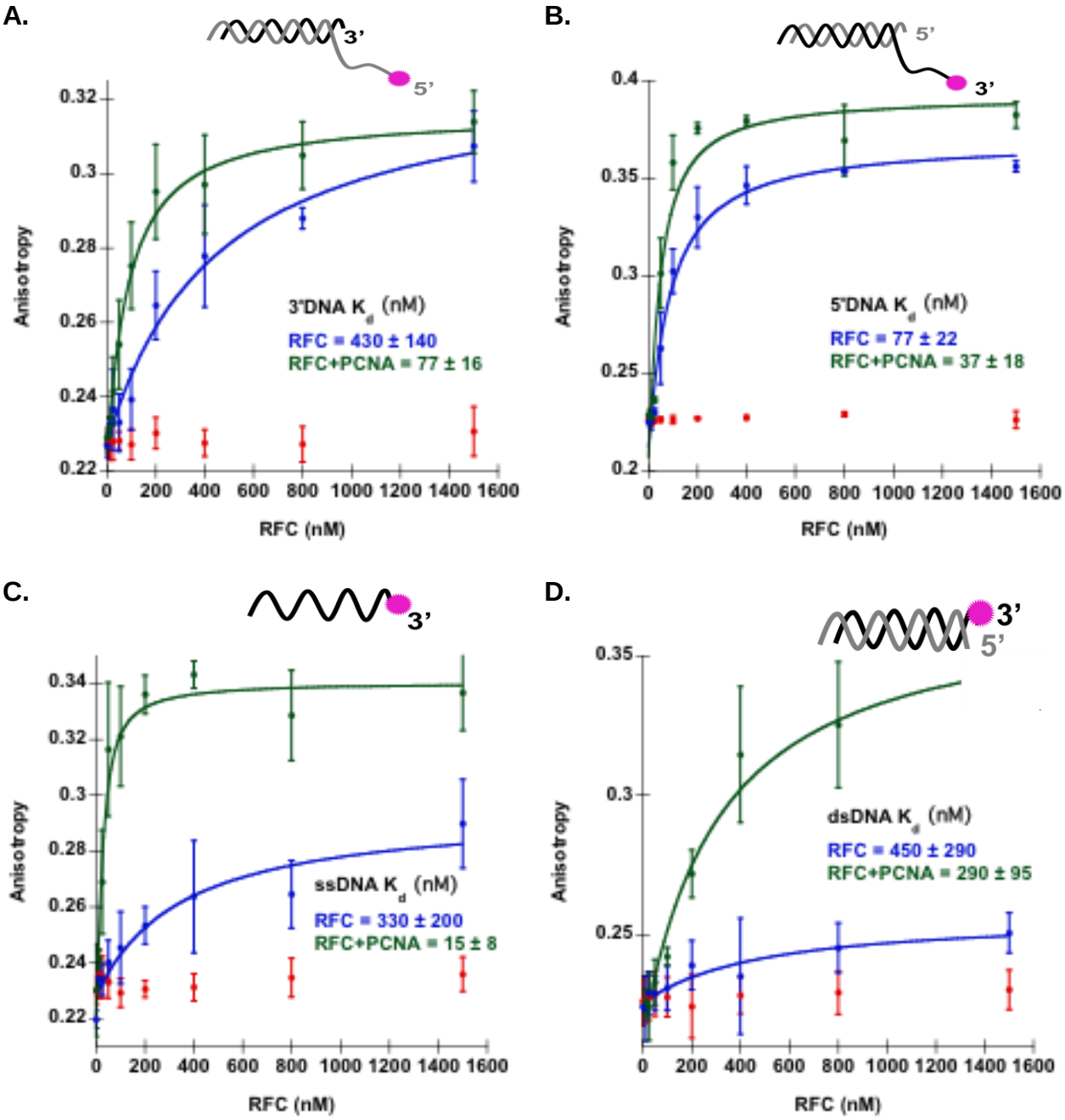


Figure 5-1. DNA binding by RFC is shown for 3'DNA (A), 5'DNA (B), ssDNA (C), and dsDNA (D). Anisotropy of free DNA is shown in red, DNA bound with RFC alone is shown in blue, and PCNA stimulated DNA binding is shown in green. $K_d$ values were calculated for DNA binding by RFC alone and RFC in the presence of PCNA using Equation 2-3.

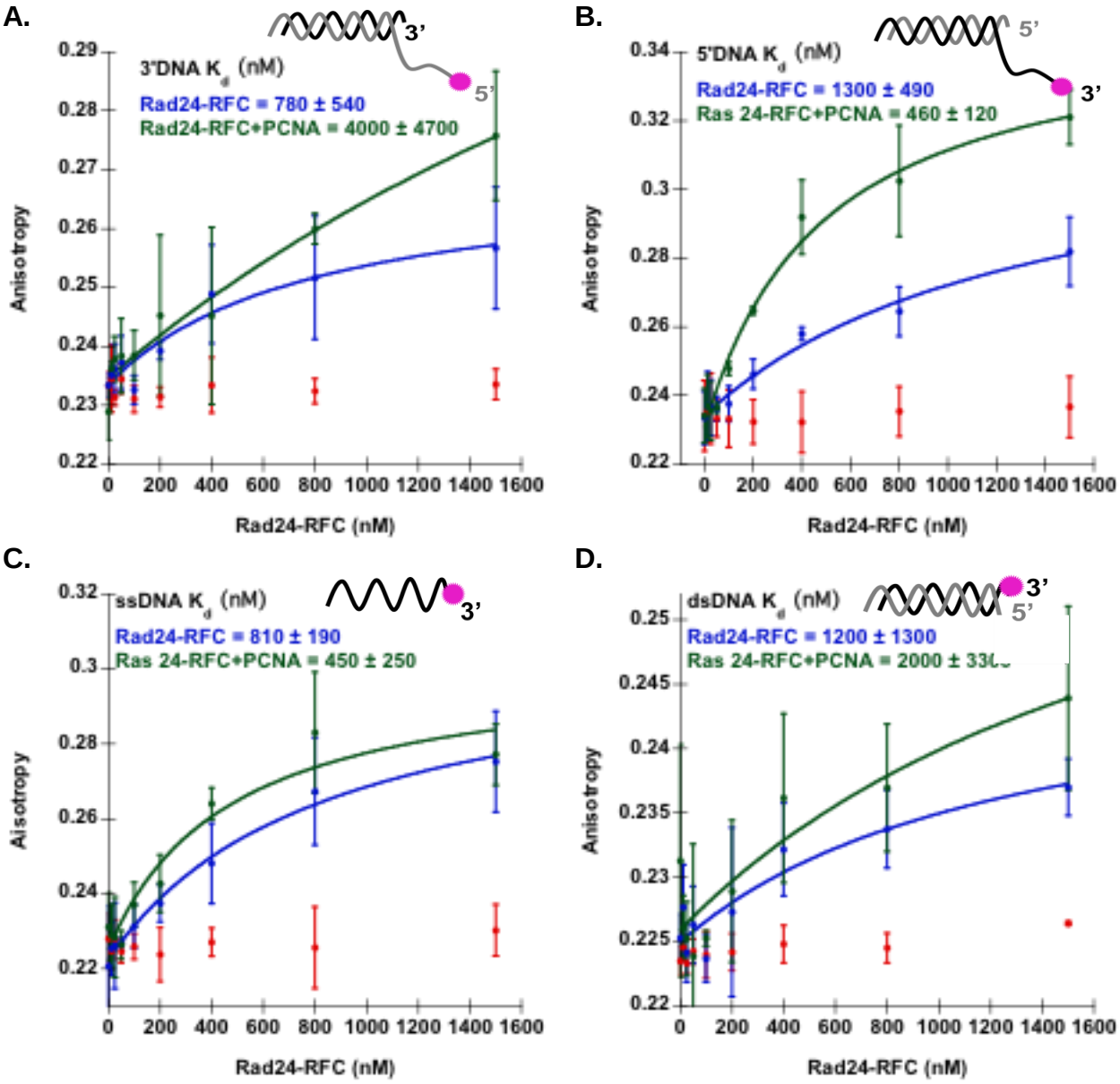


Figure 5-2. DNA binding by Rad24-RFC is shown for 3'DNA (A), 5'DNA (B), ssDNA (C), and dsDNA (D). Anisotropy of free DNA is shown in red, DNA bound with Rad24-RFC alone is shown in blue, and PCNA stimulated DNA binding is shown in green. $K_d$ values were calculated for DNA binding by Rad24-RFC alone and in the presence of PCNA using Equation 2-3.

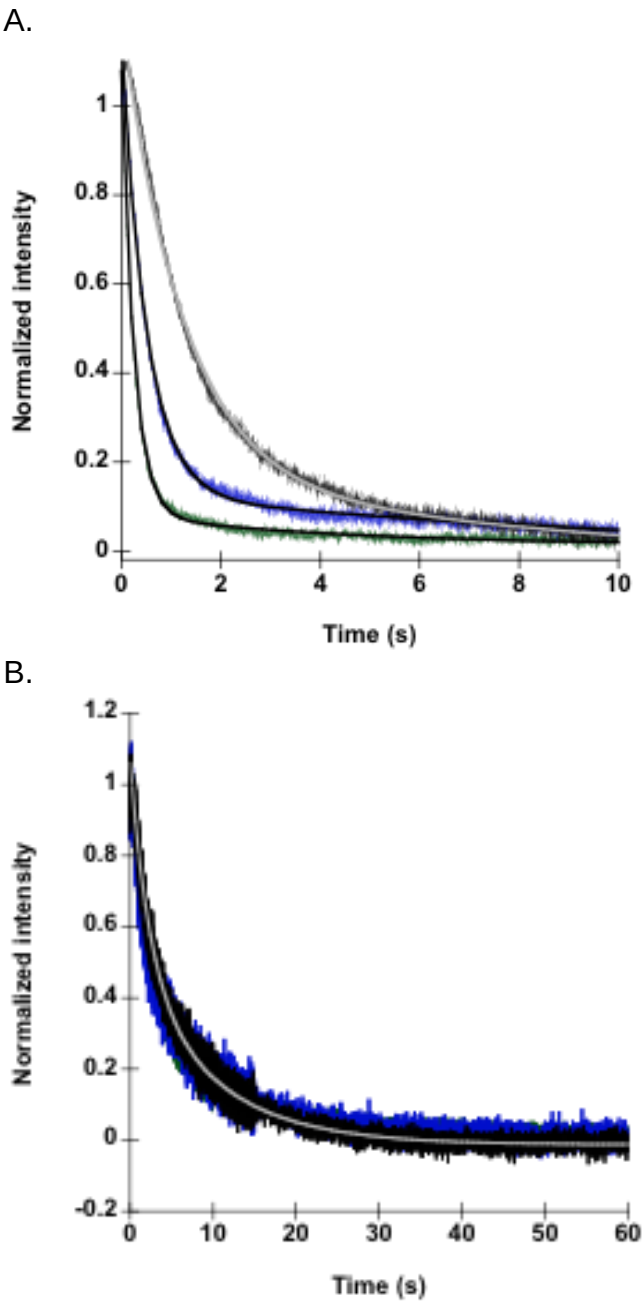


Figure 5-3. Representative time courses for PCNA closing and release on 3'DNA, ssDNA, and dsDNA. Closing is shown in A and release is shown in B are shown. Reactions contained 20 nM RFC complex, 20 nM labeled PCNA, 500 μM ATP, 40 nM DNA, and 200 nM unlabeled PCNA. DNA structures tested were 3'DNA in green (Table 2-2, JH9 and JH10), dsDNA in blue (Table 2-2, JH10), and ssDNA in black (Table 2-2, pIIIpI and JH4). Each DNA substrate was unlabeled, and the 3'DNA contained two symmetrical single stranded overhangs.

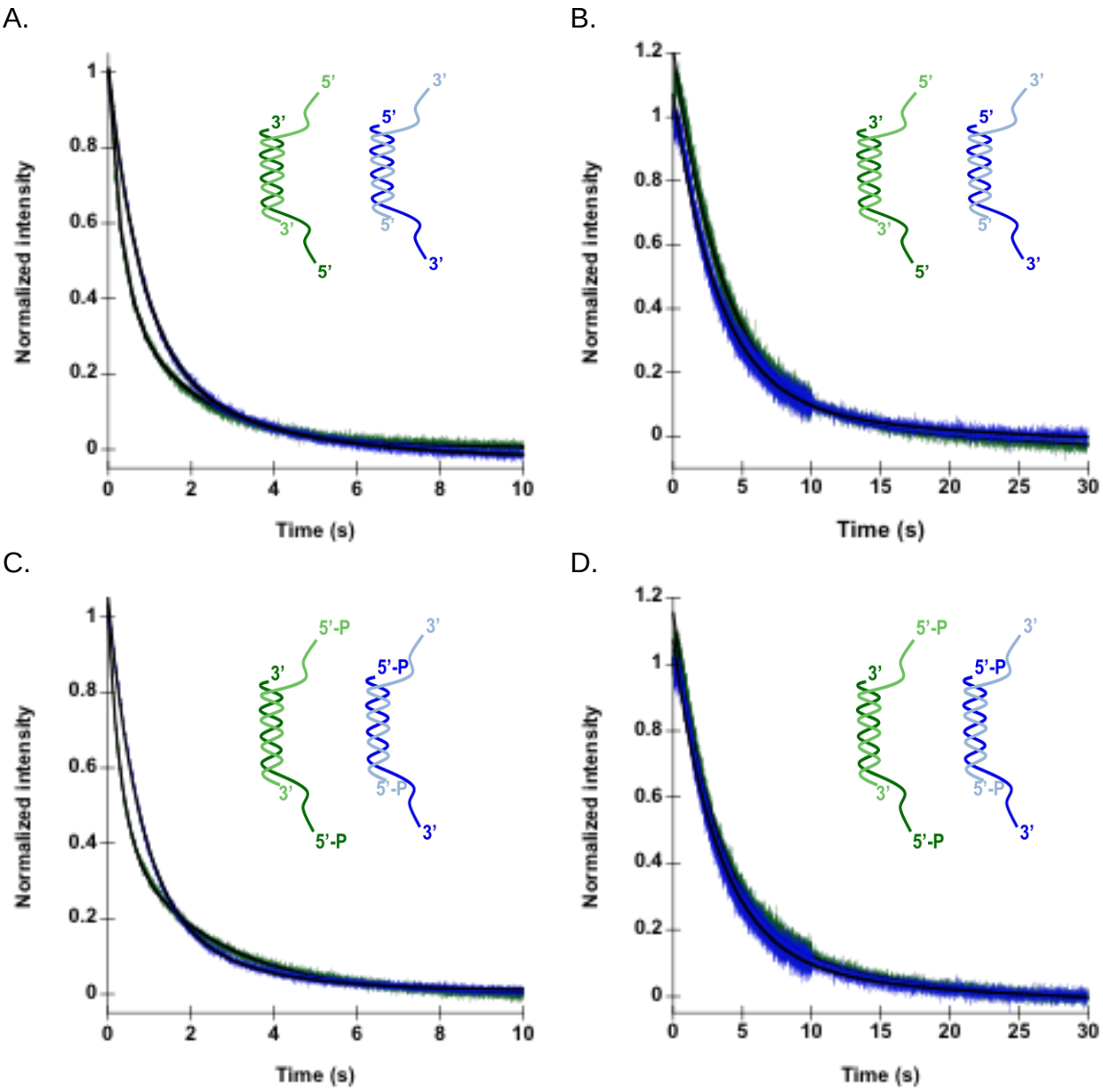


Figure 5-4. Representative PCNA closing time courses with 3'DNA (green) and 5'DNA (blue). Representative closing and release traces with DNA lacking a 5'P are shown in A and B respectively. Representative closing and release time courses where the DNA had 5'P added are shown in C and D. Reactions contained 20 nM RFC complex, 20 nM PCNA-AF488, 500 μM ATP, 40 nM DNA, and 200 nM unlabeled PCNA. DNA structures tested were 3'DNA (Table 2-2, JH9 and JH10), and 5'DNA (Table 2-2, JH10 and JH15).

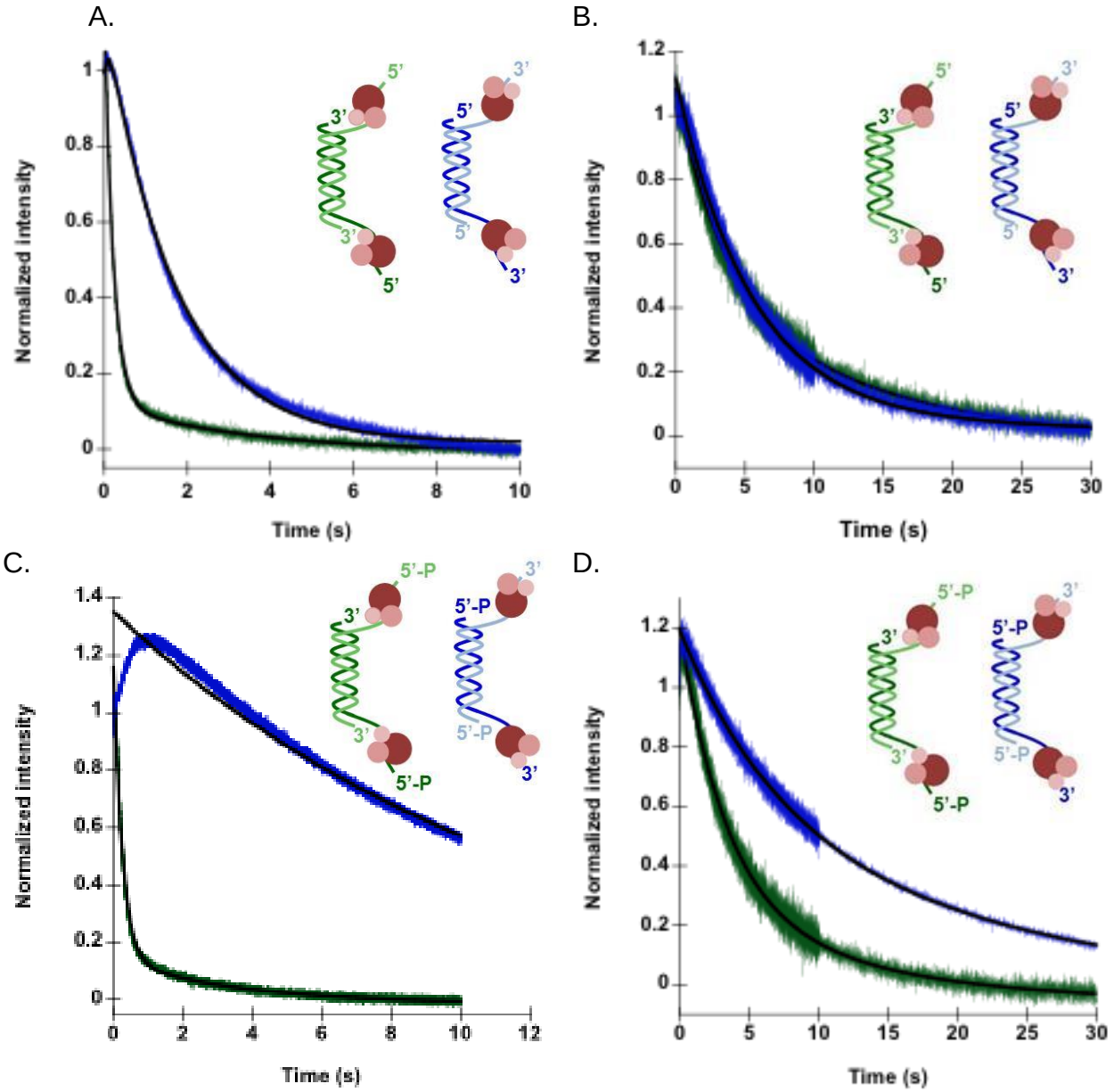


Figure 5-5. Representative PCNA closing time courses with 3'DNA (green) and 5'DNA (blue) in the presence of RPA are shown. Representative closing and release traces with DNA lacking a 5'P are shown in A and B respectively. Representative closing and release time courses where the DNA had 5'P added are shown in C and D. Reactions contained 20 nM RFC complex, 20 nM PCNA-AF488, 0.5 mM ATP, 40 nM DNA, and 200 nM unlabeled PCNA. DNA structures tested were 3'DNA (Table 2-2, JH9 and JH10), and 5'DNA (Table 2-2, JH10 and JH15).

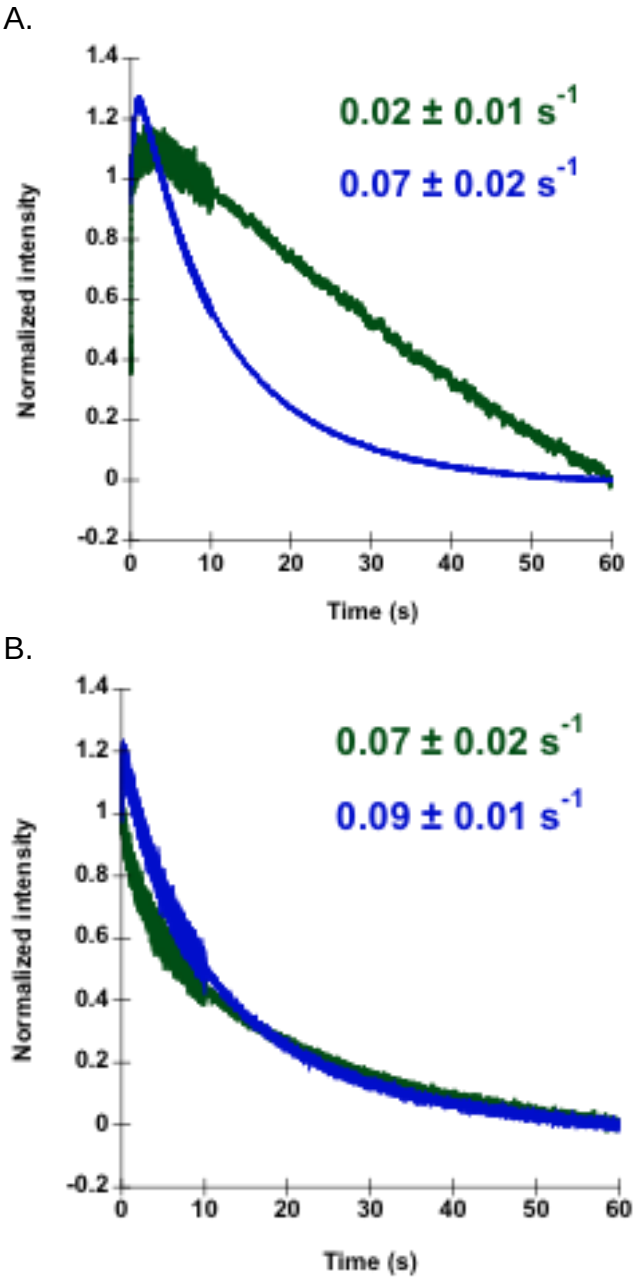


Figure 5-6. PCNA closing and release comparing 5'DNA-P in the presence of RPA to reactions with no DNA. Time courses are shown comparing PCNA closing (A) and release (B) in the absence of DNA (green) or the presence of 5'DNA-P and RPA (blue). Observed rates are reported in the graph for each trace. Reactions in green contained 20 nM RFC, 20 nM labeled PCNA, 500 μM ATP, and 400 nM PCNA. Reactions in blue contained the same components with the addition of 40 nM 5'DNA-P and 400 nM RPA.

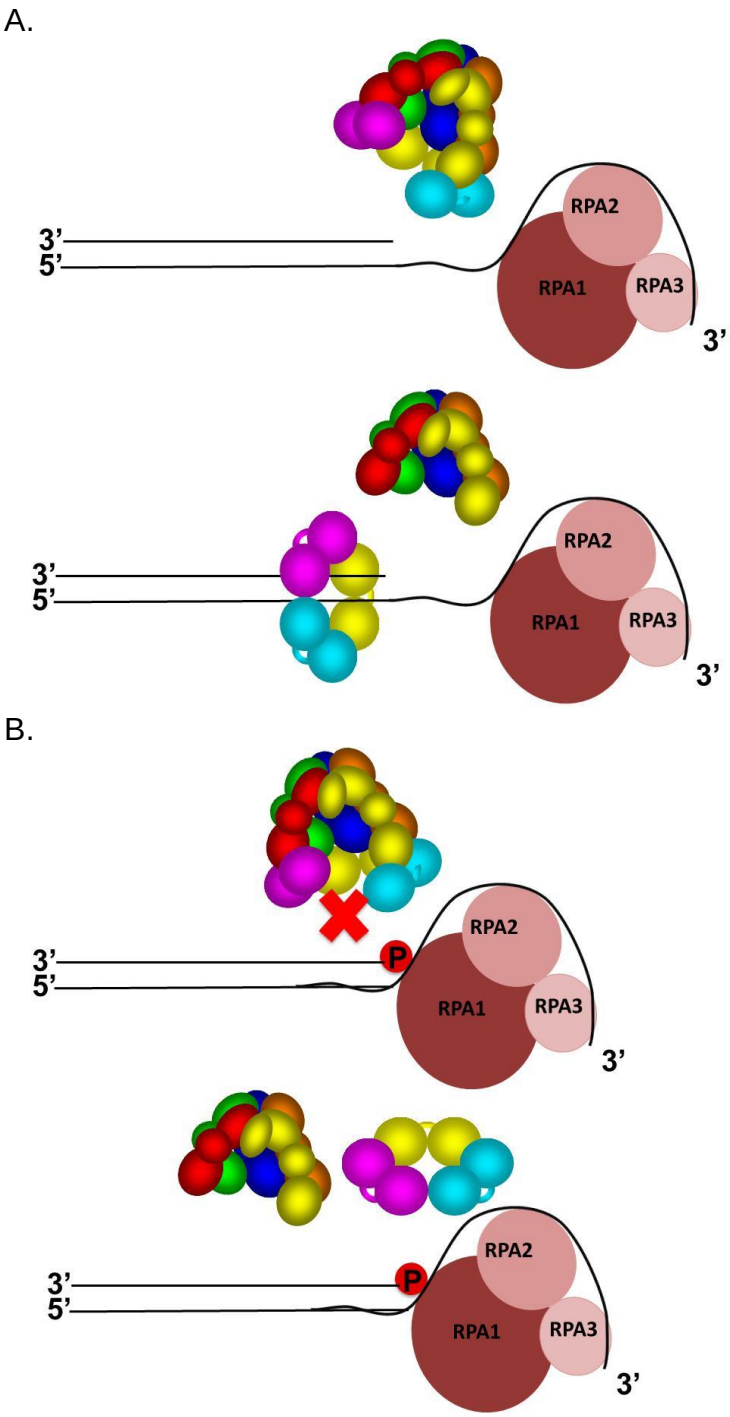


Figure 5-7. RPA could physically interact with the 5'P preventing clamp loading. A shows a cartoon of clamp loading in the absence of a 5'P (either 3'DNA or 5'DNA without a 5'P). RFC can either load PCNA around the RPA or moves RPA to load PCNA. B shows a cartoon of the inhibition of clamp loading when the 5'P is present. If RPA has tight interactions with the 5'P, RFC cannot move the RPA and there would be no gap between the RPA and the duplex region of DNA to load PCNA. Therefore, clamp loading would be inhibited.

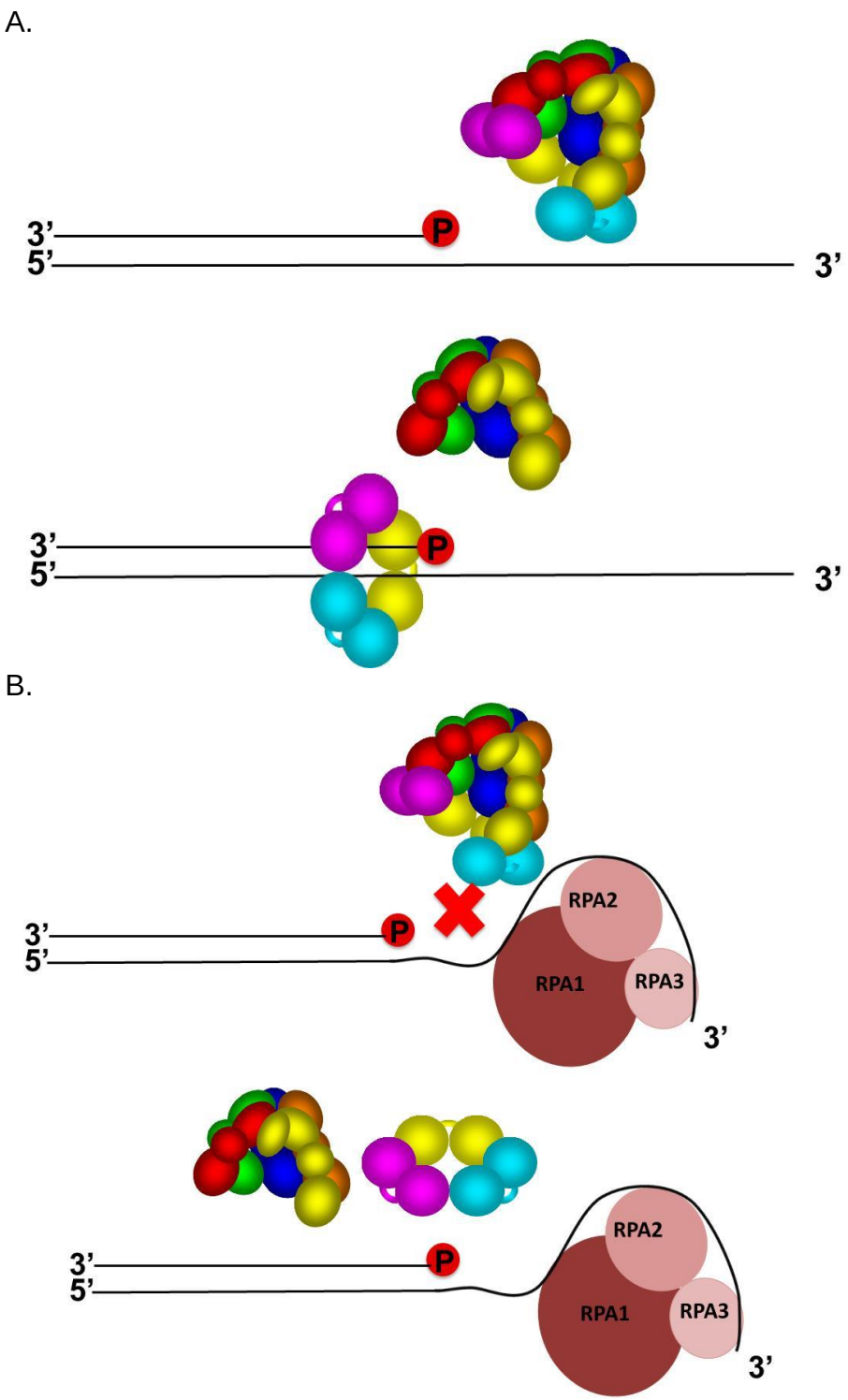


Figure 5-8. RPA could prevent alternate DNA binding modes by RFC. A shows that RFC could bind DNA in a different manner, such as the ssDNA when a 5’P is present that would allow it to still load clamps around DNA. B shows that in the presence of RPA, this alternate DNA binding mode would be suppressed, thus forcing RFC to interact with the p/t junction containing the 5’P. The presence of the 5’P would then suppress clamp loading.

Table 5-1. Calculated observed rates for PCNA closing and release with 3'DNA, ssDNA, and dsDNA.

| DNA substrate | PCNA closing | | PCNA release | |
|---|---|---|---|---|
| | $k_{obs1}$ ($s^{-1}$) | $k_{obs2}$ ($s^{-1}$) | $k_{obs1}$ ($s^{-1}$) | $k_{obs2}$ ($s^{-1}$) |
| **3'DNA** | 2.9 ± 0.3 | 0.44 ± 0.07 | 0.32 ± 0.03 | 0.10 ± 0.05 |
| **dsDNA** | 1.7 ± 0.46 | 0.29 ± 0.07 | 0.34 ± 0.08 | 0.11 ± 0.03 |
| **ssDNA** | 0.99 ± 0.22 | 0.47 ± 0.07 | 0.36 ± 0.23 | 0.12 ± 0.01 |

Table 5-2. Calculated observed rates for PCNA closing with 3'DNA and 5'DNA with and without 5'phosphates.

| DNA substrate | PCNA closing | | PCNA release | |
|---|---|---|---|---|
| | $k_{obs1}$ ($s^{-1}$) | $k_{obs2}$ ($s^{-1}$) | $k_{obs1}$ ($s^{-1}$) | $k_{obs2}$ ($s^{-1}$) |
| **3'DNA** | 2.9 ± 0.3 | 0.44 ± 0.07 | 0.32 ± 0.03 | 0.10 ± 0.05 |
| **3'DNA-P** | 3.3 ± 0.15 | 0.44 ± 0.01 | 0.31 ± 0.03 | 0.09 ± 0.02 |
| **5'DNA** | 1.2 ± 0.03 | 0.29 ± 0.03 | 0.31 ± 0.02 | 0.05 ± 0.04 |
| **5'DNA-P** | 1.3 ± 0.08 | 0.27 ± 0.03 | 0.45 ± 0.16 | 0.16 ± 0.09 |

Table 5-3. Calculated observed closing and release rates for 3'DNA and 5'DNA +RPA.

| DNA substrate | PCNA closing | | PCNA release | |
|---|---|---|---|---|
| | $k_{obs1}$ ($s^{-1}$) | $k_{obs2}$ ($s^{-1}$) | $k_{obs1}$ ($s^{-1}$) | $k_{obs2}$ ($s^{-1}$) |
| **3'DNA+RPA** | 4.6 ± 0.7 | 0.26 ± 0.02 | 0.31 ± 0.05 | 0.09 ± 0.02 |
| **3'DNA-P+RPA** | 4.4 ± 0.5 | 0.33 ± 0.07 | 0.34 ± 0.03 | 0.08 ± 0.04 |
| **5'DNA+RPA** | 0.79 ± 0.04 | 0.35 ± 0.02 | 0.22 ± 0.08 | 0.09 ± 0.07 |
| **5'DNA-P+RPA** | 0.07 ± 0.02 | N/A | 0.09 ± 0.01 | N/A |

N/A indicates no second rate was observed.

# CHAPTER 6
# THE ROLE OF THE RFC1 N-TERMINAL DOMAIN OF *S. CEREVISIAE* RFC IN PCNA LOADING

## Background

The RFC clamp loader is a member of the $AAA^+$ family of ATPase enzymes. RFC is composed of five subunits, Rfc1-5, which form a cap like structure (55, 141, 142). In general, clamp loader subunits share three domains. The N terminal domain and the middle domain in each subunit are highly conserved with other $AAA^+$ proteins and contain the ATP binding pockets. The C-terminal domains in each the subunits show divergence from the other $AAA^+$ proteins and are responsible for oligomerization of the clamp loader forming the conserved cap like structure (55, 143). Rfc1 subunit contains these domains as well as two extra domains, one at the N-terminal, and one at the C-terminal (Figure 6-1). The N-terminal domain (NTD) of Rfc1 has ligase, PARP, and BRCT homology domains, but it is unclear what these domains do and if they even play a role in clamp loading, or if they play a role in signaling at the replication fork (56, 57).

Truncation of the NTD of Rfc1 (282 amino acids in the *S. cerevisiae* Rfc1 and 555 amino acids in human Rfc1) produces clamp loaders thought to be proficient in clamp loading. Previous *in vitro* data showed that RFC with truncated Rfc1 (trRFC) had similar activity as RFC with the full length Rfc1 (flRFC). The only difference in activity was that flRFC appeared to stick non-specifically to single-stranded DNA, slowing the clamp loading reaction, whereas trRFC did not (10, 87, 95, 138). This truncation was introduced to *S. cerevisiae* to determine the effect of this mutation *in vivo*; no growth defect could be discerned under normal conditions. trRFC did not affect *S. cerevisiae*

growth even in the presence of UV irradiation or hydroxyurea; however, there was a slight deficiency in growth in the presence of MMS (138).

Other experiments however, would indicate trRFC is not proficient in clamp loading. In the Benkovic laboratory, PCNA loading by trRFC was observed to be weak and occurred successfully approximately one out or every eight or nine clamp loading attempts. RFC was therefore suggested to be an inefficient enzyme that acted stochastically instead of with a defined catalytic mechanism (45). *In vivo*, it is unlikely that RFC would be an inefficient enzyme, so it is possible that this result is due to the fact that trRFC was used. The Hingorani laboratory observed weaker ATP binding and hydrolysis by trRFC compared to flRFC (72). These data would support the idea that trRFC and flRFC have differences in clamp loading activity.

Recently, a truncation of human RFC was discovered in cells affected with Hutchinson-Gilford Progeria syndrome (HGPS), a disease characterized by DNA replication arrest and early onset aging. The RFC complex in these cells lacked the first approximately 75 kD of Rfc1, which generally aligns with the NTD deleted in *S. cerevisiae* trRFC (103). The work suggested that this truncation of RFC found in the HGPS cells could not load PCNA clamps efficiently, thus causing the replication defect and early onset aging phenotype presented in HGPS. This hypothesis suggests that the NTD of Rfc1 is important for clamp loading, and therefore trRFC might not have similar clamp loading activity as flRFC.

To compare clamp loading by the *S. cerevisiae* trRFC and flRFC, fluorescence-based assays were used to measure various steps of the clamp loading cycle. Specifically, equilibrium PCNA binding and opening were used to compare PCNA

interactions between trRFC and flRFC in the presence and absence of ATP. Pre-steady state PCNA closing and release were measured for each clamp loader to determine how the truncation of the Rfc1 subunit affects clamp loading.

## Comparing the PCNA Interactions of flRFC and trRFC

Equilibrium PCNA binding and opening was measured for both flRFC and trRFC. Results of these assays serve to compare the interactions between the clamp loaders and the PCNA clamp. Assays were performed in the absence and presence of ATP to measure ATP independent and ATP dependent PCNA clamp interactions. Final concentrations of protein and ATP are 20 nM fluorescent PCNA, 0.5 mM ATP (if present) and RFC concentrations ranging from 0 nM to 300 nM. $K_d$ values for each were calculated using Equation 2-4 and are reported in the graphs.

### PCNA binding

PCNA binding was measured using a PCNA clamp labeled with MDCC on the surface that interacts with RFC. When RFC binds PCNA-MDCC, the fluorescence of MDCC is about two-times higher than when PCNA-MDCC is free in solution (Marzahn, in preparation). The average of three independent PCNA binding experiments is shown in Figure 6-2; error bars represent a standard deviation.

The intensity of the fluorescence change as RFC binds PCNA-MDCC is reported as a function of RFC concentration in the presence (blue) and absence (green) of ATP for trRFC (A) and flRFC (B). Interestingly, in the presence of ATP, flRFC bound PCNA with an approximately 35-fold lower $K_d$ than trRFC, indicting flRFC binds PCNA with higher affinity than trRFC. The fold-change in MDCC intensity as the RFC complexes bind PCNA-MDCC saturates at around 1.6 – 1.7 for each clamp loader. This indicates

that each RFC complex interacts with the MDCC fluorophores on PCNA in the same manner. Other binding modes could result in more or less contacts with the fluorophores and thus different levels of saturating fluorescence.

Both flRFC and trRFC bind PCNA in the absence of ATP similarly, with $K_d$ values of 400 – 500 nM. PCNA binding in the absence of ATP is weak compared to in the presence of ATP; it is approximately 60-fold weaker for trRFC and approximately 2000-fold lower for flRFC. This is consistent with results from the *E. coli* clamp loader, $\gamma$ complex, which can also bind the clamp in an ATP independent manner, albeit significantly weaker than in the presence of ATP (120).

**PCNA opening**

Equilibrium PCNA opening was measured using a PCNA clamp labeled with AF488 at either end of the PCNA interface. When PCNA-AF488 is closed, the fluorophores are in close proximity and self-quench. When PCNA-AF488 is opened by RFC, the fluorophores move apart, and the self-quench is relieved (46). PCNA opening was measured in the presence and absence of ATP for both trRFC and flRFC. Averages of three independent experiments are shown in Figure 6-3 with error bars representing a standard deviation.

PCNA opening as a function of trRFC (A) and flRFC (B) concentration are shown in the presence (blue) or absence (green) of ATP. The $K_d$ for PCNA opening is about 20-fold lower for flRFC as for trRFC, indicating higher PCNA affinity and is consistent with higher binding affinity measured in Figure 6-2. Interestingly, the total intensity fold-change for flRFC is greater than for trRFC, 1.8 versus 1.5. One possible reason for the difference in fold-change is that flRFC is opening a greater population of PCNA clamps

than trRFC. The second possible reason is that the extra NTD of flRFC is contacting one or more AF488 fluorophores, thus resulting in higher total intensity.

PCNA opening in the absence of ATP resulted in no AF488 intensity change as a function of RFC concentration and therefore the $K_d$ could not be calculated. This would indicate that neither RFC complex can open PCNA in the absence of ATP. This is consistent with results from the *E. coli* clamp loader, $\gamma$ complex, which also requires ATP to open the sliding clamp (69).

## PCNA Closing and Release Comparing trRFC and flRFC

Pre-steady state PCNA closing and release assays were performed to determine if there is a difference in clamp loading between trRFC and flRFC. Assays were performed in the stopped-flow to monitor the first few seconds of the reaction. The stopped-flow mixing scheme is shown in Figure 2-4. Briefly, a solution of RFC, fluorescent PCNA, and ATP were mixed together for 4 s and then mixed with a syringe containing DNA, ATP, and excess unlabeled PCNA as chase. Final concentrations of protein and nucleotide are 20 nM RFC, 20 nM fluorescent PCNA, 40 nM DNA (if present), 0.5 mM ATP, and 200 nM unlabeled PCNA.

### PCNA release

PCNA release was measured using the PCNA-MDCC mutant described above. Figure 6-4 shows representative time courses for PCNA release in the presence (A) or absence (B) of DNA for trRFC (green) and flRFC (blue). Observed rates for reactions with DNA are calculated using a double exponential decrease shown in Equation 2-5, while the observed rate for time courses without DNA were calculated using a single

exponential decrease in Equation 2-4. Average observed rates for three independent experiments are reported in Table 6-1.

PCNA release time courses in the presence of DNA for both trRFC and flRFC show biphasic kinetics. The biphasic kinetics are consistent with previous results showing that at least two populations of RFC•PCNA•DNA complexes form, where one complex loads PCNA on DNA rapidly in a manner dependent on ATP hydrolysis, while the second loads slowly in an ATP hydrolysis independent manner (45). Therefore, the rapid phase of the PCNA release reactions likely represents the population of RFC•PCNA complexes that dissociates in an ATP hydrolysis dependent manner and represents an active clamp loading event. The slow rate represents a population of RFC•PCNA than does not participate in an active clamp loading event, and instead passively dissociates. This is supported by the fact that the slow observed rates for each RFC complex is within standard deviation of the observed rates in the absence of DNA (Table 6-1). In the absence of DNA, the RFC•PCNA complex passively dissociates in a manner independent of ATP hydrolysis and therefore does not represent an active release reaction.

The observed rates measured in both the presence and absence of DNA for trRFC are within standard deviation of those measured for flRFC (Table 6-1). This indicates that PCNA release occurs similarly for each RFC complex. This also suggests that DNA binding by both RFC•PCNA complexes triggers similar conformational changes at similar rates to promote PCNA release.

**PCNA closing**

PCNA closing was measured using the PCNA-AF488 mutant described above. Representative time courses for trRFC (green) and flRFC (blue) in the presence (A) and absence (B) of DNA are shown in Figure 6-5. Observed rates are calculated using a double exponential decrease shown in Equation 2-5 for reactions with DNA while the observed rate for time courses without DNA were calculated using a single exponential decrease in Equation 2-4. Average observed rates for three independent experiments are reported in Table 6-2.

As seen with the PCNA release, both trRFC and flRFC show biphasic closing time courses, with fast rates that are within standard deviation of one another. However, the slow rates are no longer within standard deviation of each other. The slower observed rate for PCNA closing by trRFC is within standard deviation of the passive closing rate in the absence of DNA (Figure 6-5 B and Table 6-2). Like the PCNA release reactions above, the slow closing rate likely represents a population of RFC•PCNA complexes that dissociate in a passive manner. The fast rate then represents the population of RFC•PCNA complexes that dissociate in an active, ATP dependent manner.

The slower rate in PCNA closing time courses for flRFC is about 4-fold faster than for passive PCNA closing by flRFC in the absence of DNA. This would indicate that this slower phase does not represent a population of PCNA clamps closing in a passive manner. It is interesting to note that the observed rate of this phase is within standard deviation of the fast PCNA release rate for flRFC reported in Table 6-1. This observation is also consistent with PCNA closing reactions for flRFC performed with all

other DNA substrates as well (Tables 5-1, 5-2, and 5-3). Taken together, this would seem to indicate that there is some interaction between flRFC and one or more AF488 molecules that can also sense PCNA release, and this is reflected in the biphasic observed rates. This is supported by equilibrium opening data from Figure 6-3, which shows that flRFC promotes a greater total fluorescent intensity change than trRFC. This could be due to contacts made with one of the AF488 fluorophores on PCNA by flRFC, but not trRFC. For simplicity, when referring to the observed PCNA closing rate by each RFC complex, the fast observed rate will be referenced, as this is the observed rate that corresponds to PCNA closing.

The PCNA closing rates for trRFC and flRFC are within standard deviation of each other: $3.5 \pm 0.3\ s^{-1}$ and $2.9 \pm 0.3\ s^{-1}$, respectively. Because the observed rates are similar, the RFC complexes appear to close PCNA in a similar fashion. The observed closing rates in the absence of DNA are not biphasic and are within standard deviation for the two clamp loaders. This indicates both active and passive clamp closing by the two clamp loaders are similar.

## Conclusions

trRFC and flRFC were compared in these studies to understand the role of the NTD of Rfc1 in the clamp loading mechanism. trRFC contains an Rfc1 subunit with a deletion of the first 282 amino acids containing an NTD of unknown function, while flRFC contains a Rfc1 subunit with no truncation. Previous experiments using trRFC yield conflicting results as to whether this complex functions similarly to flRFC both *in vitro* and *in vivo*. The goal of this work was to compare trRFC and flRFC side by side using *in vitro* fluorescence-based assays that report on various aspects of the clamp

loading reaction. Understanding how and at what step the two clamp loaders differ can help to determine the function of the NTD.

The biggest difference between the two clamp loader complexes is that flRFC has higher affinity interactions with PCNA than trRFC. The $K_d$ of PCNA opening and binding by flRFC are an order of magnitude lower than trRFC (Figures 6- 2 and 3). The $K_d$ is an equilibrium measurement of two components, the $k_{on}$ and $k_{off}$, which measure the rate of RFC•PCNA formation and disassociation, respectively. The $k_{off}$ can be measured from the PCNA closing and release reactions in the absence of DNA because these reactions measure the disassociation of the RFC•PCNA complex. Because the $k_{off}$ rates are similar for both clamp loaders in the closing and release assays (Table 6-1 and 2), the differences in $K_d$ values can be attributed to a faster $k_{on}$ for flRFC. Therefore, the extra NTD of flRFC does not prevent the PCNA•RFC complex from falling apart, instead, it plays a role in promoting faster formation of PCNA•RFC complex. The NTD of Rfc1 could make more interactions with PCNA that would promote faster clamp association. It was also reported that more ATP molecules bind the flRFC (72), so this might help to promote conformational changes that allow the PCNA•RFC complex to form at a faster rate.

Rates of PCNA closing and release for trRFC and flRFC are within standard deviation and therefore do not differ between clamp loaders. This indicates that the DNA induced intramolecular reactions and conformational changes promoting clamp closing and release are similar for each clamp loader.

There are still aspects of the clamp loading cycle that could be investigated using the fluorescent assays available, such as DNA binding to determine if there are

differences in how the two clamp loaders interact with DNA. The presence of the NTD was reported to cause non-specific binding to single-stranded DNA adversely affecting the clamp loading reaction (10, 87, 95, 138). Figure 5-1 shows that trRFC binds ssDNA in the presence of PCNA with higher affinity than the correct polarity of DNA, so it is not clear if flRFC has even more non-specific ssDNA binding activity or if the two clamp loaders both bind ssDNA nonspecifically. It would also be interesting to measure ATP hydrolysis by the clamp loaders using the PBP-MDCC assay described in Chapter 3 to measure differences in the first turnover of ATP hydrolysis. This could give the number of ATP molecules hydrolyzed per clamp loader, and verify claims that flRFC hydrolyzes more ATP in the first turnover than trRFC (72). The steady state ATP hydrolysis rate could also be determined from the assay, which measures the turnover of the RFC complex, or the $k_{cat}$. The $k_{cat}$ for each RFC complex can be compared to determine how the NTD affects the rate of the overall clamp loading reaction.

Based on these results, there are differences in the mechanism of the two clamp loaders indicating that the NTD plays a role in the clamp loading reaction. Specifically, it appears that flRFC has higher affinity interactions with PCNA, which could allow more efficient clamp loading based on more efficient RFC•PCNA complex formation. The NTD contains BRCT and PARP homology regions as well (56, 57), which would suggest roles outside the clamp loading reaction, such as signaling at a replication fork or mediating interactions in a DNA damage pathway. However, this work shows that the NTD does play a role in clamp loading, and therefore is important for RFC activity.

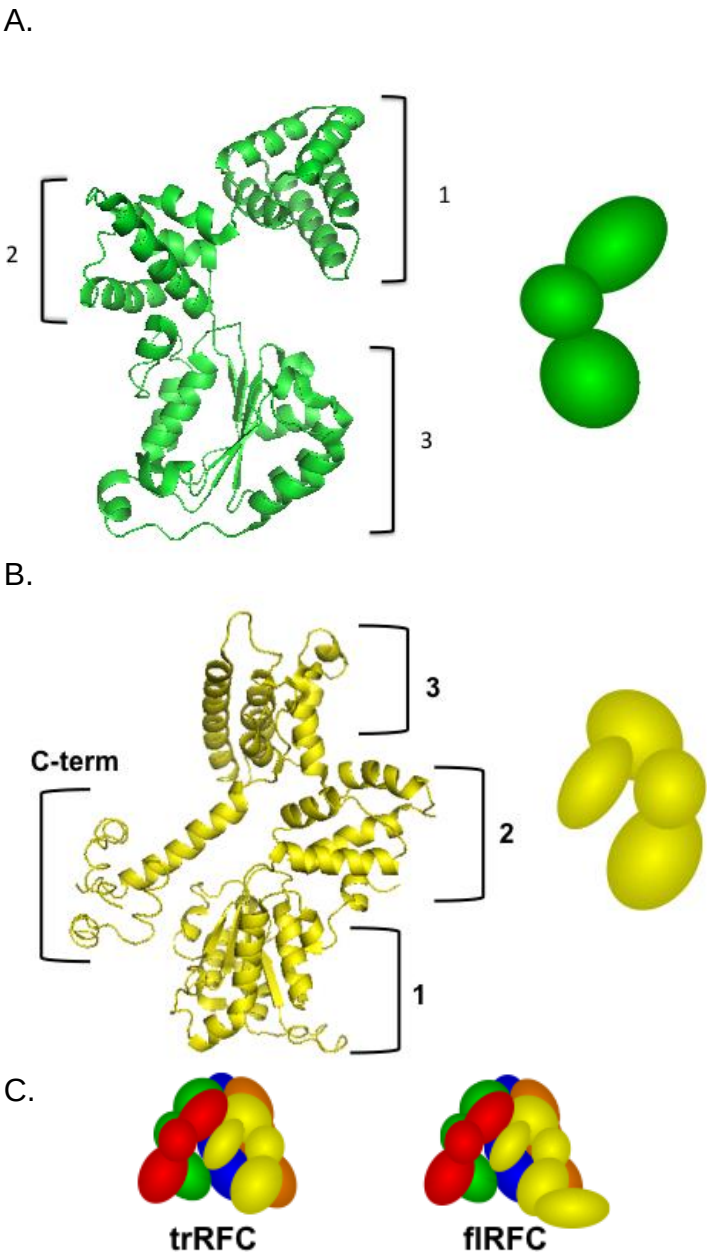


Figure 6-1. Structure of the RFC subunits and complexes used. A shows the structure of Rfc4 which contains the three conserved domains of all clamp loaders: N-terminal (1) and middle (2) contain the conserved AAA+ ATP binding pocket, while the C-terminal domain (3) is involved with subunit oligomerization. B shows the structure of the Rfc1 subunit. The extra C-terminal region is highlighted, but the extra N-terminal domain (NTD) is not shown (37). C shows cartoons of the two RFC complexes used in these studies.

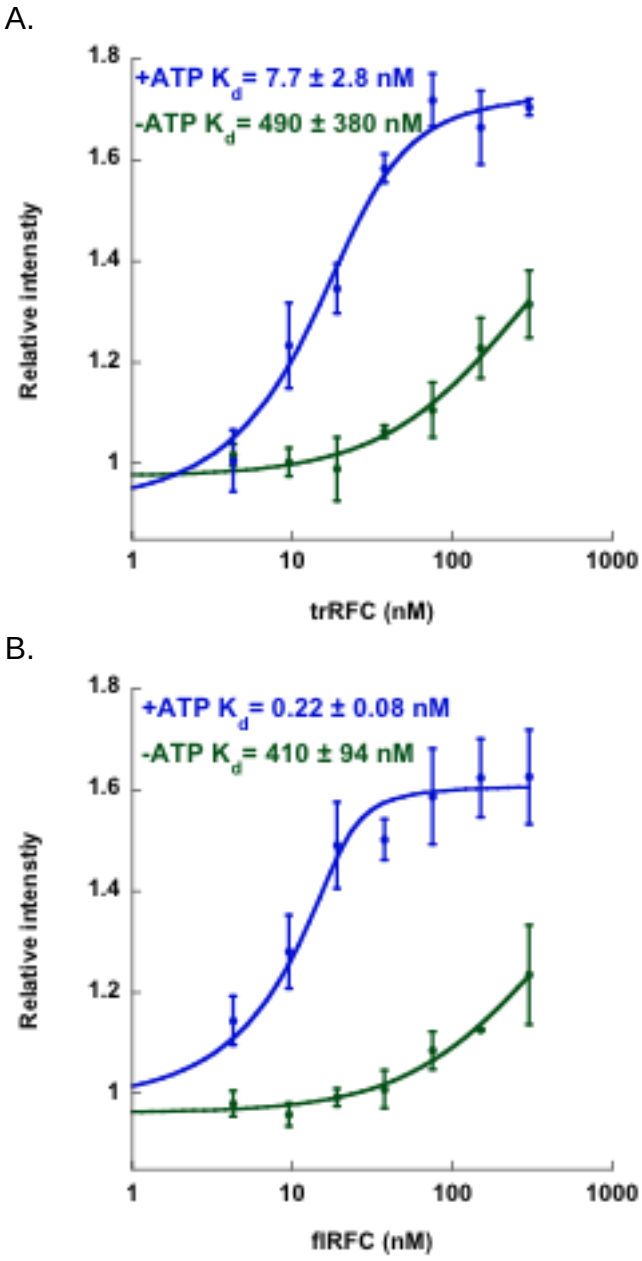


Figure 6-2. Equilibrium PCNA binding titrations for trRFC (A) and flRFC (B) are shown. Experiments are performed in the presence (blue) and absence (green) of 0.5 mM ATP. Final protein concentration was: 0 – 300 nM RFC, 20 nM PCNA-MDCC. $K_d$ values were calculated using equation 2-4.

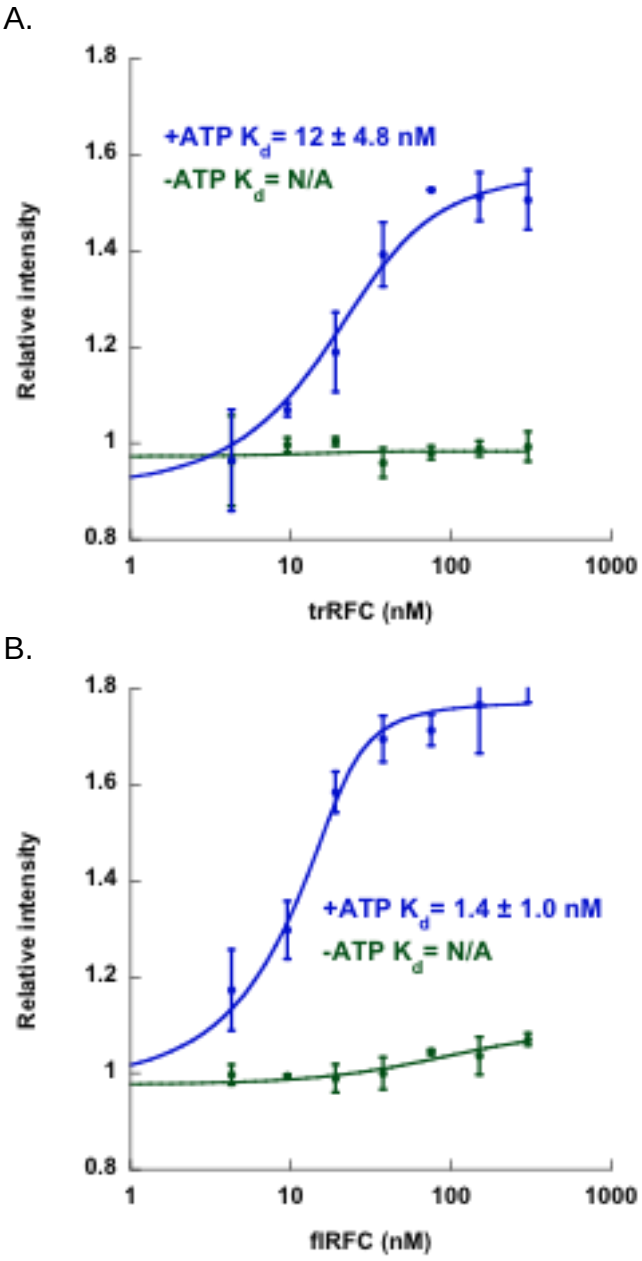


Figure 6-3. Equilibrium PCNA opening titrations for trRFC (A) and flRFC (B) are shown. Experiments are performed in the presence (blue) and absence (green) of 0.5 mM ATP. Final protein concentration was: 0 – 300 nM RFC and 20 nM PCNA-AF488. $K_d$ values were calculated using equation 2-4.

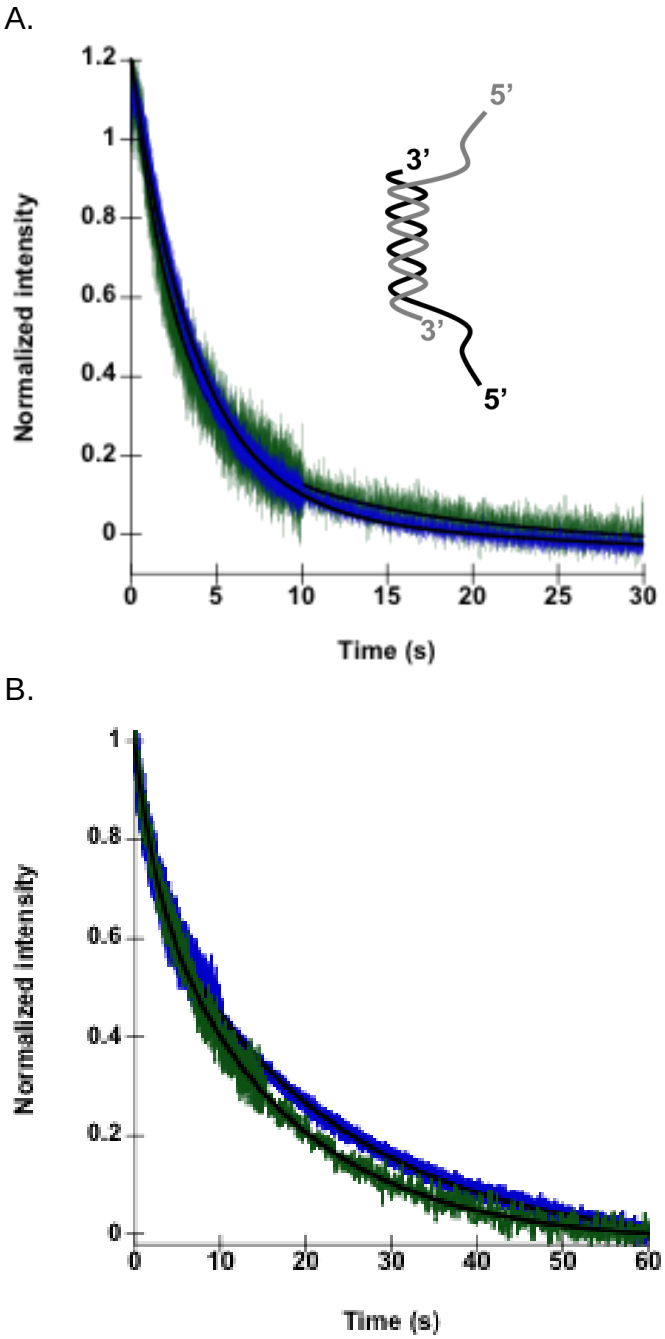


Figure 6-4. Representative time courses for PCNA release by trRFC (green) and flRFC (blue) are shown. Time courses in A contained 40 nM DNA, while time courses in B lacked DNA. Final concentration of proteins and DNA are 20 nM RFC, 20 nM PCNA-AF488, 0.5 mM ATP, 40 nM DNA (or none in B), and 200 nM unlabeled PCNA. The DNA used in these assays was composed of JH9 and JH10 to make a 30nt duplex region and two symmetrical 30nt single-stranded overhangs.

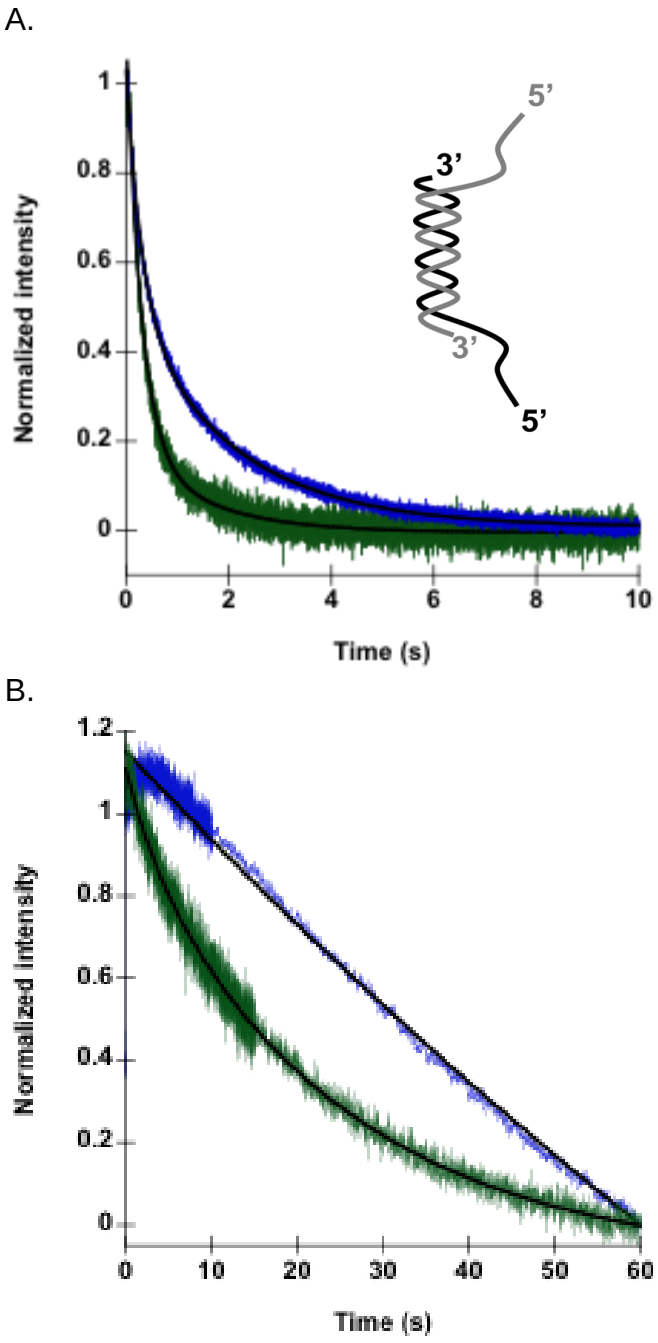


Figure 6-5. Representative time courses for passive PCNA closing by trRFC (green) and flRFC (blue) are shown. Time courses in A contained 40 nM DNA, while time courses in B lacked DNA. Final concentration of proteins and DNA are 20 nM RFC, 20 nM PCNA-AF488, 0.5 mM ATP, 40 nM DNA (or none in B), and 200 nM unlabeled PCNA. The DNA used in these assays was composed of JH9 and JH10 to make a 30nt duplex region and two symmetrical 30nt single-stranded overhangs.

Table 6-1. Calculated observed rates of PCNA release for trRFC and flRFC

| RFC complex | DNA | | No DNA |
|---|---|---|---|
| | $k_{obs1}$ ($s^{-1}$) | $k_{obs2}$ ($s^{-1}$) | |
| trRFC | 0.37 ± 0.06 | 0.09 ± 0.03 | 0.07 ± 0.02 |
| flRFC | 0.32 ± 0.03 | 0.10 ± 0.05 | 0.04 ± 0.01 |

Table 6-2. Calculated observed rates of PCNA closing for trRFC and flRFC

| RFC complex | DNA | | No DNA |
|---|---|---|---|
| | $k_{obs1}$ ($s^{-1}$) | $k_{obs2}$ ($s^{-1}$) | |
| trRFC | 3.5 ± 0.32 | 0.09 ± 0.05 | 0.03 ± 0.02 |
| flRFC | 2.9 ± 0.33 | 0.44 ± 0.07 | 0.02 ± 0.01 |

# CHAPTER 7
# DISCUSSION AND FUTURE DIRECTIONS

Experiments were performed here to compare the mechanism and DNA specificity of the *E. coli* and *S. cerevisiae* clamp loaders. Fluorescence-based assays reporting on various aspects of the clamp loading cycle were used in each system to compare different aspects of the clamp loading reaction. These assays helped to understand the mechanism by which the clamp loaders quickly and efficiently load clamps. Specifically, in Chapter 3, the timing of events in the clamp loading cycle was compared for γ complex and RFC. In Chapter 4, the mechanism of DNA binding by γ complex was investigated. In Chapter 5, the mechanism of DNA specificity of the eukaryotic clamp loaders was examined. Finally in Chapter 6, the fluorescence-based assays were used to compare the activity of two forms of the RFC clamp loader.

## Clamp Closing Before Release

In Chapter 3, the timing of clamp closing and release was assayed. Results indicated that both *E. coli* γ complex and *S. cerevisiae* RFC close clamps around DNA before releasing them onto DNA. Because of the high stability of the sliding clamps in the closed conformation, it was previously unclear if clamp loaders were even needed to close clamps around DNA, or if the clamp loaders just released an open clamp on DNA and allowed it to snap shut on its own. This represents a conserved mechanism for the two clamp loaders and likely serves to prevent an open clamp from slipping away from the DNA before it shuts.

It is still unclear if the clamp loaders physically shut the sliding clamps around DNA, or if some clamp loader•clamp contacts are destabilized allowing the clamp to shut on its own while still bound to the clamp loader. To test this hypothesis, clamp

mutants could be used in which the interface is weakened to decrease the high stability in the closed conformation (70, 144, 145). The fluorescence-based assays could be adapted to these mutants to determine how the reaction kinetics change given that the sliding clamps no longer have high stability in the closed conformation. If the clamp loaders destabilize some contacts with the clamp allowing the clamp to shut on its own, pre-steady state kinetics with the clamp mutants would be expected to show little to no change in fluorescence upon addition of DNA. In this situation, where no other force is closing the clamp, the clamp loader•clamp would be stuck in an open conformation, because closed clamp state is no longer favorable. If the clamp loader physically closes the clamp, experiments with the clamp mutants should show the clamps being forced closed upon addition of DNA. Because the closed clamp states are no longer favorable, the clamps would begin to open again until they reached an equilibrium of open and closed populations in solution.

In addition, a burst of ATP hydrolysis occurs before β closing by γ complex indicating at least two molecules of ATP are hydrolyzed before the closing step can occur. Previously, it was unclear if hydrolysis of individual ATP molecules corresponded to specific steps in the clamp loading cycle, or if all molecules were hydrolyzed before the next step could be achieved. The ATP hydrolysis step was not measured for the RFC clamp loader, so it is not clear if this step is similar to γ complex. The γ complex binds all molecules of ATP before it binds β (50) and conversely hydrolyzes all ATP molecules before closing β. However, RFC binds ATP molecules in a manner where the binding of a specific number of ATP molecules is correlated with specific actions of the clamp loader (63). RFC binds two ATP molecules to bind either PCNA or DNA, and

then binds a third ATP molecule to bind both PCNA and DNA. After PCNA and DNA binding, the fourth ATP molecule is allowed to bind RFC leading to hydrolysis and release of PCNA around DNA. Because ATP binding correlates to specific steps in the formation of the ternary RFC•PCNA•DNA complex, does hydrolysis of specific ATP sites correlate to individual steps in the disassembly of the ternary complex to result in PCNA•DNA?

### The DNA Specificity and Binding Mechanism of γ Complex

In Chapter 4, the DNA specificity of the *E. coli* γ complex was measured using fluorescence-based assays to report on β closing and release. The closing and release assays were used in conjunction with a variety of DNA substrates to determine how γ complex recognizes the correct DNA structure. The first set of experiments was performed with DNA substrates varying the length of the single-stranded overhang (SSO). From this data, γ complex closes β with the fastest observed rate on DNA with at least 1nt of SSO when the 5'P is absent, but requires 3 – 5nt of SSO when the 5'P is present. Comparing the DNA concentration dependence of the closing reactions suggests a DNA binding mechanism where the SSO mediates γ complex binding to the p/t junction, instead of the γ complex binding the p/t junction directly (Figure 4-6). This is similar to a sliding or threading mechanism proposed previously (88).

This mechanism could be further explored by increasing the length of the SSO beyond 30nt to see if this has any effect on the β closing rates. Also, a FRET-based assay could be designed to measure distances between the p/t junction and the γ complex•β. This assay could be used to monitor the FRET changes in real-time and could better support the sliding model. This model could also be tested using two

fluorescence-based DNA binding assays present in the laboratory. One assay, described in Chapter 5, uses p/t DNA labeled with RhX to measure changes in the rotational motion of the DNA-RhX as large macromolecules bind. This assay would report on binding of γ complex•β to any region of the DNA, not necessarily the physiologically relevant p/t junction. The second assay uses p/t DNA labeled with DCC at the p/t junction. This assay reports on binding of γ complex•β specifically to the p/t junction, but does not measure binding on any other portion of the DNA. Pre-steady state analysis of DNA binding by γ complex•β using both of these assays would give a reading of when the complex binds DNA, and when it reaches the p/t junction. If the timing of these two events is distinct, it would support the sliding model.

This sliding mechanism is called into question once complications at the replication fork are considered. For example, SSB is present at a replication fork *in vivo* and would bind the SSO and presumably make it inaccessible to γ complex. Unless the SSB is physically removed, it would also inhibit sliding on the SSO. Also, the chromosome is circular, so an SSO with a free end would not be present and would actually signal DNA damage to the cell. Therefore, it seems like this mechanism may only explain how γ complex binds these artificial short linear p/t DNA structures and may not translate to more physiologically relevant DNA structures found in the cell.

The second set of experiments performed focused on addressing the question of how γ complex differentiates between the two polarities of DNA found within the cell. The β clamps are required at 3'DNA sites, therefore γ complex must have a way of targeting these sites over 5'DNA sites. These studies implicate SSB as the major contributor to γ complex specificity toward 3'DNA. In the absence of SSB, there is only a

2-fold difference in observed closing rates between the two polarities, but the addition of SSB results in a 50 – 100 fold difference. Interestingly, there are two different mechanisms by which SSB confers specificity, depending on the presence of a 5'P at the p/t junction. When the 5'P is absent, an interaction between the $\chi$ subunit of $\gamma$ complex and SSB is required to prevent loading on 5'DNA. When the $\chi$•SSB interaction is lost, there is only a 2-fold difference in observed closing rates, similar to if SSB was absent. When the 5'P is present, loading on SSB coated 5'DNA is inhibited regardless of whether the $\chi$•SSB interaction is present. Therefore, this suggests that either there is some type of 5'P•SSB interaction that prevents clamp loading or there are additional $\gamma$ complex•SSB interactions as suggested previously by the McHenry group (129). It is possible that the presence of the 5'P and SSB forces $\gamma$ complex into a conformation where an additional contact with SSB, not mediated by $\chi$, could be made and influence the clamp loading reaction. This study raises some interesting questions about the $\gamma$ complex•SSB dynamics as well as how SSB behaves at p/t junctions and will be discussed in more detail below.

**The DNA Specificity of the Eukaryotic Clamp Loaders**

In Chapter 5, the DNA specificity of the *S. cerevisiae* clamp loaders RFC and Rad24-RFC were investigated. DNA binding by these clamp loaders was tested with different DNA structures in the presence and absence of PCNA (Figure 5-1 and 2). Results indicated that RFC had little specificity toward 3'DNA in the presence or absence of PCNA. Rad24-RFC bound DNA weakly compared to RFC, but did show slight specificity toward 5'DNA when PCNA was present. These results would indicate that neither clamp loader is adept at recognizing a p/t DNA junction, which is surprising,

as sliding clamps are required at these specific sites. DNA binding in the presence of the 9-1-1 clamp should be measured to determine how the correct sliding clamp affects DNA binding by Rad24-RFC.

The DNA specificity of RFC was investigated further using PCNA closing and release assays to measure clamp loading triggered by different DNA structures. These assays concluded that there is little difference between clamp loading on 3'DNA, dsDNA, ssDNA, and naked 5'DNA (Table 5-1 and 2). However, In the presence of RPA and a 5'P at the p/t junction, clamp loading was inhibited on 5'DNA, indicating that like $\gamma$ complex, the single-stranded binding protein is required to prevent clamp loading on the wrong polarity of DNA. It was previously reported that RPA plays a role in targeting RFC to 3'DNA (100), however it was not shown that this function of RPA is dependent on the presence of a 5'P. Implications of the 5'P and RPA are discussed below.

Rad24-RFC was not investigated further, as there is currently no 9-1-1 closing or release assays in place. To measure clamp loading triggered by different DNA structures, ATP hydrolysis could be monitored. This would give a more dynamic measurement of the DNA specificity of Rad24-RFC. Measuring 9-1-1 closing and release likely cannot be measured using similar methods as PCNA, where 9-1-1 is selectively labeled with a fluorophore. The *S. cerevisiae* 9-1-1 clamp contains 29 native cysteine residues that would either need to be removed or would have to be buried in the clamp loader to prevent off-target labeling. Some of these cysteine residues may be involved in disulfide bonds, essential to the structure of the 9-1-1 clamp, and therefore could not be mutated without consequence to the overall 9-1-1 structure.

## The N-terminal Domain of the Rfc1 Subunit of RFC

In Chapter 6, the role of the N-terminal domain (NTD) of Rfc1 was investigated to determine how it affects clamp loading by the *S. cerevisiae* clamp loader, RFC. Previous work suggested that the NTD is dispensable for RFC activity, however more recent work highlights anomalies in the activity of the truncated version that would indicate it is not as proficient at clamp loading as once thought (10, 45, 72, 87, 95, 103, 138). Fluorescence-based assays were used to measure individual steps in the clamp loading reaction to compare the activity of RFC with a truncated Rfc1 (trRFC) to wild type RFC (flRFC). Results from these experiments indicated that the biggest difference between trRFC and flRFC is that the flRFC has higher affinity for PCNA. The $K_d$ measured for PCNA binding and opening are an order of magnitude lower for flRFC than trRFC. This could suggest additional interactions present between flRFC and PCNA not present between trRFC and PCNA. A greater number of ATP molecules bind to flRFC than trRFC (72), which could promote faster conformational changes that might explain the tighter interactions with PCNA observed for flRFC.

It would be interesting to perform structural analysis on the flRFC bound to PCNA to verify the hypothesis of additional contacts. From the structure of trRFC bound to PCNA, it appears that after contacting PCNA, the most N-terminal region of the Rfc1 subunit visible in the structure folds back toward the other Rfc subunits. It could be possible that this conformation results in more contacts with PCNA. It would also be interesting to perform high-resolution structural analysis on the flRFC clamp loader to determine any structural differences that would explain why flRFC was reported to bind more ATP molecules as well as have stronger ATP hydrolysis activity (72).

Previous studies reported that when genomic Rfc1 was mutated to produce *S. cerevisiae* expressing only trRFC, there was no growth defect detected (138). It would be interesting to repeat this study while monitoring protein levels. It is possible that trRFC does lead to defects, but the yeast cells compensate by increasing the expression of trRFC or another protein. The NTD has BRCT and PARP homology domains, so it must play a role in some aspect of DNA replication or repair. More rigorous analysis of growth could be performed by using an array of DNA damaging agents to determine if the NTD has a role outside the clamp loading reaction.

**Role of the DNA SSO in Clamp Loading**

In Chapter 4 and 5, the DNA specificity of the $\gamma$ complex and RFC clamp loaders were measured. Comparing the results, there is a divergence on the importance of the SSO for each clamp loader. The $\gamma$ complex requires at least 1nt of SSO when DNA structures lack the 5'P, as $\beta$ closing on 0nt DNA was 20-fold slower than 30nt DNA (Table 4-1). However, RFC does not require any SSO because PCNA closing on 0nt DNA (dsDNA) is only 2-fold slower than closing on 30nt DNA (3'DNA) (Table 5-1). This marks a clear difference in function between the two clamp loaders, and suggests that $\gamma$ complex relies more on DNA structural cues than RFC.

There is currently no structural data for RFC bound to DNA, so it is not clear if RFC makes different contacts with the SSO, or what other structural basis can explain the difference between the two clamp loaders. The Rfc1 subunit was shown to crosslink to the SSO (91), so there is conservation to $\gamma$ complex in that regard, but it does not translate to the need for an SSO for RFC.

The DNA concentration dependence of PCNA closing on different DNA structures can be measured to determine if the binding mechanism for RFC on the short linear p/t structures is similar to γ complex. It would be interesting to perform similar analysis using nicked or gapped DNA structures for both γ complex and RFC to determine how binding to these structures, which have no free SSO end, differ from other structures. Different lengths of the duplex region could also be measured to understand how this aspect of the DNA structure is important for triggering clamp loading by RFC and γ complex. Another possibility is measuring clamp loading on p/t structures with an RNA primer and a DNA template. This is the physiologically relevant structure recognized by the γ complex at a replication fork, but it is not thought to be the physiologically relevant structure for RFC. Because an RNA:DNA hybrid assumes an A-DNA form, where the diameter of the helix is wider and the rise is smaller, it could make different contacts with the clamp loaders potentially affecting the clamp loading reaction. Because RNA:DNA is not the physiologically relevant structure for RFC, it would be interesting to see if RFC could load PCNA onto this structure. Unfortunately, previous attempts to purify an RNA oligomer resulted in low RNA yield and potential RNA precipitation, therefore an alternate purification strategy will need to be adapted.

It would be interesting to determine how the SSO affects clamp loading by Rad24-RFC. This could be measured using the fluorescent ATP hydrolysis assay described in Chapter 3. Interactions with the SSO are likely mediated via the Rad24 subunit, so Rad24-RFC could behave similar to RFC.

## SSB and RPA Interactions at the Replication Fork

For both *E. coli* γ complex, and *S. cerevisiae* RFC, interactions with the SSBs prevent clamp loading on the incorrect polarity of DNA. This represents a conserved mechanism between the two clamp loaders and helps to define a common role for SSBs in the clamp loading reaction. Data from Chapter 4 and 5 would suggest that the presence of the 5'P at the replication fork plays a role in preventing clamp loading when the SSBs are present. It is unclear if this is due to an interaction between the 5'P and the SSBs, or if it simply forces a conformation of DNA•SSBs not conducive for clamp loading.

SSB binds ssDNA with a defined polarity through the oligonucleotide binding (OB) domain folds (146). However, since the protein is a homotetramer, it is symmetrical and the C-terminal tails would likely make similar contacts with γ complex regardless of the polarity of DNA. In fact, previous work using an artificial DNA structure with a reversed SSO relative to the duplex region indicated that the polarity of the SSO and therefore the orientation of the SSB did not affect DNA specificity. The template strand of the p/t DNA was modified with an internal linker to produce p/t DNA with a normal duplex region, but a reversed polarity SSO. This linker made a p/t DNA structure that appeared to be the correct polarity at the p/t junction, but was the incorrect polarity at the SSO, or vice versa. Results measuring clamp loading on these structures in the presence of SSB indicated that the polarity of the SSO did not affect the clamp loading reaction; if the duplex portion was a 5'DNA structure, the clamps would not load, even if the SSO mimicked a 3'DNA structure (90). Because the SSO is switched for these structures, the SSB orientation on the SSO would also be reversed, but this showed no

effect on clamp loading, indicating the conformation of SSB on the SSO does not likely play a role in preventing clamp loading on 5'DNA.

Interactions between SSB and the 5'P at the p/t junction are possible, but it is not clear how they would be mediated. All known *E. coli* SSB interactions with proteins are mediated via an acidic C-terminal tail (reviewed in (147)), but an interaction with the 5'P of the primer strand seems unlikely, as this tail is highly negatively charged. It is possible that the 5'P repels the C-terminal tail enough from the p/t junction that it adopts a different conformation where it can no longer interact with the $\gamma$ complex, creating a situation not conducive for clamp loading.

RPA is an asymmetric heterotrimer, which binds ssDNA with a defined polarity that would result in two different orientations at the replication fork, depending on the polarity of the SSO. The N-terminal domain of Rpa1 is oriented toward the 5' end of the SSO, while the C-terminal region of Rpa3 is oriented toward the 3' end of the SSO (139, 140). On a 3'DNA structure, the Rpa3 subunit would be facing the p/t junction, and the Rpa1 subunit would be facing away, so it is possible that this conformation of RPA makes contacts with RFC that allow clamp loading at these sites. Inversely, on 5'DNA, Rpa1 would be facing the p/t junction, while Rpa3 would be facing away from the junction. This conformation could either make incorrect contacts with RFC or repel RFC binding at this structure. This could be a similar mechanism for how Rad24-RFC is targeted to 5'DNA sites. Rad24-RFC interactions with the Rpa3 subunit at a 3'DNA junction may repel DNA binding, thus biasing clamp loading to 5'DNA sites.

It was surprising to note that the inhibitory effect of RPA was dependent on the presence of a 5'P, indicating that interactions with the individual subunits alone do not

mediate RFC specificity towards 3'DNA. Instead, the 5'P could force RFC to interact with the RPA in such a way that would influence DNA specificity. Interactions between RPA and the 5'P that physically block RFC binding to the p/t are possible, but like *E. coli* SSB, it is not clear how this interaction would be mediated. If RPA tightly interacts with the 5'P preventing clamp loading, this would also inhibit Rad24-RFC binding to 5'DNA, which is the physiologically relevant DNA structure for Rad24-RFC. It would be interesting to measure clamp loader activity on the DNA structures with the SSO polarity modified by the internal linker. This could help to understand if the orientation of RPA affects RFC and Rad24-RFC DNA specificity.

Little work had been done measuring SSB or RPA conformation and binding dynamics in the context of a p/t junction as opposed to ssDNA. Using DNA binding assays currently available in the laboratory, the affinity of RPA and SSB for various p/t junctions with and without a 5'P present could be assayed to determine if the SSBs bind any p/t DNA structure with higher affinity that could be attributed to interactions with a p/t junction. Another interesting experiment would be to measure PCNA closing in the presence of *E. coli* SSB, and measure β closing in the presence of *S. cerevisiae* RPA. These experiments could give insight into species specific interactions between the clamp loaders and the SSBs that could mediate DNA specificity.

# APPENDIX
# DEVELOPING A PURIFICATION PROTOCOL FOR THE 9-1-1 CLAMP

## 9-1-1 Plasmid

The alternative sliding clamp in *S. cerevisiae*, the 9-1-1 clamp is a heterotrimer composed of Rad17, Mec3, and Ddc1. The plasmid expressing these three proteins is a pET-11a based plasmid and was a gift of the O'Donnell laboratory. This plasmid has each protein subunit under control of individual T7 promoters and an N-terminal histidine tag added to the Rad17 subunit (Figure A-1).

## Protein Expression Times

To determine the length of induction time needed to maximize 9-1-1 protein expression, a test expression was performed. The plasmid was transformed into BL21 (DE3) Rosetta cells, which are supplemented with rare codons to prevent lower protein yields because of codon bias. An extra plasmid within the Rosetta cells supplemented tRNAs coding for the following rare codons: AGG, AGA, AUA, CUA, CCC, and GGA. Colonies were selected for using ampicillin (Amp) resistance for the 9-1-1 plasmid, and chloramphenicol (Cm) resistance for the rare tRNA plasmid. A single colony was picked and grown at 37°C overnight in a 2-mL LB Amp/Cm culture. The 2-mL culture was used to inoculate two 50-mL LB Amp/Cm cultures. The cells in the 2-mL culture were isolated by centrifugation at 6,810 x g for 5 minutes. The cells were resuspended in 2 mL of fresh LB media and isolated a second time by centrifugation. This cell pellet was resuspended in 2 mL fresh LB media and was used to inoculate the two 50-mL flasks of LB Amp and Cm. These cultures were grown to an OD of 0.6 – 0.8 and then induced with IPTG to a final concentration of 1 mM. Induction of one 50-mL culture was performed at 20°C, while the other was performed at 37°C. Each culture was sampled

at 0, 1, 2, 4, 6, and 24 hour post-induction, where 2 mL of culture was removed and frozen at -20°C.

The samples were each resuspended in 250 μL of 1X SDS PAGE buffer consisting of 25 mM Tris, 250 mM glycine and 0.1% SDS. The samples were boiled for 15 min and then centrifuged at 10,640 x g for 5 min. The resulting supernatants and pellets were analyzed via a 12% SDS-PAGE gel, using 10 μL of each supernatant and resuspended pellet. The gel for samples at 20°C is shown below (Figure A-2).

Ddc1 migrates at about 75 kD, Mec3 migrates at about 50 kD, and Rad17 migrates at about 40 kD. At both temperatures, the 9-1-1 subunits were not soluble and appeared in the pellet fractions. This does not necessarily mean that the protein will be insoluble in a full-scale preparation, but it is possible that boiling the samples in 1X SDS buffer does not give efficient lysis. The best time point and temperature for 9-1-1 expression is 20°C for 6 hours, therefore this is the protein expression protocol adopted.

**Full Scale 9-1-1 Expression**

The 9-1-1 plasmid was transformed into BL21 (DE3) Rosetta cells. A single colony was used to inoculate 2 mL of LB/Amp/Cm. This culture was grown for 8 hr at 37°C. The 2-mL culture was used to inoculate four 600-mL LB Amp/Cm cultures using the protocol described for the 50-mL cultures above. The 9-1-1 cultures were grown to an OD of 0.6 – 0.7 before induction with IPTG to a final concentration of 1 mM. The cultures were incubated for 6 hours at 20°C to promote protein expression. Cells were isolated by centrifugation at 4,650 x g for 30 min at 4°C. The cell pellets were stored at -80°C.

## Lysis

To purify 9-1-1 protein, bacterial cells were lysed in 30 mM HEPES pH 7.5, 500 mM NaCl, 10% glycerol, 0.5 mM EDTA, and SigmaFast protease inhibitor cocktail (EDTA free). Cells were lysed using the French press at 14,000 psi inside the cell. Cells were lysed three times in the French press to ensure complete lysis. The lysate was centrifuged at 17,420 x g for 30 min at 4°C. The supernatant was used for purification in the subsequent steps.

The NaCl concentration at lysis was tested in later experiments, and it was determined that lysis buffer containing 750 mM NaCl yielded a higher amount of soluble 9-1-1 than 500 mM NaCl.

## Ammonium Sulfate Precipitation

Previously published methods for purification of *S. cerevisiae* 9-1-1 indicated that 9-1-1 would precipitate around 40% ammonium sulfate saturation (148). For an ammonium sulfate precipitation, ammonium sulfate is mixed slowly into the lysis supernatant over the course of 1 – 2 hours. The protein/ammonium sulfate mixture was centrifuged at 31,000 x g for 30 min at 4°C. Initial experiments were performed at various ammonium sulfate concentrations to determine the best concentration to yield 9-1-1 purity. Ammonium sulfate cuts equating to 20%, 40%, 60%, and 80% saturation were performed. From SDS-PAGE analysis, it appears that 9-1-1 is in the 40% pellet (Figure A-3).

However, when this portion was used in subsequent steps, there was low yield of 9-1-1. It is possible that 9-1-1 was also in the 20% pellet, but just not visible on the gel. Therefore, subsequent 9-1-1 purifications that included an ammonium sulfate

precipitation step used only a 40% ammonium sulfate cut instead of removing the 20% cut.

### Nickel Column

Rad17 contains an N-terminal histidine tag, which has high affinity for $Ni^{2+}$, therefore, the first column used was a nickel column. HiTrap chelating columns (GE Healthcare) were charged with 100 mM $NiSO_4$. Various column sizes were used: first two 1-mL columns in tandem were used, but this did not have a large enough binding capacity, so a 5-mL column was used in later experiments. The buffer used for this column was 30 mM HEPES pH 7.5, 500 mM NaCl, and elution was performed with a 10 column volume linear gradient from 0 to 500 mM imidazole. In each purification attempt, the 9-1-1 protein eluted in approximately 200 – 350 mM imidazole. Therefore, throughout each purification attempt, the nickel column was used as the first column.

### Heparin Column

A HiTrap heparin column (GE Healthcare) was tested to determine if it would give another level of purification to 9-1-1 that had already been through a nickel column. The heparin resin mimics the DNA phosphate backbone, and since 9-1-1 binds DNA, it may stick to this column, thus giving another purification step. The 9-1-1 protein did stick to the heparin column in 30 mM HEPES pH 7.5, 10% glycerol, and 125 nM NaCl. However, a gradient from 125 – 500 nM NaCl showed the 9-1-1 clamp falling apart, where the Ddc1 subunit seemed to be in a lower ratio as compared to Mec3 and Rad17. Because 9-1-1 disassociated on the heparin column, this column was not used.

## Ion Exchange Columns

Binding of 9-1-1 to both a cation exchange (HiTrap SP, GE Healthcare) and an anion exchange (HiTrap Q, GE Healthcare) were tested to determine if either column provided a purification step after 9-1-1 had been run on the nickel column. Initial experiments with the HiTrap SP indicated that in 30 mM HEPES pH 7.5, 10% glycerol, and 125 nM NaCl, 9-1-1 did not stick to the column. The 9-1-1 protein did stick to a HiTrap Q column in this buffer, and eluted at approximately 400 mM NaCl. This peak was very broad and still contained a few contaminants. This HiTrap Q column step was incorporated after the nickel column in each of the subsequent purification attempts. A representative gel showing the purification of 9-1-1 using ammonium sulfate precipitation, a nickel column and the Q column is shown in Figure A-4.

## Size Exclusion

The 9-1-1 clamp *in vivo* is a heterotrimer, but *in vitro* partial complexes can be formed (149). To remove partial complexes and ensure that only a heterotrimer is purified, a Superose size exclusion column (GE Healthcare) was used to purify 9-1-1 by size. Protein standards (BioRad) of known molecular weight were run to calibrate the column, and based on the protein standards, 9-1-1 should elute at 10.6 mL. The 9-1-1 clamp was first run through the nickel column and HiTrap Q column before loading onto the size exclusion column.

The 9-1-1 protein was run on the Superose size column, and four peaks eluted. The peaks were analyzed by SDS-PAGE gels (Figure A-5). The first peak eluted in the void volume, but gel analysis did not reveal any proteins present. It is not clear what this peak represents, but it occurred in three separate attempts. The second peak was the

largest, and eluted close to the void volume, at 7 mL and was larger than 9-1-1. Gel analysis shows that this peak has 9-1-1, although not in a 1:1:1 ratio as expected. It appears as if the Ddc1 subunit is in a lower ratio compared to the other subunits, and likely represents a partial 9-1-1 complex. There was also a high molecular weight band present in this lane that may indicate a contaminating interacting partner or aggregate of 9-1-1 subunits. The third peak was at 10 mL, the correct size for a 9-1-1 heterotrimer, and gel analysis verifies that this is 9-1-1. The last peak was the smallest, and eluted at 19 mL. Gel analysis did not show any protein, and this peak may represent a buffer component such as DTT.

Use of the size exclusion column yielded 9-1-1 complex that was the correct size, but the resulting protein yield was very low. In each of the three times the size exclusion column was used, 1.5 – 3 mg of protein was loaded, but only 0.2 – 0.4 mg of protein was recovered. This represented a significant loss of 9-1-1 protein. About half of the protein was lost in the second size exclusion peak that had the higher molecular weight band, but that does not account for all of the loss in protein. Most likely, there was also some protein precipitation at the resin bed that prevented some of the 9-1-1 from entering the column in the first place.

## Conclusions

These data show attempts to maximize purity and yield of 9-1-1. From this data, a single 40% ammonium sulfate precipitation appears to be the best ammonium sulfate cut to perform; it removes contaminating proteins as well as retains the most 9-1-1 protein. The nickel column and Q column are the best columns to use for purification.

The 9-1-1 protein did not stick to the HiTrap S column and disassembled on the HiTrap heparin column.

The size exclusion column served two purposes, first it removed impurities from 9-1-1 and second it removed 9-1-1 subcomplexes. However a significant amount of protein was lost during the process, so it is not worth using this column in the purification process. Instead, a MonoQ column can be used, which has higher resolution than the HiTrap Q column used previously. This will help to separate 9-1-1 from contaminants and may also help to separate 9-1-1 from any subcomplexes.

Based on the results here, the best plan for purifying 9-1-1 is:

- Express 9-1-1 for 6 hours at 20°C
- Lyse bacterial pellets in 30 mM HEPES pH 7.5, 1 M NaCl, 10% glycerol, 0.5 mM EDTA, and SigmaFast protease inhibitor cocktail (EDTA free)
- 40% ammonium precipitation
- Use a 5-mL nickel column with 50 mM imidazole added to the lysate to prevent non-specific interactions between other proteins and the nickel resin. Addition of the imidazole to the lysate should help with purity.
- MonoQ column, which will have better resolution than the HiTrap Q column. This will help to remove any contaminants and may be able to separate any subcomplexes if present.

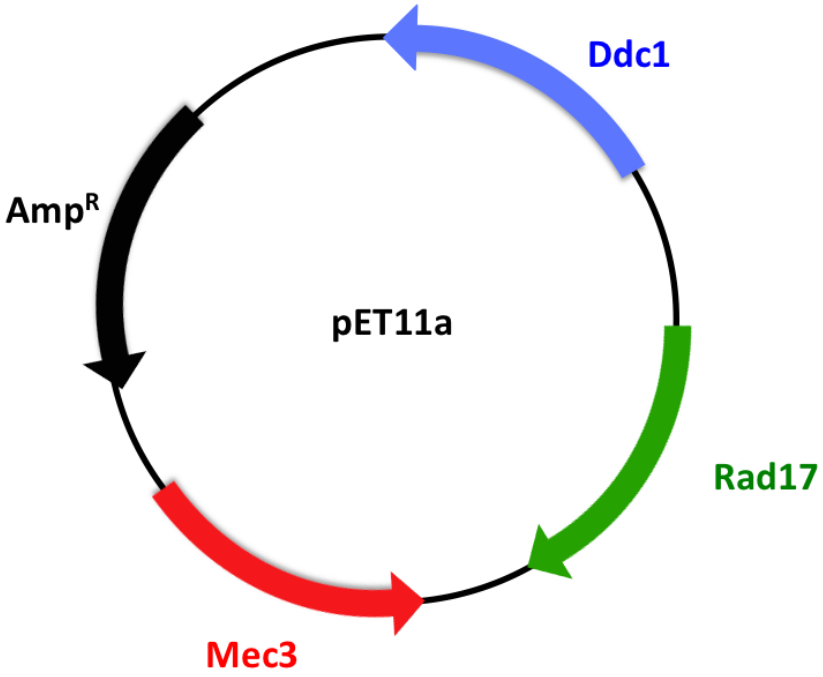


Figure A-1. Map of the 9-1-1 vector obtained from the O'Donnell laboratory. Each gene was cloned into the multiple cloning site of pET11a in individual vectors. Rad17 and Mec3 were cut out of the pET11a vectors using BglII and AatI sites, which flank the T7 casette. The genes were blunted with Klenow and the Rad17 gene was cloned into the Eag1 site, while the Mec3 gene was cloned into the Bst1107 site.

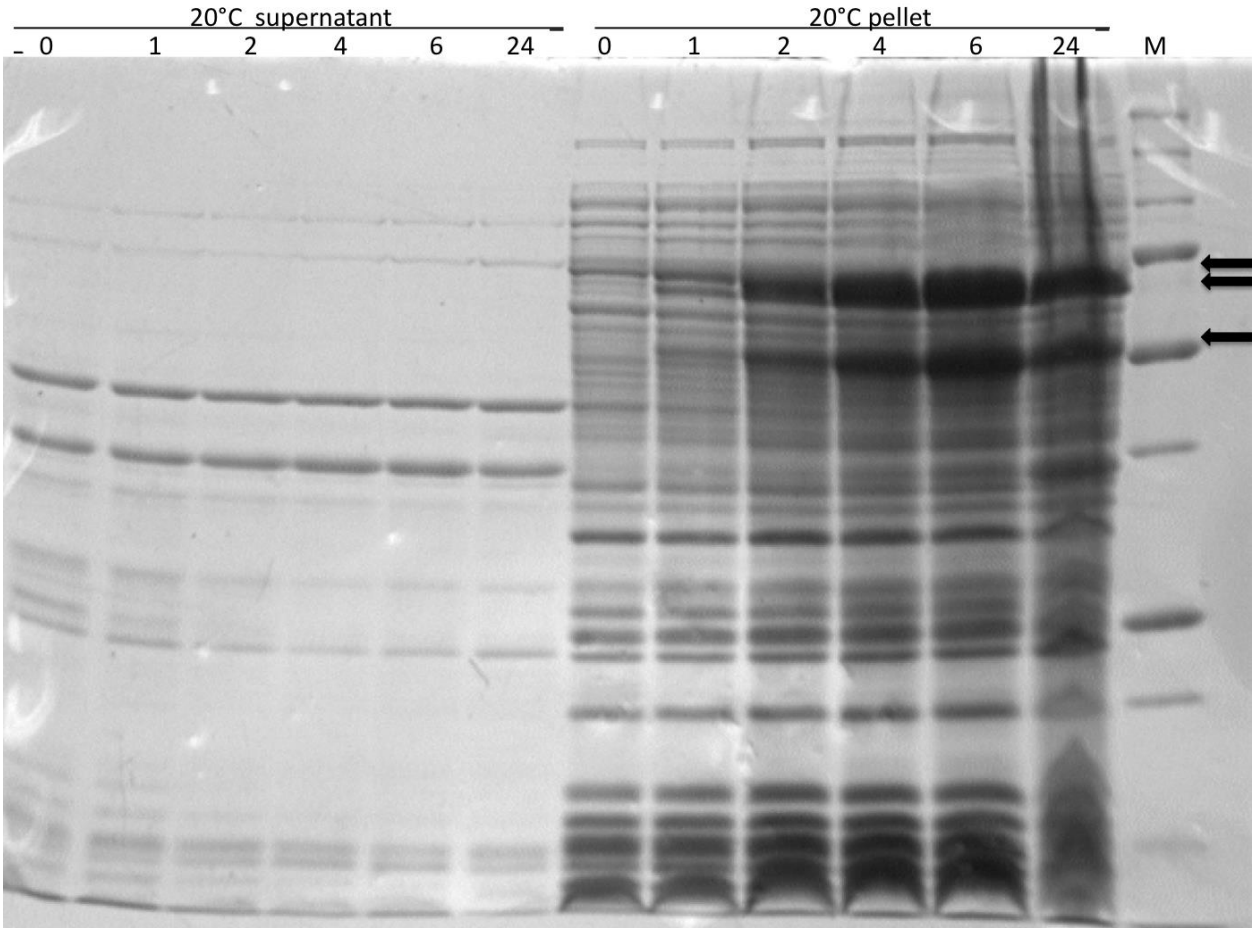


Figure A-2. SDS-PAGE gels of 9-1-1 expression time points at 20°C. For each time point, 9-1-1 appeared in the pellet fractions. The best induction time appears to be 6 hours. Arrows indicate the 9-1-1 subunits.

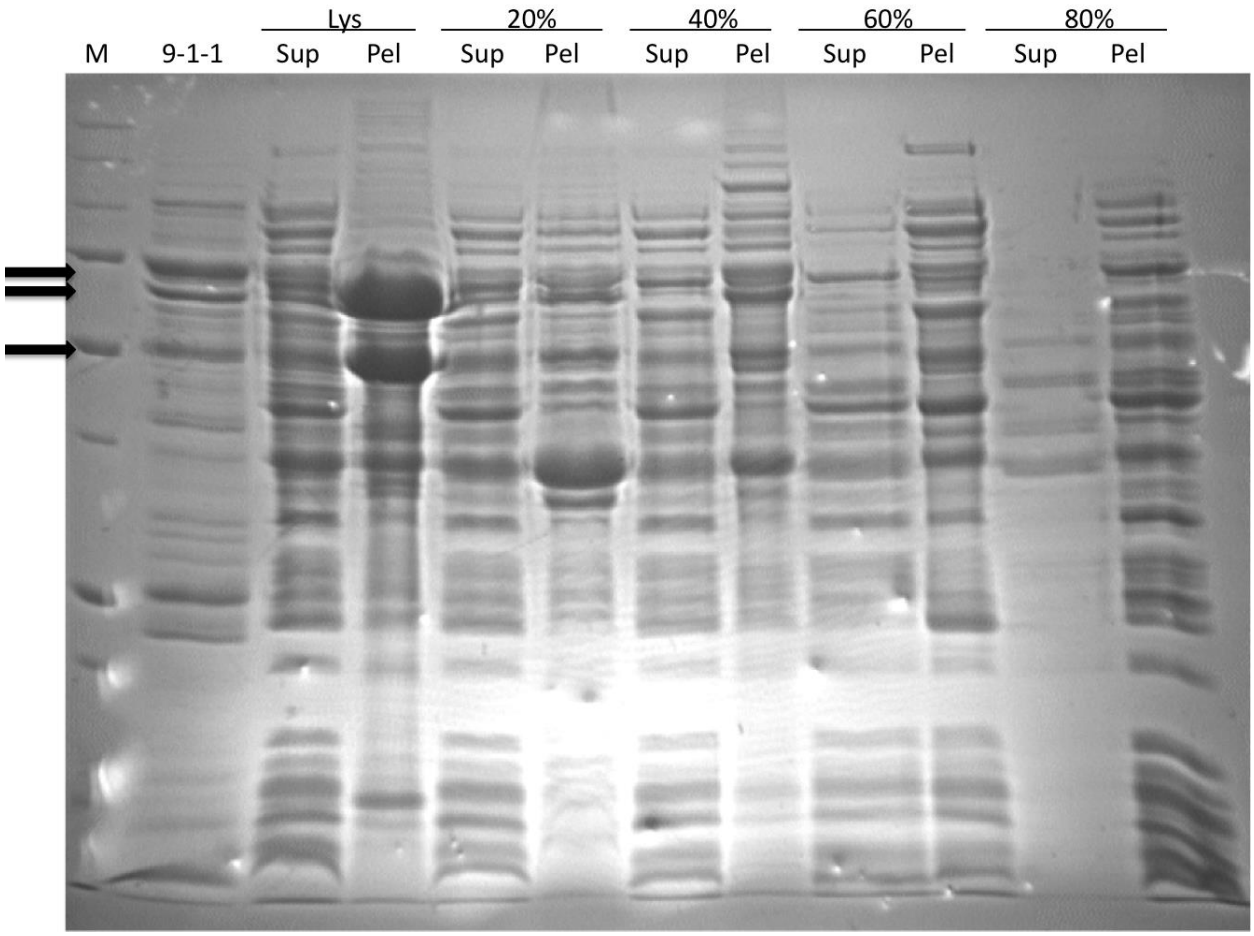


Figure A-3. Gel showing the ammonium sulfate precipitation steps tested. The first lane is a protein standard marker, the second lane is a sample of 9-1-1 run on a nickel column as reference. The supernatant and pellet are shown for lysis, 20%, 40%, 60%, and 80% ammonium sulfate cuts.

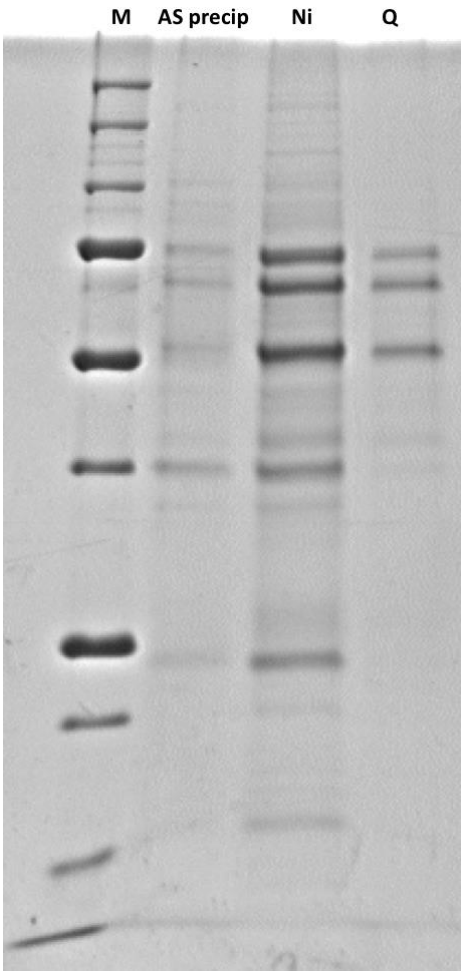


Figure A-4. Final gel showing 9-1-1 purification. The first lane is a protein marker, and the second lane shows 9-1-1 after the ammonium sulfate precipitation step. The third lane shows 9-1-1 after the nickel column. The fourth lane shows 9-1-1 after the Q column.

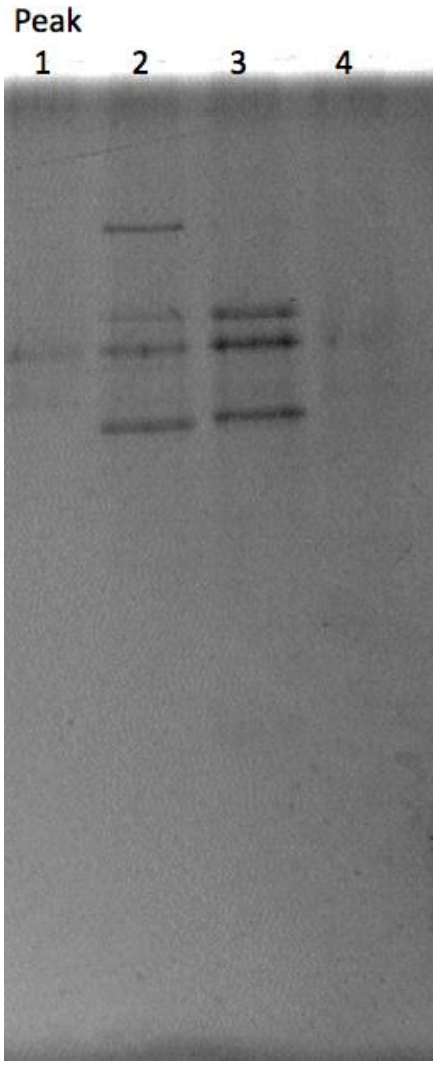


Figure A-5. Gel analysis of peaks from the size exclusion column. Four peaks resulted from each size exclusion run of 9-1-1 that had been purified through ammonium sulfate, nickel column, and Q column before this column. Purified 9-1-1 appears in peak 3.

LIST OF REFERENCES


1. Kong, X. P., Onrust, R., O'Donnell, M., and Kuriyan, J. (1992) Three-dimensional structure of the beta subunit of *E. coli* DNA polymerase III holoenzyme: a sliding DNA clamp. *Cell* **69**, 425–437
2. Krishna, T. S., Kong, X. P., Gary, S., Burgers, P. M., and Kuriyan, J. (1994) Crystal structure of the eukaryotic DNA polymerase processivity factor PCNA. *Cell* **79**, 1233–1243
3. Georgescu, R. E., Kim, S.-S., Yurieva, O., Kuriyan, J., Kong, X.-P., and O'Donnell, M. (2008) Structure of a sliding clamp on DNA. *Cell* **132**, 43–54
4. LaDuca, R. J., Crute, J. J., McHenry, C. S., and Bambara, R. A. (1986) The beta subunit of the Escherichia coli DNA polymerase III holoenzyme interacts functionally with the catalytic core in the absence of other subunits. *J Biol Chem* **261**, 7550–7557
5. Fay, P. J., Johanson, K. O., McHenry, C. S., and Bambara, R. A. (1981) Size classes of products synthesized processively by DNA polymerase III and DNA polymerase III holoenzyme of Escherichia coli. *J Biol Chem* **256**, 976–983
6. Fay, P. J., Johanson, K. O., McHenry, C. S., and Bambara, R. A. (1982) Size classes of products synthesized processively by two subassemblies of Escherichia coli DNA polymerase III holoenzyme. *J Biol Chem* **257**, 5692–5699
7. Dohrmann, P. R., and Mchenry, C. S. (2005) A bipartite polymerase-processivity factor interaction: only the internal beta binding site of the alpha subunit is required for processive replication by the DNA polymerase III holoenzyme. *Journal of Molecular Biology* **350**, 228–239
8. Kim, D. R., and McHenry, C. S. (1996) Identification of the beta-binding domain of the alpha subunit of Escherichia coli polymerase III holoenzyme. *J Biol Chem* **271**, 20699–20704
9. Kim, S., Dallmann, H. G., McHenry, C. S., and Marians, K. J. (1996) tau couples the leading- and lagging-strand polymerases at the Escherichia coli DNA replication fork. *J Biol Chem* **271**, 21406–21412
10. Podust, V. N., Tiwari, N., Stephan, S., and Fanning, E. (1998) Replication factor C disengages from proliferating cell nuclear antigen (PCNA) upon sliding clamp formation, and PCNA itself tethers DNA polymerase delta to DNA. *J Biol Chem* **273**, 31992–31999
11. Stoimenov, I., and Helleday, T. (2009) PCNA on the crossroad of cancer. *Biochem. Soc. Trans* **37**, 605–613
12. López de Saro, F. J., Georgescu, R. E., Goodman, M. F., and O'Donnell, M. (2003) Competitive processivity-clamp usage by DNA polymerases during DNA replication and repair. *EMBO J.* **22**, 6408–6418

13. Beattie, T. R., and Bell, S. D. (2011) The role of the DNA sliding clamp in Okazaki fragment maturation in archaea and eukaryotes. *Biochem. Soc. Trans* **39**, 70–76

14. Beattie, T. R., and Bell, S. D. (2012) Coordination of multiple enzyme activities by a single PCNA in archaeal Okazaki fragment maturation. *EMBO J.* **31**, 1556–1567

15. López de Saro, F. J., and O'Donnell, M. (2001) Interaction of the beta sliding clamp with MutS, ligase, and DNA polymerase I. *Proc Natl Acad Sci USA* **98**, 8376–8380

16. López de Saro, F. J., Marinus, M. G., Modrich, P., and O'Donnell, M. (2006) The beta sliding clamp binds to multiple sites within MutL and MutS. *J Biol Chem* **281**, 14340–14349

17. Pluciennik, A., Burdett, V., Lukianova, O., O'Donnell, M., and Modrich, P. (2009) Involvement of the beta clamp in methyl-directed mismatch repair in vitro. *J Biol Chem* **284**, 32782–32791

18. Pillon, M. C., Miller, J. H., and Guarné, A. (2011) The endonuclease domain of MutL interacts with the β sliding clamp. *DNA Repair* **10**, 87–93

19. Iyer, R. R., Pohlhaus, T. J., Chen, S., Hura, G. L., Dzantiev, L., Beese, L. S., and Modrich, P. (2008) The MutSalpha-proliferating cell nuclear antigen interaction in human DNA mismatch repair. *J Biol Chem* **283**, 13310–13319

20. Pluciennik, A., Dzantiev, L., Iyer, R. R., Constantin, N., Kadyrov, F. A., and Modrich, P. (2010) PCNA function in the activation and strand direction of MutLα endonuclease in mismatch repair. *Proc Natl Acad Sci USA* **107**, 16066–16071

21. Guo, S., Presnell, S. R., Yuan, F., Zhang, Y., Gu, L., and Li, G.-M. (2004) Differential requirement for proliferating cell nuclear antigen in 5" and 3" nick-directed excision in human mismatch repair. *J Biol Chem* **279**, 16912–16917

22. Hughes, A. J., Bryan, S. K., Chen, H., Moses, R. E., and McHenry, C. S. (1991) Escherichia coli DNA polymerase II is stimulated by DNA polymerase III holoenzyme auxiliary subunits. *J Biol Chem* **266**, 4568–4573

23. Bonner, C. A., Stukenberg, P. T., Rajagopalan, M., Eritja, R., O'Donnell, M., McEntee, K., Echols, H., and Goodman, M. F. (1992) Processive DNA synthesis by DNA polymerase II mediated by DNA polymerase III accessory proteins. *J Biol Chem* **267**, 11431–11438

24. Tang, M., Pham, P., Shen, X., Taylor, J. S., O'Donnell, M., Woodgate, R., and Goodman, M. F. (2000) Roles of E. coli DNA polymerases IV and V in lesion-targeted and untargeted SOS mutagenesis. *Nature* **404**, 1014–1018

25. Wagner, J., Fujii, S., Gruz, P., Nohmi, T., and Fuchs, R. P. (2000) The beta clamp targets DNA polymerase IV to DNA and strongly increases its processivity. *EMBO Rep* **1**, 484–488

26. Hoege, C., Pfander, B., Moldovan, G.-L., Pyrowolakis, G., and Jentsch, S. (2002) RAD6-dependent DNA repair is linked to modification of PCNA by ubiquitin and SUMO. *Nature* **419**, 135–141

27. Watanabe, K., Tateishi, S., Kawasuji, M., Tsurimoto, T., Inoue, H., and Yamaizumi, M. (2004) Rad18 guides poleta to replication stalling sites through physical interaction and PCNA monoubiquitination. *EMBO J.* **23**, 3886–3896

28. Kannouche, P. L., Wing, J., and Lehmann, A. R. (2004) Interaction of human DNA polymerase eta with monoubiquitinated PCNA: a possible mechanism for the polymerase switch in response to DNA damage. *Molecular Cell* **14**, 491–500

29. Bienko, M., Green, C. M., Crosetto, N., Rudolf, F., Zapart, G., Coull, B., Kannouche, P., Wider, G., Peter, M., Lehmann, A. R., Hofmann, K., and Dikic, I. (2005) Ubiquitin-binding domains in Y-family polymerases regulate translesion synthesis. *Science* **310**, 1821–1824

30. Kemp, M., and Sancar, A. (2009) DNA distress: just ring 9-1-1. *Curr Biol* **19**, R733–4

31. St Onge, R. P., Besley, B. D., Park, M., Casselman, R., and Davey, S. (2001) DNA damage-dependent and -independent phosphorylation of the hRad9 checkpoint protein. *J Biol Chem* **276**, 41898–41905

32. St Onge, R. P., Besley, B. D. A., Pelley, J. L., and Davey, S. (2003) A role for the phosphorylation of hRad9 in checkpoint signaling. *J Biol Chem* **278**, 26620–26628

33. Chen, M. J., Lin, Y. T., Lieberman, H. B., Chen, G., and Lee, E. Y. (2001) ATM-dependent phosphorylation of human Rad9 is required for ionizing radiation-induced checkpoint activation. *J Biol Chem* **276**, 16580–16586

34. Roos-Mattjus, P., Hopkins, K. M., Oestreich, A. J., Vroman, B. T., Johnson, K. L., Naylor, S., Lieberman, H. B., and Karnitz, L. M. (2003) Phosphorylation of human Rad9 is required for genotoxin-activated checkpoint signaling. *J Biol Chem* **278**, 24428–24437

35. Navadgi-Patil, V. M., and Burgers, P. M. (2009) The unstructured C-terminal tail of the 9-1-1 clamp subunit Ddc1 activates Mec1/ATR via two distinct mechanisms. *Molecular Cell* **36**, 743–753

36. Dore, A. S., Kilkenny, M. L., Rzechorzek, N. J., and Pearl, L. H. (2009) Crystal structure of the rad9-rad1-hus1 DNA damage checkpoint complex--implications for clamp loading and regulation. *Molecular Cell* **34**, 735–745

37. Sohn, S. Y., and Cho, Y. (2009) Crystal structure of the human rad9-hus1-rad1 clamp. *Journal of Molecular Biology* **390**, 490–502

38. Xu, M., Bai, L., Gong, Y., Xie, W., Hang, H., and Jiang, T. (2009) Structure and functional implications of the human rad9-hus1-rad1 cell cycle checkpoint complex. *J Biol Chem* **284**, 20457–20461

39. Oakley, A. J., Prosselkov, P., Wijffels, G., Beck, J. L., Wilce, M. C. J., and Dixon, N. E. (2003) Flexibility revealed by the 1.85 A crystal structure of the beta sliding-clamp subunit of *Escherichia coli* DNA polymerase III. *Acta Crystallogr D Biol Crystallogr* **59**, 1192–1199

40. Mcnally, R., Bowman, G. D., Goedken, E. R., O'Donnell, M., and Kuriyan, J. (2010) Analysis of the role of PCNA-DNA contacts during clamp loading. *BMC Struct. Biol.* **10**, 3

41. Zhou, Y., and Hingorani, M. M. (2012) Impact of Individual PCNA-DNA Contacts on Clamp Loading and Function on DNA. *J Biol Chem*

42. Leu, F. P., Hingorani, M. M., Turner, J., and O'Donnell, M. (2000) The delta subunit of DNA polymerase III holoenzyme serves as a sliding clamp unloader in Escherichia coli. *J Biol Chem* **275**, 34609–34618

43. Podust, L. M., Podust, V. N., Sogo, J. M., and Hübscher, U. (1995) Mammalian DNA polymerase auxiliary proteins: analysis of replication factor C-catalyzed proliferating cell nuclear antigen loading onto circular double-stranded DNA. *Molecular and Cellular Biology* **15**, 3072–3081

44. Yao, N., Turner, J., Kelman, Z., Stukenberg, P. T., Dean, F., Shechter, D., Pan, Z. Q., Hurwitz, J., and O'Donnell, M. (1996) Clamp loading, unloading and intrinsic stability of the PCNA, beta and gp45 sliding clamps of human, *E. coli* and T4 replicases. *Genes Cells* **1**, 101–113

45. Kumar, R., Nashine, V. C., Mishra, P. P., Benkovic, S. J., and Lee, T.-H. (2010) Stepwise loading of yeast clamp revealed by ensemble and single-molecule studies. *Proc Natl Acad Sci USA* **107**, 19736–19741

46. Thompson, J. A., Marzahn, M. R., O'Donnell, M., and Bloom, L. B. (2011) Replication factor C is a more effective PCNA opener than the checkpoint clamp loader, RAD24-RFC. *J Biol Chem*

47. Ogura, T., and Wilkinson, A. J. (2001) AAA+ superfamily ATPases: common structure--diverse function. *Genes Cells* **6**, 575–597

48. Bertram, J. G., Bloom, L. B., Hingorani, M. M., Beechem, J. M., O'Donnell, M., and Goodman, M. F. (2000) Molecular mechanism and energetics of clamp assembly in *Escherichia coli*. The role of ATP hydrolysis when gamma complex loads beta on DNA. *J Biol Chem* **275**, 28413–28420

49. Williams, C. R., Snyder, A. K., Kuzmic, P., O'Donnell, M., and Bloom, L. B. (2004) Mechanism of loading the *Escherichia coli* DNA polymerase III sliding clamp: I. Two distinct activities for individual ATP sites in the gamma complex. *J Biol Chem* **279**, 4376–4385

50. Johnson, A., and O'Donnell, M. (2003) Ordered ATP hydrolysis in the gamma complex clamp loader AAA+ machine. *J Biol Chem* **278**, 14406–14413

51. Simonetta, K. R., Kazmirski, S. L., Goedken, E. R., Cantor, A. J., Kelch, B. A., Mcnally, R., Seyedin, S. N., Makino, D. L., O'Donnell, M., and Kuriyan, J. (2009) The mechanism of ATP-dependent primer-template recognition by a clamp loader complex. *Cell* **137**, 659–671

52. Glover, B. P. (1998) The chi psi Subunits of DNA Polymerase III Holoenzyme Bind to Single-stranded DNA-binding Protein (SSB) and Facilitate Replication of an SSB-coated Template. *Journal of Biological Chemistry* **273**, 23476–23484 [online] http://eutils.ncbi.nlm.nih.gov/entrez/eutils/elink.fcgi?dbfrom=pubmed&id=9722585&retmode=ref&cmd=prlinks.

53. Kelman, Z., Yuzhakov, A., Andjelkovic, J., and O'Donnell, M. (1998) Devoted to the lagging strand-the subunit of DNA polymerase III holoenzyme contacts SSB to promote processive elongation and sliding clamp assembly. *EMBO J.* **17**, 2436–2449

54. Anderson, S. G., Williams, C. R., O'Donnell, M., and Bloom, L. B. (2007) A function for the psi subunit in loading the Escherichia coli DNA polymerase sliding clamp. *J Biol Chem* **282**, 7035–7045

55. Bowman, G. D., O'Donnell, M., and Kuriyan, J. (2004) Structural analysis of a eukaryotic sliding DNA clamp-clamp loader complex. *Nature* **429**, 724–730

56. Burbelo, P. D., Utani, A., Pan, Z. Q., and Yamada, Y. (1993) Cloning of the large subunit of activator 1 (replication factor C) reveals homology with bacterial DNA ligases. *Proc Natl Acad Sci USA* **90**, 11543–11547

57. Kobayashi, M., Figaroa, F., Meeuwenoord, N., Jansen, L. E. T., and Siegal, G. (2006) Characterization of the DNA binding and structural properties of the BRCT region of human replication factor C p140 subunit. *J Biol Chem* **281**, 4308–4317

58. Green, C. M., Erdjument-Bromage, H., Tempst, P., and Lowndes, N. F. (2000) A novel Rad24 checkpoint protein complex closely related to replication factor C. *Curr Biol* **10**, 39–42

59. Kai, M., Tanaka, H., and Wang, T. S. (2001) Fission yeast Rad17 associates with chromatin in response to aberrant genomic structures. *Molecular and Cellular Biology* **21**, 3289–3301

60. Griffith, J. D., Lindsey-Boltz, L. A., and Sancar, A. (2002) Structures of the human Rad17-replication factor C and checkpoint Rad 9-1-1 complexes visualized by glycerol spray/low voltage microscopy. *J Biol Chem* **277**, 15233–15236

61. Shiomi, Y., Shinozaki, A., Nakada, D., Sugimoto, K., Usukura, J., Obuse, C., and Tsurimoto, T. (2002) Clamp and clamp loader structures of the human checkpoint protein complexes, Rad9-1-1 and Rad17-RFC. *Genes Cells* **7**, 861–868

62. Davey, M. J., Jeruzalmi, D., Kuriyan, J., and O'Donnell, M. (2002) Motors and switches: AAA+ machines within the replisome. *Nat. Rev. Mol. Cell Biol.* **3**, 826–835

63. Gomes, X. V., Schmidt, S. L., and Burgers, P. M. (2001) ATP utilization by yeast replication factor C. II. Multiple stepwise ATP binding events are required to load proliferating cell nuclear antigen onto primed DNA. *J Biol Chem* **276**, 34776–34783

64. Naktinis, V., Onrust, R., Fang, L., and O'Donnell, M. (1995) Assembly of a chromosomal replication machine: two DNA polymerases, a clamp loader, and sliding clamps in one holoenzyme particle. II. Intermediate complex between the clamp loader and its clamp. *J Biol Chem* **270**, 13358–13365

65. Hingorani, M. M., and O'Donnell, M. (1998) ATP binding to the *Escherichia coli* clamp loader powers opening of the ring-shaped clamp of DNA polymerase III holoenzyme. *J Biol Chem* **273**, 24550–24563

66. Turner, J., Hingorani, M. M., Kelman, Z., and O'Donnell, M. (1999) The internal workings of a DNA polymerase clamp-loading machine. *EMBO J.* **18**, 771–783

67. Gomes, X. V., and Burgers, P. M. (2001) ATP utilization by yeast replication factor C. I. ATP-mediated interaction with DNA and with proliferating cell nuclear antigen. *J Biol Chem* **276**, 34768–34775

68. Schmidt, S. L., Gomes, X. V., and Burgers, P. M. (2001) ATP utilization by yeast replication factor C. III. The ATP-binding domains of Rfc2, Rfc3, and Rfc4 are essential for DNA recognition and clamp loading. *J Biol Chem* **276**, 34784–34791

69. Paschall, C. O., Thompson, J. A., Marzahn, M. R., Chiraniya, A., Hayner, J. N., O'Donnell, M., Robbins, A. H., McKenna, R., and Bloom, L. B. (2011) The *E. coli* clamp loader can actively pry open the beta-sliding clamp. *J Biol Chem*

70. Bertram, J. G., Bloom, L. B., Turner, J., O'Donnell, M., Beechem, J. M., and Goodman, M. F. (1998) Pre-steady state analysis of the assembly of wild type and mutant circular clamps of *Escherichia coli* DNA polymerase III onto DNA. *J Biol Chem* **273**, 24564–24574

71. Hingorani, M. M., Bloom, L. B., Goodman, M. F., and O'Donnell, M. (1999) Division of labor--sequential ATP hydrolysis drives assembly of a DNA polymerase sliding clamp around DNA. *EMBO J.* **18**, 5131–5144

72. Chen, S., Levin, M. K., Sakato, M., Zhou, Y., and Hingorani, M. M. (2009) Mechanism of ATP-driven PCNA clamp loading by S. cerevisiae RFC. *Journal of Molecular Biology* **388**, 431–442

73. Anderson, S. G., Thompson, J. A., Paschall, C. O., O'Donnell, M., and Bloom, L. B. (2009) Temporal correlation of DNA binding, ATP hydrolysis, and clamp release in the clamp loading reaction catalyzed by the *Escherichia coli* gamma complex. *Biochemistry* **48**, 8516–8527

74. Sakato, M., Zhou, Y., and Hingorani, M. M. (2011) ATP-Binding- and Hydrolysis-Driven Rate-Determining Events in the RFC-Catalyzed PCNA Clamp Loading Reaction. *Journal of Molecular Biology*

75. Sakato, M., O'Donnell, M., and Hingorani, M. M. (2011) A Central Swivel Point in the RFC Clamp Loader Controls PCNA Opening and Loading on DNA. *Journal of Molecular Biology*

76. Bermudez, V. P., Lindsey-Boltz, L. A., Cesare, A. J., Maniwa, Y., Griffith, J. D., Hurwitz, J., and Sancar, A. (2003) Loading of the human 9-1-1 checkpoint complex onto DNA by the checkpoint clamp loader hRad17-replication factor C complex in vitro. *Proc Natl Acad Sci USA* **100**, 1633–1638

77. Majka, J., Chung, B. Y., and Burgers, P. M. J. (2004) Requirement for ATP by the DNA damage checkpoint clamp loader. *J Biol Chem* **279**, 20921–20926

78. Ellison, V., and Stillman, B. (2003) Biochemical characterization of DNA damage checkpoint complexes: clamp loader and clamp complexes with specificity for 5' recessed DNA. *PLoS Biol.* **1**, E33

79. Griffiths, D. J., Barbet, N. C., McCready, S., Lehmann, A. R., and Carr, A. M. (1995) Fission yeast rad17: a homologue of budding yeast RAD24 that shares regions of sequence similarity with DNA polymerase accessory proteins. *EMBO J.* **14**, 5812–5823

80. Naiki, T., Shimomura, T., Kondo, T., Matsumoto, K., and Sugimoto, K. (2000) Rfc5, in cooperation with rad24, controls DNA damage checkpoints throughout the cell cycle in Saccharomyces cerevisiae. *Molecular and Cellular Biology* **20**, 5888–5896

81. Dalrymple, B. P. (2001) A universal protein-protein interaction motif in the eubacterial DNA replication and repair systems. *Proc Natl Acad Sci USA* **98**, 11627–11632

82. Warbrick, E. (1998) PCNA binding through a conserved motif. *Bioessays* **20**, 195–199

83. Parker, A. E., Van de Weyer, I., Laus, M. C., Verhasselt, P., and Luyten, W. H. (1998) Identification of a human homologue of the Schizosaccharomyces pombe rad17+ checkpoint gene. *J Biol Chem* **273**, 18340–18346

84. Rauen, M., Burtelow, M. A., Dufault, V. M., and Karnitz, L. M. (2000) The human checkpoint protein hRad17 interacts with the PCNA-like proteins hRad1, hHus1, and hRad9. *J Biol Chem* **275**, 29767–29771

85. Caspari, T., Dahlen, M., Kanter-Smoler, G., Lindsay, H. D., Hofmann, K., Papadimitriou, K., Sunnerhagen, P., and Carr, A. M. (2000) Characterization of Schizosaccharomyces pombe Hus1: a PCNA-related protein that associates with Rad1 and Rad9. *Molecular and Cellular Biology* **20**, 1254–1262

86. Venclovas, C., Colvin, M. E., and Thelen, M. P. (2002) Molecular modeling-based analysis of interactions in the RFC-dependent clamp-loading process. *Protein Sci.* **11**, 2403–2416

87. Yao, N. Y., Johnson, A., Bowman, G. D., Kuriyan, J., and O'Donnell, M. (2006) Mechanism of proliferating cell nuclear antigen clamp opening by replication factor C. *J Biol Chem* **281**, 17528–17539

88. Kelch, B. A., Makino, D. L., O'Donnell, M., and Kuriyan, J. (2011) How a DNA polymerase clamp loader opens a sliding clamp. *Science* **334**, 1675–1680

89. Goedken, E. R., Kazmirski, S. L., Bowman, G. D., O'Donnell, M., and Kuriyan, J. (2005) Mapping the interaction of DNA with the Escherichia coli DNA polymerase clamp loader complex. *Nat Struct Mol Biol* **12**, 183–190

90. Park, M. S., and O'Donnell, M. (2009) The clamp loader assembles the beta clamp onto either a 3' or 5' primer terminus: the underlying basis favoring 3' loading. *J Biol Chem* **284**, 31473–31483

91. Magdalena Coman, M., Jin, M., Ceapa, R., Finkelstein, J., O'Donnell, M., Chait, B. T., and Hingorani, M. M. (2004) Dual functions, clamp opening and primer-template recognition, define a key clamp loader subunit. *Journal of Molecular Biology* **342**, 1457–1469

92. Chen, S., Coman, M. M., Sakato, M., O'Donnell, M., and Hingorani, M. M. (2008) Conserved residues in the delta subunit help the *E. coli* clamp loader, gamma complex, target primer-template DNA for clamp assembly. *Nucleic Acids Res.* **36**, 3274–3286

93. Tsurimoto, T., and Stillman, B. (1991) Replication factors required for SV40 DNA replication in vitro. I. DNA structure-specific recognition of a primer-template junction by eukaryotic DNA polymerases and their accessory proteins. *J Biol Chem* **266**, 1950–1960

94. Fotedar, R., Mossi, R., Fitzgerald, P., Rousselle, T., Maga, G., Brickner, H., Messier, H., Kasibhatla, S., Hübscher, U., and Fotedar, A. (1996) A conserved domain of the large subunit of replication factor C binds PCNA and acts like a dominant negative inhibitor of DNA replication in mammalian cells. *EMBO J.* **15**, 4423–4433

95. Uhlmann, F., Cai, J., Gibbs, E., O'Donnell, M., and Hurwitz, J. (1997) Deletion analysis of the large subunit p140 in human replication factor C reveals regions required for complex formation and replication activities. *J Biol Chem* **272**, 10058–10064

96. Allen, B. L., Uhlmann, F., Gaur, L. K., Mulder, B. A., Posey, K. L., Jones, L. B., and Hardin, S. H. (1998) DNA recognition properties of the N-terminal DNA binding domain within the large subunit of replication factor C. *Nucleic Acids Res.* **26**, 3877–3882

97. Keller, R. C., Mossi, R., Maga, G., Wellinger, R. E., Hübscher, U., and Sogo, J. M. (1999) Electron microscopic analysis reveals that replication factor C is sequestered by single-stranded DNA. *Nucleic Acids Res.* **27**, 3433–3437

98. Hingorani, M. M., and Coman, M. M. (2002) On the specificity of interaction between the Saccharomyces cerevisiae clamp loader replication factor C and primed DNA templates during DNA replication. *J Biol Chem* **277**, 47213–47224

99. Li, J., Holzschu, D. L., and Sugiyama, T. (2013) PCNA is efficiently loaded on the DNA recombination intermediate to modulate polymerase δ, η, and ζ activities. *Proc Natl Acad Sci USA* **110**, 7672–7677

100. Majka, J., Binz, S. K., Wold, M. S., and Burgers, P. M. J. (2006) Replication protein A directs loading of the DNA damage checkpoint clamp to 5'-DNA junctions. *J Biol Chem* **281**, 27855–27861

101. Querol-Audí, J., Yan, C., Xu, X., Tsutakawa, S. E., Tsai, M.-S., Tainer, J. A., Cooper, P. K., Nogales, E., and Ivanov, I. (2012) Repair complexes of FEN1 endonuclease, DNA, and Rad9-Hus1-Rad1 are distinguished from their PCNA counterparts by functionally important stability. *Proc Natl Acad Sci USA*

102. Peoples, R., Perez-Jurado, L., Wang, Y. K., Kaplan, P., and Francke, U. (1996) The gene for replication factor C subunit 2 (RFC2) is within the 7q11.23 Williams syndrome deletion. *Am. J. Hum. Genet.* **58**, 1370–1373

103. Tang, H., Hilton, B., Musich, P. R., Fang, D. Z., and Zou, Y. (2012) Replication factor C1, the large subunit of replication factor C, is proteolytically truncated in Hutchinson-Gilford progeria syndrome. *Aging Cell* **11**, 363–365

104. Bell, D. W., Sikdar, N., Lee, K.-Y., Price, J. C., Chatterjee, R., Park, H.-D., Fox, J., Ishiai, M., Rudd, M. L., Pollock, L. M., Fogoros, S. K., Mohamed, H., Hanigan, C. L., NISC Comparative Sequencing Program, Zhang, S., Cruz, P., Renaud, G., Hansen, N. F., Cherukuri, P. F., Borate, B., McManus, K. J., Stoepel, J., Sipahimalani, P., Godwin, A. K., Sgroi, D. C., Merino, M. J., Elliot, G., Elkahloun, A., Vinson, C., Takata, M., Mullikin, J. C., Wolfsberg, T. G., Hieter, P., Lim, D.-S., and Myung, K. (2011) Predisposition to cancer caused by genetic and functional defects of mammalian Atad5. *PLoS Genet* **7**, e1002245

105. Kim, Y. R., Song, S. Y., Kim, S. S., An, C. H., Lee, S. H., and Yoo, N. J. (2010) Mutational and expressional analysis of RFC3, a clamp loader in DNA replication, in gastric and colorectal cancers. *Hum. Pathol.* **41**, 1431–1437

106. Maniwa, Y., Yoshimura, M., Bermudez, V. P., Okada, K., Kanomata, N., Ohbayashi, C., Nishimura, Y., Hayashi, Y., Hurwitz, J., and Okita, Y. (2006) His239Arg SNP of HRAD9 is associated with lung adenocarcinoma. *Cancer* **106**, 1117–1122

107. Warbrick, E. (2006) A functional analysis of PCNA-binding peptides derived from protein sequence, interaction screening and rational design. *Oncogene* **25**, 2850–2859

108. Georgescu, R. E., Yurieva, O., Kim, S.-S., Kuriyan, J., Kong, X.-P., and O'Donnell, M. (2008) Structure of a small-molecule inhibitor of a DNA polymerase sliding clamp. *Proc Natl Acad Sci USA* **105**, 11116–11121

109. Zhao, H., Lo, Y.-H., Ma, L., Waltz, S. E., Gray, J. K., Hung, M.-C., and Wang, S.-C. (2011) Targeting tyrosine phosphorylation of PCNA inhibits prostate cancer growth. *Mol. Cancer Ther.* **10**, 29–36

110. Wijffels, G., Johnson, W. M., Oakley, A. J., Turner, K., Epa, V. C., Briscoe, S. J., Polley, M., Liepa, A. J., Hofmann, A., Buchardt, J., Christensen, C., Prosselkov, P., Dalrymple, B. P., Alewood, P. F., Jennings, P. A., Dixon, N. E., and Winkler, D. A. (2011) Binding inhibitors of the bacterial sliding clamp by design. *J. Med. Chem.* **54**, 4831–4838

111. Tan, Z., Wortman, M., Dillehay, K. L., Seibel, W. L., Evelyn, C. R., Smith, S. J., Malkas, L. H., Zheng, Y., Lu, S., and Dong, Z. (2012) Small-molecule targeting of proliferating cell nuclear antigen chromatin association inhibits tumor cell growth. *Mol. Pharmacol.* **81**, 811–819

112. Punchihewa, C., Inoue, A., Hishiki, A., Fujikawa, Y., Connelly, M., Evison, B., Shao, Y., Heath, R., Kuraoka, I., Rodrigues, P., Hashimoto, H., Kawanishi, M., Sato, M., Yagi, T., and Fujii, N. (2012) Identification of Small Molecule Proliferating Cell Nuclear Antigen (PCNA) Inhibitor That Disrupts Interactions with PIP-box Proteins and Inhibits DNA Replication. *J Biol Chem* **287**, 14289–14300

113. Actis, M., Inoue, A., Evison, B., Perry, S., Punchihewa, C., and Fujii, N. (2013) Small molecule inhibitors of PCNA/PIP-box interaction suppress translesion DNA synthesis. *Bioorg. Med. Chem.* **21**, 1972–1977

114. Bozza, W. P., Yang, K., Wang, J., and Zhuang, Z. (2012) Developing peptide-based multivalent antagonists of proliferating cell nuclear antigen and a fluorescence-based PCNA binding assay. *Analytical Biochemistry* **427**, 69–78

115. Onrust, R., Finkelstein, J., Naktinis, V., Turner, J., Fang, L., and O'Donnell, M. (1995) Assembly of a chromosomal replication machine: two DNA polymerases, a clamp loader, and sliding clamps in one holoenzyme particle. I. Organization of the clamp loader. *J Biol Chem* **270**, 13348–13357

116. Dong, Z., Onrust, R., Skangalis, M., and O'Donnell, M. (1993) DNA polymerase III accessory proteins. I. holA and holB encoding delta and delta'. *J Biol Chem* **268**, 11758–11765

117. Olson, M. W., Dallmann, H. G., and McHenry, C. S. (1995) DnaX complex of *Escherichia coli* DNA polymerase III holoenzyme. The chi psi complex functions by increasing the affinity of tau and gamma for delta.delta' to a physiologically relevant range. *J Biol Chem* **270**, 29570–29577

118. Maki, S., and Kornberg, A. (1988) DNA polymerase III holoenzyme of *Escherichia coli*. I. Purification and distinctive functions of subunits tau and gamma, the dnaZX gene products. *J Biol Chem* **263**, 6547–6554

119. Johanson, K. O., Haynes, T. E., and McHenry, C. S. (1986) Chemical characterization and purification of the beta subunit of the DNA polymerase III holoenzyme from an overproducing strain. *J Biol Chem* **261**, 11460–11465

120. Thompson, J. A., Paschall, C. O., O'Donnell, M., and Bloom, L. B. (2009) A slow ATP-induced conformational change limits the rate of DNA binding but not the rate of beta clamp binding by the *Escherichia coli* gamma complex clamp loader. *J Biol Chem* **284**, 32147–32157

121. Yao, N., Hurwitz, J., and O'Donnell, M. (2000) Dynamics of beta and proliferating cell nuclear antigen sliding clamps in traversing DNA secondary structure. *J Biol Chem* **275**, 1421–1432

122. Finkelstein, J., Antony, E., Hingorani, M. M., and O'Donnell, M. (2003) Overproduction and analysis of eukaryotic multiprotein complexes in Escherichia coli using a dual-vector strategy. *Analytical Biochemistry* **319**, 78–87

123. Yao, N., Coryell, L., Zhang, D., Georgescu, R. E., Finkelstein, J., Coman, M. M., Hingorani, M. M., and O'Donnell, M. (2003) Replication factor C clamp loader subunit arrangement within the circular pentamer and its attachment points to proliferating cell nuclear antigen. *J Biol Chem* **278**, 50744–50753

124. Ayyagari, R., Impellizzeri, K. J., Yoder, B. L., Gary, S. L., and Burgers, P. M. (1995) A mutational analysis of the yeast proliferating cell nuclear antigen indicates distinct roles in DNA replication and DNA repair. *Molecular and Cellular Biology* **15**, 4420–4429

125. Bauer, G. A., and Burgers, P. M. (1988) The yeast analog of mammalian cyclin/proliferating-cell nuclear antigen interacts with mammalian DNA polymerase delta. *Proc Natl Acad Sci USA* **85**, 7506–7510

126. Brune, M., Hunter, J. L., Corrie, J. E., and Webb, M. R. (1994) Direct, real-time measurement of rapid inorganic phosphate release using a novel fluorescent probe and its application to actomyosin subfragment 1 ATPase. *Biochemistry* **33**, 8262–8271

127. Indiani, C., and O'Donnell, M. E. (2006) The replication clamp-loading machine at work in the three domains of life. *Nat. Rev. Mol. Cell Biol.* **7**, 751–761

128. Bloom, L. B., Turner, J., Kelman, Z., Beechem, J. M., O'Donnell, M., and Goodman, M. F. (1996) Dynamics of loading the beta sliding clamp of DNA polymerase III onto DNA. *J Biol Chem* **271**, 30699–30708

129. Downey, C. D., and Mchenry, C. S. (2010) Chaperoning of a replicative polymerase onto a newly assembled DNA-bound sliding clamp by the clamp loader. *Molecular Cell* **37**, 481–491

130. Brune, M., Hunter, J. L., Howell, S. A., Martin, S. R., Hazlett, T. L., Corrie, J. E., and Webb, M. R. (1998) Mechanism of inorganic phosphate interaction with phosphate binding protein from Escherichia coli. *Biochemistry* **37**, 10370–10380

131. Anderson, S. G., Thompson, J. A., Paschall, C. O., O'Donnell, M., and Bloom, L. B. (2009) Temporal Correlation of DNA Binding, ATP Hydrolysis, and Clamp Release in the Clamp Loading Reaction Catalyzed by the Escherichia coliγ complex. *Biochemistry* **48**, 8516–8527

132. Jeruzalmi, D., Yurieva, O., Zhao, Y., Young, M., Stewart, J., Hingorani, M., O'Donnell, M., and Kuriyan, J. (2001) Mechanism of processivity clamp opening by the delta subunit wrench of the clamp loader complex of *E. coli* DNA polymerase III. *Cell* **106**, 417–428

133. Fang, J., Engen, J. R., and Beuning, P. J. (2011) *Escherichia coli* processivity clamp β from DNA polymerase III is dynamic in solution. *Biochemistry* **50**, 5958–5968

134. Tainer, J. A., McCammon, J. A., and Ivanov, I. (2010) Recognition of the ring-opened state of proliferating cell nuclear antigen by replication factor C promotes eukaryotic clamp-loading. *J. Am. Chem. Soc.* **132**, 7372–7378

135. Bloom, L. B. (2006) Dynamics of loading the Escherichia coli DNA polymerase processivity clamp. *Crit. Rev. Biochem. Mol. Biol.* **41**, 179–208

136. Parrilla-Castellar, E. R., Arlander, S. J. H., and Karnitz, L. (2004) Dial 9-1-1 for DNA damage: the Rad9-Hus1-Rad1 (9-1-1) clamp complex. *DNA Repair* **3**, 1009–1014

137. Eichinger, C. S., and Jentsch, S. (2011) 9-1-1: PCNA's specialized cousin. *Trends Biochem. Sci.* **36**, 563–568

138. Gomes, X. V., Gary, S. L., and Burgers, P. M. (2000) Overproduction in Escherichia coli and characterization of yeast replication factor C lacking the ligase homology domain. *J Biol Chem* **275**, 14541–14549

139. Bochkarev, A., Pfuetzner, R. A., Edwards, A. M., and Frappier, L. (1997) Structure of the single-stranded-DNA-binding domain of replication protein A bound to DNA. *Nature* **385**, 176–181

140. Bochkareva, E., Korolev, S., Lees-Miller, S. P., and Bochkarev, A. (2002) Structure of the RPA trimerization core and its role in the multistep DNA-binding mechanism of RPA. *EMBO J.* **21**, 1855–1863

141. Waga, S., and Stillman, B. (1994) Anatomy of a DNA replication fork revealed by reconstitution of SV40 DNA replication in vitro. *Nature* **369**, 207–212

142. Cullmann, G., Fien, K., Kobayashi, R., and Stillman, B. (1995) Characterization of the five replication factor C genes of Saccharomyces cerevisiae. *Molecular and Cellular Biology* **15**, 4661–4671

143. Jeruzalmi, D., O'Donnell, M., and Kuriyan, J. (2001) Crystal structure of the processivity clamp loader gamma (gamma) complex of *E. coli* DNA polymerase III. *Cell* **106**, 429–441

144. Ionescu, C. N., Shea, K. A., Mehra, R., Prundeanu, L., and McAlear, M. A. (2002) Monomeric yeast PCNA mutants are defective in interacting with and stimulating the ATPase activity of RFC. *Biochemistry* **41**, 12975–12985

145. Freudenthal, B. D., Gakhar, L., Ramaswamy, S., and Washington, M. T. (2009) A charged residue at the subunit interface of PCNA promotes trimer formation by destabilizing alternate subunit interactions. *Acta Crystallogr D Biol Crystallogr* **65**, 560–566

146. Raghunathan, S., Kozlov, A. G., Lohman, T. M., and Waksman, G. (2000) Structure of the DNA binding domain of E. coli SSB bound to ssDNA. *Nat. Struct. Biol.* **7**, 648–652

147. Shereda, R. D., Kozlov, A. G., Lohman, T. M., Cox, M. M., and Keck, J. L. (2008) SSB as an Organizer/Mobilizer of Genome Maintenance Complexes. *Crit. Rev. Biochem. Mol. Biol.* **43**, 289–318

148. Bylund, G. O., Majka, J., and Burgers, P. M. J. (2006) Overproduction and purification of RFC-related clamp loaders and PCNA-related clamps from Saccharomyces cerevisiae. *Meth. Enzymol.* **409**, 1–11

149. Majka, J., and Burgers, P. M. (2005) Function of Rad17/Mec3/Ddc1 and its partial complexes in the DNA damage checkpoint. *DNA Repair* **4**, 1189–1194

# BIOGRAPHICAL SKETCH

Jaclyn Hayner was born in Mt. Kisco, New York in 1985. In 1990, she moved to Tampa, FL and graduated with honors from Gaither High School in 2003. She attended the University of South Florida for undergraduate work. In 2008, she received a Bachelor of Science in Biology, and a Bachelor of Art in Chemistry with an emphasis in Biochemistry. She performed undergraduate research under the guidance of Dr. Lindsey Shaw and Dr. Edward Turros, investigating the role of virulence factors in *S.aureus* pathogenicity as well as synthesizing novel antibiotics targeting MRSA. In 2008, she joined the graduate program in the College of Medicine at the University of Florida. In 2009, she joined the laboratory of Dr. Linda Bloom investigating the mechanism and DNA specificity of *E. coli* and *S. cerevisiae* clamp loaders.